Investigating the regulation of divalent cation homeostasis during fertilization and preimplantation embryo development in mice

Investigating the regulation of divalent cation homeostasis during fertilization and preimplantation embryo development in mice

A Dissertation Presented

By

NEHA GUPTA

Submitted to the Graduate School of the

University of Massachusetts in partial fulfillment

of the requirements for the degree of

DOCTOR OF PHILOSOPHY

May 2024

Animal Biotechnology and Biomedical Sciences

Investigating the regulation of divalent cation homeostasis during fertilization and preimplantation embryo development in mice

A Dissertation Presented

By

NEHA GUPTA

Approved as to style and content by:

_____

Rafael Fissore, Chair

_____

Dominique Alfandari, Member

_____

Wei Cui, Member

_____

Thomas Maresca, Member

_____

Kathleen Arcaro, Graduate Program Director

Department of Veterinary and Animal Sciences

ACKNOWLEDGEMENTS

I am profoundly grateful for the unwavering support and guidance provided by numerous individuals who have accompanied me throughout my PhD journey. Without their invaluable assistance, this achievement would not have been possible.

First and foremost, I extend my heartfelt gratitude to my advisor, **Dr. Rafael Fissore**. His expertise, encouragement, and insightful guidance have played a pivotal role in shaping this research. I am deeply appreciative of the opportunity to learn under his mentorship.

I would like to express sincere appreciation to the members of my thesis committee, **Dr. Dominique Afandari, Dr. Wei Cui,** and **Dr. Thomas Maresca**, for their constructive feedback and expertise, which have greatly enriched the quality and depth of this study. Special thanks also go to our collaborators, including **Dr. Dominique Alfandari, Dr. Wei Cui, Dr. Carmen Williams, Dr. Pablo Visconti,** and **Dr. Mariano Buffone**, for their invaluable insights and assistance in obtaining essential data for the projects.

The willingness of participants such as **Lei Zhang, Goli Ardestani, Cristina Soriano Ubeda,** and **Hiroki Akizawa** to share their experiences and insights has been integral to the completion of this thesis. I am also grateful to our former lab manager, **Changli He**, for her unwavering support throughout these studies. I am also deeply indebted to our administrative staff, especially **Laura Looman, James Wright**, and **Mary Schneider**, along with IPO advisor **Katie Ahlman**, for their patience in providing me with all the necessary information throughout my PhD milestone and lab organization. Their support has been invaluable in ensuring the smooth progress of my academic journey.

I extend my gratitude to my friends and colleagues, including **Ana Clara, Nidhi Thaker, Emily Lopes, Francesca Carpentiero** and **Oguz Koc** for their encouragement, moral support, and assistance whenever needed. Your companionship has made this journey more meaningful and enjoyable.

I am thankful for the financial support provided by all the funds from NIH (R24OD021485, R01DE016289, 1R21 HD10734, RO1 HD092499), BTP, Hong fellowship, and various travel grants, which have enabled me to conduct these studies and share my research with the broader academic community.

To my family, your unconditional love, support, and understanding have been my rock throughout this endeavor. Your belief in me has been my greatest source of strength, and I am profoundly grateful for your constant presence in my life.

Finally, I extend my deepest appreciation to all individuals, institutions, and organizations whose contributions, whether direct or indirect, have facilitated the completion of this research thesis.

Thank you all for being an integral part of this significant milestone in my academic journey.

ABSTRACT

INVESTIGATING THE REGULATION OF DIVALENT CATION HOMEOSTASIS DURING FERTILIZATION AND PREIMPLANTATION EMBRYO DEVELOPMENT IN MICE

MAY 2024

NEHA GUPTA, B.TECH HINDUSTAN COLLEGE OF SCIENCE AND TECHNOLOGY, INDIA

M.TECH, INDIAN INSTITUTE OF SCIENCE AND TECHNOLOGY, GANDHINAGAR, INDIA

PH.D., UNIVERSITY OF MASSACHUSETTS AMHERST

Directed by: Professor Rafael Fissore

The role of calcium ions (Ca^{2+}) as the universal signal for egg activation has been acknowledged for nearly a century, with subsequent research unveiling the necessity of Ca^{2+} oscillations for egg activation in mammals. However, understanding the precise triggering pathway(s) behind the prolonged and protracted Ca^{2+} responses during mammalian fertilization posed a challenge due to limited methods to investigate these events and knowledge of the mechanisms involved. Pivotal breakthroughs came with the discovery of fluorescent dyes to monitor ion changes and that injecting sperm extracts into eggs replicated fertilization-induced oscillations and egg activation. The culminating demonstration of this process was the birth of offspring through Intra Cytoplasmic Sperm Injection (ICSI) without previous interaction of the gametes. This milestone was molecularly underpinned by the identification of sperm-specific PLCζ, whose injection in the form of mRNA, induced Ca^{2+} oscillations identical to those observed during

fertilization. Interestingly, infertile patients with repeated ICSI failure exhibited the absence of PLCζ expression or point mutations on the sequence of PLCζ, suggesting that PLCζ represented the main, and possibly sole Ca^{2+}-active factor in mammalian sperm. However, this notion was challenged by the observation that *Plcζ*-null males initiated subdued Ca^{2+} oscillations and displayed subfertility, indicating the existence of an additional factor(s) in mouse sperm triggering sufficient Ca^{2+} responses to support embryo development. Yet, its identity and involvement during fertilization with wild-type sperm remain unknown. Our contribution here is to identify the remaining Ca^{2+} active component(s) in sperm that could function as a "backup mechanism" of egg activation. This contribution is significant because it is a necessary step in our goal to identify all the sperm molecules that induce the Ca^{2+} signal required for embryo development.

TRPM7 is expressed ubiquitously across cell types and tissues, and exhibits diverse subcellular localization, including the plasma membrane, cytoplasm, and nucleus, suggesting multifunctionality. Numerous studies have highlighted the essential role of TRPM7 in numerous cell types and organs, including a vital role in pre-implantation embryo development, where its absence causes embryonic death. Significantly, its molecular mechanism in embryogenesis remains unknown. Additionally, despite its fundamental role in fertility, the expression and localization of TRPM7 in gametes and embryos have not been fully elucidated. Our contribution seeks to precisely identify the expression, localization, and molecular mechanism of TRPM7 in embryo development, a crucial step in understanding the function of this essential channel regulating divalent cation homeostasis during embryogenesis.

Overall, this contribution holds significant implications for perfecting parthenogenetic methods to address egg activation failure, enhancing embryo development, identifying new indicators of male and female fertility, and exploring potential contraception targets. This study helped in understanding the molecules and regulatory mechanisms initiating embryo development in these species and advances our knowledge substantially.

TABLE OF CONTENTS

LIST OF TABLES

LIST OF FIGURES

CHAPTER 1

INTRODUCTION

1.1 Sperm Factor, fertilization and Ca^{2+} oscillations

The widespread participation of Ca^{2+} in invertebrate and vertebrate fertilization and the near-universal involvement of the phosphoinositide pathway and 1,4,5-inositol trisphosphate (IP_3), raised expectations for a one size-fits-all mechanism of egg activation (Stricker, 1999). Nevertheless, experimental evidence showed that none of the proposed models at the time could replicate the whole gamut of Ca^{2+} responses during fertilization. We will not discuss the main features of each model, for that, we refer the reader to comprehensive published works on the subject (Jones, 2007; Kashir et al., 2014). We will focus instead on the work that led to the elucidation of the signaling mechanism(s) responsible for the Ca^{2+}oscillations in mammals, driven from the outset by widely divergent hypotheses (Runft et al., 2002). The mechanistic chasm arose in no small part because it was conceptually difficult to envisage how the ephemeral interaction of the gametes at the plasma membrane could induce Ca^{2+} oscillations that lasted for hours. Further, this "receptor hypothesis" was primarily based on findings from hormone and neurotransmitter signaling, which were the most studied and best understood signaling models at the time, but that displayed a short lifespan. An alternative model advanced the view that after gamete fusion, a sperm component(s), the sperm factor, SFs, induced the persistent Ca^{2+} oscillations, the "fusion hypothesis." The initial supporting evidence showed that injection of sperm extracts, SFs, into eggs induced activation and embryo development. These results were first reported in sea urchin and ascidians (Dale, 1988; Dale et al., 1985) and later in hamster and rabbit eggs (Stice & Robl, 1990; Swann, 1990),

including the demonstration in hamster eggs that SFs initiated Ca^{2+} oscillations indistinguishable from those at fertilization (Swann, 1990). Despite the physiological nature of the SF-triggered oscillations, the specificity of its responses was challenged, and it was not until the success of the intracytoplasmic sperm injection technique (Iritani et al., 1988) highlighted by the birth of offspring in humans (Palermo et al., 1992), that this hypothesis became consolidated. It is remarkable, however, that the results of Uehara and Yanagimachi in 1976 (Uehara & Yanagimachi, 1976) showing that injection of mammalian sperm heads into hamster eggs induced complete egg activation did not receive more scrutiny and stimulated immediate replication, despite the confounding effects of the injection procedure (Uehara & Yanagimachi, 1977), as this data foreshadowed the true mechanism of egg activation a decade ahead of the SF results and the birth of offspring by ICSI.

The recognition of the significance of the Sperm Factor (SF) in triggering egg activation spurred efforts to pinpoint its molecular identity. Through biochemical analyses and calcium monitoring studies, several distinctive traits of SF, such as its ability to stimulate the production of IP3(Galione et al., 1997; Jones et al., 2000; Kurokawa et al., 2005; Wu et al., 1998), were revealed. However, the identification of PLCζ1 was achieved after conducting BLAST searches of a mouse EST testis database utilizing sequences of mammalian PLCs(Saunders et al., 2002). Subsequent studies across multiple investigations confirmed the pivotal role of PLCζ1 in initiating calcium oscillations in various mammalian species. Further research delved into intricacies such as the functional roles of its individual domains, differences in activity and localization among species, and its implications for infertility, topics discussed extensively in other sections of this publication.

Yet, significant questions persist, including how PLCζ1 is released during fertilization and where it acts within the egg. Notably, studies utilizing Intracytoplasmic Sperm Injection (ICSI) and sperm from genetically modified models(Hachem et al., 2017a; Nozawa et al., 2018) have reaffirmed PLCζ1 as the key SF in mammals, while simultaneously posing additional inquiries whose answers promise to offer valuable insights into mammalian fertilization processes.

1.2 SF release, PLCζ1 PN homing, and nuclear positioning in the sperm

While identification of the active component of the SF demanded a few years, the advent of ICSI firmly established the notion that the diffusion of a sperm factor into the ooplasm underpinned the events of activation in mammalian eggs. A series of studies extended these results by demonstrating that following ICSI, the sperm's active component(s) diffuse into the ooplasm within 15-30 min post-injection, and release appears to be complete by 120 min. The conclusions were obtained by re-injecting sperm heads into unfertilized eggs and monitoring Ca^{2+} rises. Sperm heads that have resided in the ooplasm for less than 1 hour initiated oscillations when injected into MII eggs but failed when re-injected after 120 min despite continuing rises in the donor egg (Knott et al., 2003). These studies also showed that the M-phase state of the MII ooplasm was not required for the release of SF and that exposure and solubilization but not the disintegration of the perinuclear theca (PT), the presumed site of the residence of PLCζ1 in the mature sperm, are needed for its release (Knott et al., 2003). A follow-up study demonstrated that the loss of the sperm heads' Ca^{2+} oscillation-inducing activity coincided with the loss of PLCζ1 reactivity (Yoon & Fissore, 2007). Unfortunately, the ooplasm's high fluorescent background has prevented thus far to track the distribution of PLCζ1 in the ooplasm,

although PLCζ1 reappears and its detection raises well above background in the PNs, which are a recognized site of PLCζ1 accumulation in mouse zygotes (Ito et al., 2008; Larman et al., 2004; Sone et al., 2005). Remarkably, it is this property of mouse PLCζ1, its nuclear localization signal and concentration in the PN, which can explain results that remained unexplained for years. Those observations noted that injections of PNs from fertilized mouse zygotes but not from parthenogenetically activated eggs triggered oscillations in fresh mouse eggs (Kono et al., 1995), which were likely due to the accumulation of PLCζ1 in the fertilized PNs . These results are among the most robust demonstrations that PLCζ1 represents the primary and possibly sole active SF in mammals during natural fertilization.

The molecules involved in determining the location of PLCζ1 in mature sperm are presently unknown but using ICSI has provided essential clues that have led to the discovery of previously unknown proteins required for PLCζ1 to find or be anchored to the PT, its final destination before fertilization. In non-capacitated mouse sperm, a fraction of PLCζ1 is detected overlaying the acrosome, although the highest concentration centers on the post-acrosome region where it appears as a continuous band (Grasa et al., 2008; Yoon & Fissore, 2007). Following the acrosome reaction, the post-acrosomal localization becomes predominant (Grasa et al., 2008), which is appropriate given the need to rapidly access the ooplasm after fusion. ICSI's importance in these studies emanates from its routine application to overcome total fertilization failure (TFF) cases following IVF or for patients with abnormally shaped sperm heads and/or acrosomes. The inability in some patients' sperm to induce egg activation in conjunction with the absence or mislocalization of PLCζ1 led to genomic analysis that identified essential determinants in PT organization.

One of these proteins is *ACTL9*, an Actin-Like 9 protein, for which homozygous mutations underlie the abnormal organization of the PT, mislocalization of PLCζ1, and inability to trigger steady oscillations (Dai et al., 2021). Another protein uncovered following TTF after ICSI is associated with ~70% of the type I cases of human globozoospermia (Harbuz et al., 2011). An initial study showed that the repeated TFF commonly observed in globozoospermic patients after ICSI was associated with the absence of PLCζ1 expression in these patient's sperm and inability to trigger Ca^{2+} oscillations (Yoon et al., 2008). Genomics studies of these men led to research demonstrating that most of these patients had a homozygous deletion of *DPY19L2,* a gene highly expressed in testes and of unknown function until then. The induced deletion of the homolog gene in mice also caused globozoospermic and activation failure, later demonstrated to be due to the absence of Plcζ1 in mature sperm (Yassine et al., 2015). *Dpy19l2* expression was found to be restricted to the inner nuclear membrane facing the acrosomal vesicle, and its absence destabilized the nuclear dense lamina and caused the elimination of the unbound acrosomal vesicle presumably with the associated loss of Plcζ1. Therefore, the ability to inject whole nuclei, including sperm into eggs, has been leveraged to gain fundamental insights that are proving indispensable as we aim to understand the mechanisms that underlie mammalian fertilization.

1.3 Divalent cations and fertilization

Divalent cations play essential roles in fertilization and early embryo development, including cellular processes associated with egg activation, implantation, and gastrulation (Komiya et al., 2014; Krauchunas & Wolfner, 2013; Stein et al., 2020; Wozniak & Carlson, 2020). The role of calcium (Ca^{2+}) in egg activation, the first stage of development, is

broadly recognized in all species, including in mammals, where the signal consists of repeated changes in its intracellular concentration that lasts for several hours (hr) and are known as Ca^{2+} oscillations (Stein et al., 2020; Stricker, 1999; Wakai & Fissore, 2019). The realization of Zn^{2+} contributions to fertilization is more recent, and the full scope of its actions remains unrevealed. However, Zn^{2+} undergoes exocytosis during fertilization producing the Zn^{2+} sparks (Kim et al., 2011), and it participates in molecular events associated with the exit of meiosis and polyspermy block (Burkart et al., 2012; Suzuki et al., 2010; Tokuhiro & Dean, 2018). Lastly, the precise role of Mg^{2+} in early development is least understood, but the content of extracellular Mg^{2+} influences the periodicity of Ca^{2+} oscillations and impacts embryo development (Bernhardt et al., 2018; Ozil et al., 2017). Thus, divalent cations play essential roles in the initiation and progression of embryo development, although many of the molecules and mechanisms regulating their homeostasis and the molecular effectors of their actions remain unspecified.

The stereotypical fertilization-induced calcium (Ca^{2+}) oscillations of mammals underpin all events of egg activation necessary for embryo development, and elucidation of all the molecules responsible for triggering these responses has potential diagnostic and therapeutic benefits. In most species, the fertilization signal involves a single or few Ca^{2+}

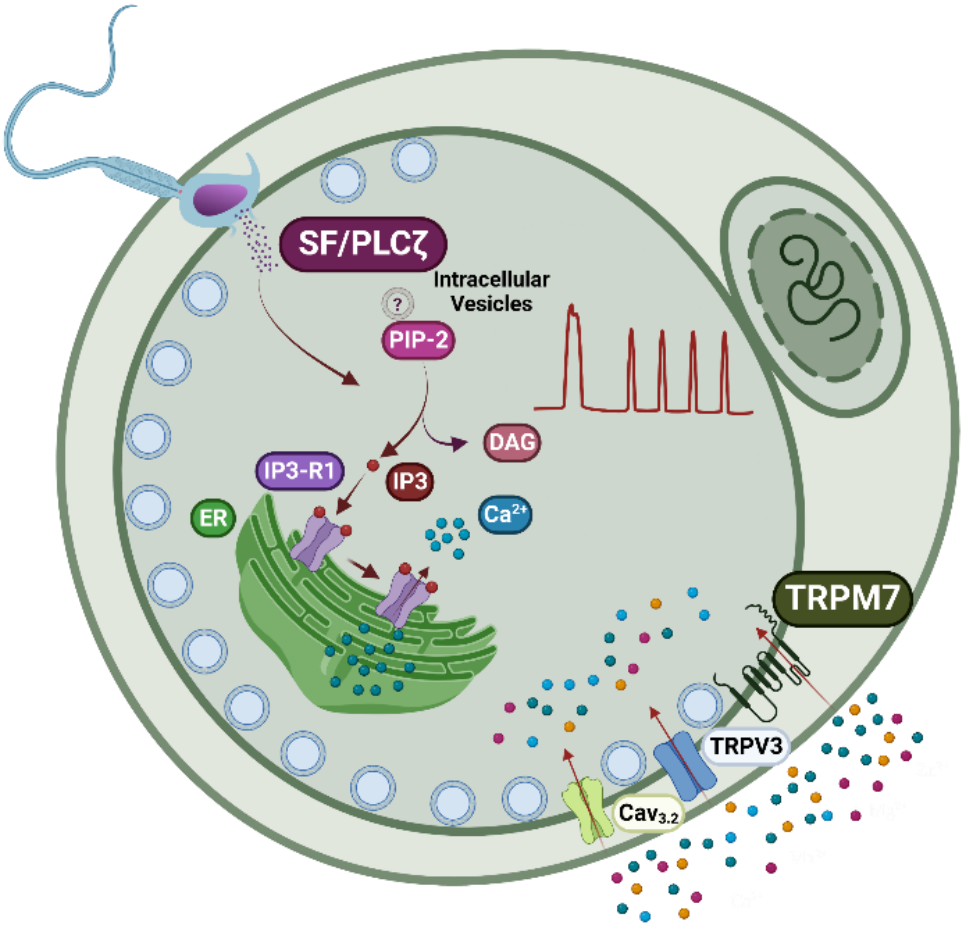

Figure 1. Molecules involved in post-fertilization events.

rises, but it is complex and protracted in mammals. In this species, the Ca^{2+} rises are periodical, slow, occur every 10 to 20 min, and persistent, extending from 4 to more than 10 hr. (Miyazaki & Ito, 2006) (**Figure 1**) It is accepted that following gamete fusion, sperm molecule(s) induce and maintain the Ca^{2+} oscillations. It is recognized that the phosphoinositide pathway of the egg is engaged, resulting in the production of inositol 1,4,5-trisphosphate (IP_3), which mediates Ca^{2+} release through its cognate receptor (Miyazaki, 1993). The sperm-specific phospholipase C Zeta 1 (PLCζ) has emerged as the central molecule capable of producing IP_3 and inducing oscillations, and its expression replicates the Ca^{2+} responses of fertilization (Saunders et al., 2002). PLCζ is member of

the domain-based PLC family, and possess the unique characteristics of lacking a pleckstrin homology (PH) domain (see for review (Thanassoulas et al., 2022)) (**Figure 2**) and has a high specific activity at basal levels of Ca^{2+}. (Rice et al., 2000) Whether PLCζ represents the complete

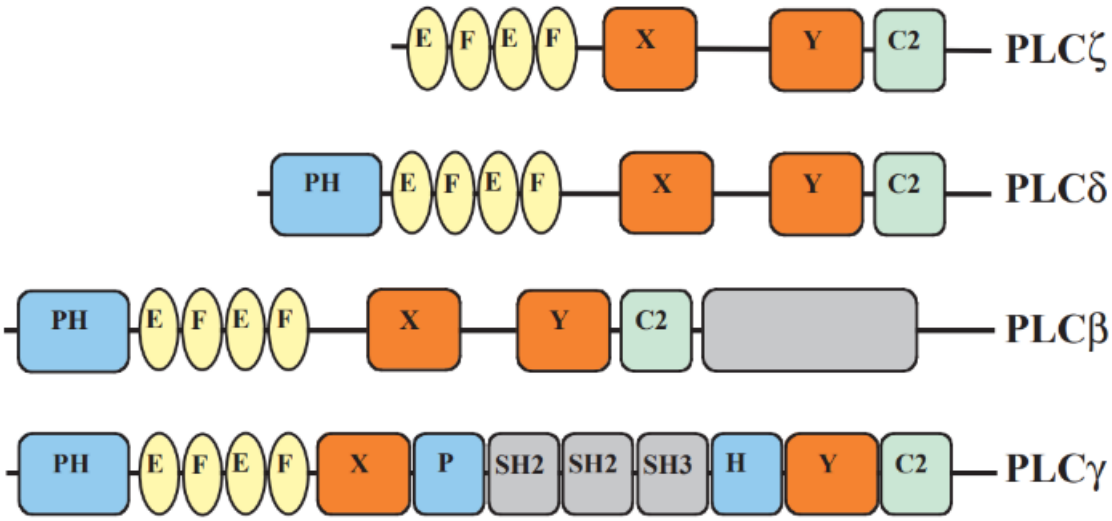

Figure 2. Schematic illustrating predicted domains of mPLCs. (Saunders et al.,

"*sperm's Ca^{2+} activating load*" is unknown (Hachem et al., 2017b; Nozawa et al., 2018). There *is a need to fill this gap*, as this knowledge will make it possible to control Ca^{2+} activation parameters, ascertain the extent to which defects/mutations in these molecules influence fertility in this species, and extend focused studies of egg-activating molecules to all mammals.

1.4 Divalent cations and their channels in mouse gametes and embryos

Gametes and embryos influx the divalent cations from their environment to refill the stores and involve in essential molecular processes, but the array of specific and non-specific plasma membrane (PM) channels and transporters they employ remains poorly characterized. Mammalian eggs and embryos express a complete Ca^{2+} toolkit (Stein et al.,

2020; Wakai et al., 2011), but the molecules that mediate Ca^{2+} influx remain unexplored except for mouse eggs and to some extent, early mouse embryos (Carvacho et al., 2016). Mouse eggs functionally express three channels, $Ca_v3.2$ or T-channel (*Canah1h*) (Bernhardt et al., 2015; Peres, 1987), a voltage-gated channel, and two Transient Receptor Potential (TRP) family members, Vanilloid-3 (Carvacho et al., 2013) and Melastatin-7 (TRPV3 and TRPM7) (Bernhardt et al., 2017; Carvacho et al., 2016) **(Figure 1)**. Eggs null for any of these channels (*Trpm7* is a conditional KO) mount somewhat altered Ca^{2+} responses after fertilization, and KO females display varying degrees of subfertility when paired with WT males. *Trpv3*- or *$Ca_v3.2$*-null females are fertile even after homozygous mating or combined deletion, which contrasts with the early development arrest caused by the homozygous deletion of *Trpm7* (Jin et al., 2008). TRPM7 is notable among all the mentioned channels because of its widespread expression and effective permeation of Zn^{2+}, Mg^{2+}, and, to a lesser extent, Ca^{2+} (Li et al., 2006; Monteilh-Zoller et al., 2003; Nadler et al., 2001). It is unknown if the absence of TRPM7 affects one or all these cations in gametes and zygotes.

TRPM7 is a unique bifunctional molecule that, besides the channel domain, is outfitted on its intracellular-C-terminal end with an active α-type serine-threonine kinase. **(Figure 3.)** (Schmitz et al., 2003) It is a cationic, non-selective channel with a permeability sequence favoring divalent cations, and that under physiological ionic conditions supports small inward currents (Monteilh-Zoller et al., 2003; Nadler et al.,

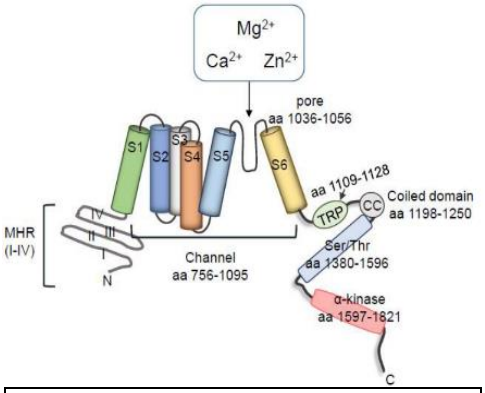

Fig. 3. Schematic structure of channel and kinase domain of TRPM7. (Zou et al., 2019)

2001). TRPM7 forms active homomeric complexes and undergoes cleavage in a cell type-specific manner that releases a C-term kinase (C-kinase) capable of nuclear translocation (Krapivinsky et al., 2014). Whether this occurs in gametes and embryos during development is unknown. Several studies reported on the essential role of TRPM7 in embryogenesis. Research showed that its ablation caused developmental arrest before embryonic day 7 (E7) (Jin et al., 2008; Jin et al., 2012), and a recent investigation found earlier demise of KO embryos, ~E5, and reported defective implantation due to failure of trophectoderm differentiation (Schütz et al., 2021). Neither study pinpointed the underlying molecular mechanism(s). Remarkably, the null *Trpm7* embryos used in those studies resulted from heterozygous pairings, raising the possibility that due to the oocyte's ability to synthesize and store mRNA and protein from the WT allele (Wu & Dean, 2020), they may express TRPM7 post-fertilization, delaying KO embryos from acquiring null status. In support of this view, inhibition of TRPM7 with the pharmacological compound NS8593 caused embryonic arrest during cleavage stages (Carvacho et al., 2016), suggesting that TRPM7 is essential at earlier stages of development than reported thus far by genetic studies. However, the precise expression, distribution, and function of TRPM7 in gametes and early mammalian embryos are unknown.

1.5 Aim1. Identify the factor(s) that supports fertilization-initiated Ca^{2+} oscillations in the absence of PLCZ1.

Fertilization-induced Ca^{2+} oscillations are essential for egg activation and initiation of embryo development. These oscillations are generally the function of the primary sperm factor, PLCZ1(**Fig. 4**, **A)**. However, the sperm of PLCZ1-null males generate residual Ca^{2+} oscillations post IVF (Hachem et al., 2017b; Nozawa et al., 2018) (**Fig. 4**, **B**), making them subfertile and with average litter sizes of 2.3 ± 0.8. Interestingly, the same sperm are unable to induce Ca^{2+} oscillations post ICSI (Hachem et al., 2017b; Nozawa et al., 2018) (**Fig. 4**, **C**). PLCZ1 engages the phosphoinositide pathway to induce Ca^{2+} oscillations wherein it hydrolyses the eggs' PIP2 and generates IP_3, which binds to its cognate receptor on the ER membrane and release Ca^{2+}. This suggests that these residual oscillations are potentially being generated by another sperm PLCs. An equally abundant PLC in mouse sperm is PLCD4, which is involved in the acrosome reaction (AR) during fertilization. (Fukami et al., 2001) *Our working hypothesis is that PLCD4 acts as a backup molecule in absence of PLCZ1 and generates the residual Ca^{2+} oscillations*.

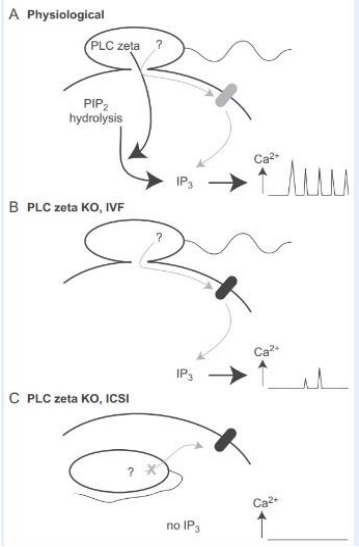

Fig 4. Ca^{2+} oscillations in WT (A) and in PLCZ KO sperm post IVF (B) and ICSI (C).(Jones, 2018)

1.6 Aim 2. Characterize the functional role of TRPM7 in gametes and preimplantation embryos

TRPM7 is one of the three known Ca^{2+} channels expressed in mouse oocytes/eggs essential for egg activation and preimplantation embryo development. (Bernhardt et al., 2017; Carvacho et al., 2016) Previous studies reported the *Trpm7* null embryos are embryonically lethal at day ~E7. (Jin et al., 2008; Jin et al., 2012) However, these embryos were generated by mating heterozygous animals, and the oocyte's WT allele likely produced TRPM7 during oogenesis. In support of this view, when our lab used a TRPM7-specific pharmacological inhibitor, NS8593, we found that the embryonic arrest was much earlier than reported (**Table 1**; (Carvacho et al., 2016)).

Table 1. In vitro embryo development in control and TRPM7 inhibitor (NS8593) group

Treatment	#2nd PB/2PN[a]	#2-Cells (%)[b]	#4-cells (%)	#8 -cells (%)
Control	32	26 (81)	26 (100)	21 (81)
NS8593-10 μM	35	31 (88)	21 (69)	6 (29)

We, therefore, hypothesized that the presence of maternal mRNA in the embryos generated by mating heterozygous animals delays the acquisition of *Trpm7* null status. Thus, we wanted to examine the effect of the deletion of *Trpm7* from gametes (conditional KO; cKOs) to produce embryos that lack TRPM7 from the outset and evaluate the impact on development. Thus, after generating those animals, we evaluate divalent cation homeostasis in gametes and embryos as well as the effect on pre-implantation embryo development. *Our working hypothesis is that TRPM7 is required for preimplantation embryo development because is essential for regulating the homeostasis of one or more of divalent cations.*

CHAPTER 2

THE ROLE OF SPERM FACTORS IN GENERATING THE CA^{2+} OSCILLATIONS OF FERTILIZATION IN THE MOUSE

2.1 Abstract

Fertilization-induced calcium (Ca^{2+}) oscillations play a pivotal role in egg activation and the onset of embryo development in mammals, holding significant diagnostic and therapeutic implications. Research spanning several decades has identified the sperm-derived molecules that are released into the ooplasm post-gamete fusion and that initiate the signaling pathways leading to the generation of Ca^{2+} oscillations. Among these, sperm-specific phospholipase C (PLCζ1) stands out for triggering Ca^{2+} release through the production of inositol 1,4,5-triphosphate (IP3), which binds to its receptor in the endoplasmic reticulum (ER). However, whether PLCζ1 represents the sole activator of sperm-induced Ca^{2+} release remains uncertain. Notably, studies including ours reveal that male mice lacking PLCζ1 exhibit sub-fertility, generating smaller litters, and their sperm trigger diminished Ca^{2+} oscillations upon fertilization, suggesting the presence of a compensatory mechanism in place. We identified PLCδ4 as a potentially upregulated molecule in *Plcζ1* knockout sperm, implicating it as a backup mechanism. By generating *Plcδ4* knockout mice, we demonstrated that their sperm induce diminished Ca^{2+} oscillations during in vitro fertilization (IVF) and intra-cytoplasmic sperm injection (ICSI), underscoring its contribution to egg activation in mice. By generating double knockout males lacking both *Plc*ζ1 and *Plc*δ4 genes, we demonstrated that they are sterile and generate no or a single rise, which is not enough to activate the eggs. Unraveling the complete repertoire of molecules involved in triggering Ca^{2+} oscillations in mice and other

mammals holds paramount importance in understanding this critical stage of embryo development. Such insights not only will shed light on the functional regulation of sperm molecules but also offer valuable diagnostic and therapeutic avenues for reproductive management in both humans and animals.

2.2 Introduction

Ca^{2+} plays an essential role in fertilization and egg activation. Three pivotal discoveries guided the search for the sperm's egg activating factor, namely, the observation that ionic changes underlie egg activation, the discovery that Ca^{2+} is the physiological ion, and the finding that in mammals the Ca^{2+} changes are periodical, separated by dozens of minutes and persists for hours. The widespread participation of Ca^{2+} in invertebrate and vertebrate fertilization and the near-universal involvement of the phosphoinositide pathway and 1,4,5-inositol trisphosphate (IP_3), raised expectations for a one-size-fits-all mechanism of egg activation (Stricker, 1999). Nevertheless, experimental evidence showed that none of the proposed models at the time could replicate the whole gamut of Ca^{2+} responses during fertilization. The mechanistic chasm arose in no small part because it was conceptually difficult to envisage how the ephemeral interaction of the gametes at the plasma membrane could induce Ca^{2+} oscillations that lasted for hours. Further, this "receptor hypothesis" was primarily based on findings from hormone and neurotransmitter signaling, which were the most studied and best understood signaling models at the time, but that displayed a short lifespan. An alternative model advanced the view that after gamete fusion, a sperm component(s), the sperm factor, SFs, induced the persistent Ca^{2+} oscillations, the "fusion hypothesis." The initial supporting evidence showed that injection of sperm extracts, SFs, into eggs induced activation and embryo development. These

results were first reported in sea urchin and ascidians (Dale, 1988; Dale et al., 1985) and later in hamster and rabbit eggs (Stice & Robl, 1990; Swann, 1990), including the demonstration in hamster eggs that SFs initiated Ca^{2+} oscillations indistinguishable from those at fertilization (Swann, 1990). Despite the physiological nature of the SF-triggered oscillations, the specificity of its responses was challenged, and it was not until the success of the intracytoplasmic sperm injection technique (Iritani et al., 1988) highlighted by the birth of offspring in humans (Palermo et al., 1992), that this hypothesis became consolidated. It is remarkable, however, that the results of Uehara and Yanagimachi in 1976 (Uehara & Yanagimachi, 1976) showing that injection of mammalian sperm heads into hamster eggs induced complete egg activation did not receive more scrutiny and stimulated immediate replication, despite the confounding effects of the injection procedure (Uehara & Yanagimachi, 1977), as this data foreshadowed the true mechanism of egg activation a decade ahead of the SF results and the birth of offspring by ICSI.

The realization of the role of SF in egg activation prompted the search for its molecular identity. Biochemical and Ca^{2+} monitoring studies uncovered many unique features of the SF including its ability to induce production of IP_3 (Galione et al., 1997; Jones et al., 2000; Kurokawa et al., 2005; Wu et al., 1998), but identification of PLCζ1 was accomplished after BLAST searches of a mouse EST testis database using mammalian PLC sequences (Saunders et al., 2002). Multiple studies confirmed the role of PLCζ1 in the initiation of Ca^{2+} oscillations in mammalian species. Furthermore, more detailed studies followed, including the elucidation of the functional role of each of its domains, species-specific differences in activity and localization, and its implications on infertility. Nevertheless, unanswered questions remain, such as the mechanism of PLCζ1 release

during fertilization and the site of action in the egg. Remarkably, the use of ICSI and sperm from genetic models (Hachem et al., 2017a; Nozawa et al., 2018) have confirmed the role of PLCζ1 as the pivotal SF in mammals while at the same time raising some outstanding questions, the answers to which will provide valuable insights about fertilization in mammals such as how PLCζ1 gets to the peri-nuclear theca (PT) and its release from it. Similarly, once in the ooplasm, how PLCζ1 finds its substrate and what organelle(s) hosts the substrate remain to be determined. Lastly, and possibly most importantly, is whether PLCζ1 is the only factor required for egg activation in mammals. Two sets of findings lead to profoundly different interpretations. First, the ever-growing list of *PLCζ1* mutations found underlying cases of human infertility despite these patients' normal sperm parameters and otherwise normal genome profiles strongly supports the view that in humans, PLCζ1 is "the sole SF." Against this line of thought is the evidence by several laboratories that *Plcζ1* KO mice sire offspring (Hachem et al., 2017a; Nozawa et al., 2018), albeit the litters are of drastically reduced size. The interpretation of these results is that a "backup mechanism" exists, at least in mice, and the implications are it might be capable of supporting "basal levels" of egg activation and offspring development to ensure reproduction. A caveat to the interpretation of all genetics studies is that elimination or inactivation of a gene in a target organ or cells from the outset can produce significant changes in the gene expression of others, which might obscure the full impact of the function of the deleted gene. Therefore, further proteomic studies are needed to demonstrate whether the deletion/inactivation of *Plcζ1* alters the expression of other enzymes that can "make up" for the loss of *PLCζ1*. Further, the deletion of *PLCζ1* should be extended to other mammals to determine how widespread is the reliance of mammals

on PLCζ1. In other words, does a backup mechanism exist in other mammals? Regardless, studies over the last twenty years have established the preeminent role of PLCζ1 in egg activation in mammals. With this knowledge at hand, the available *Plcζ1 KO* models, and the increased ability to generate new ones, coupled with the capacity to induce timely fertilization by ICSI, all the tools are at our disposal to answer the remaining questions and continue uncovering the molecules and mechanisms of fertilization.

Regarding the search for a possible mechanism(s) that sperm without PLCζ1 could support minimal oscillations and fertility, there are several mechanisms whereby oscillations can be initiated in mouse eggs. One possibility is without producing IP_3. Two compounds can initiate oscillations this way, thimerosal and $SrCl_2$, which modify the IP_3R1 by a different mechanism(s), but they are naturally toxic and require μM or mM concentrations, respectively, which is unlikely to be present in a single sperm. Other proposed mechanisms, such as NADP, cADPR, or the sperm-derived PAWP or citrate synthase proteins, (Kang et al., 2020) besides failing to initiate oscillations like fertilization, suffer other limitations that make them unlikely SFs. (Escoffier et al., 2016; Kashir et al., 2015; Swann & Lai, 2016) Mouse eggs can produce IP_3 by stimulating their PLCs and promoting Ca^{2+} influx can activate these enzymes. However, in eggs, this approach triggers a Ca^{2+} rise but no oscillations (Miyazaki, 1993). Lastly, one of the other sperm-expressed PLC isoforms, individually or collectively, can serve as the Ca^{2+}-backup mechanism. Genetic deletion studies showed that homozygous mating of *PLcγ1*$^{-/-}$ or *Plcδ3*$^{-/-}$ animals produced embryonic death, ~embryonic day 8.0 or later, but initial stages of development were normal (Ji et al., 1997; Nakamura & Fukami, 2017). Deletion of other *Plc* isoforms present in sperm was seemingly without effect on fertility except for *Plcδ4.*

(Fukami et al., 2001) *Plcδ4* null males were infertile, and mating with WT females failed to produce offspring in most cases. PLCδ4, splice variant II, is abundantly expressed in the testes and sperm of mice and rats. In mouse sperm, PLCδ4 localizes to the acrosome, where it regulates the acrosome reaction (**AR**) (Fukami et al., 2003). How loss of *Plcz* affects the expression of other sperm PLCs is unknown, but upregulation of one or more could compensate for the loss of *Plcz*. Thus, the role of the sperm-enriched PLCδ4, or other isoforms as the Ca^{2+} backup mechanism in *Plcz*$^{-/-}$ sperm represents *a gap in our knowledge* we propose to answer in this aim.

In this study, we investigated the possible backup mechanism of PLCZ1 by exploring the role of other sperm's PLCs. We generated PLCZ1 CRISPR KO animals and examined if other sperm PLCs were upregulated. We found that PLCD4 expression is markedly upregulated in these sperm and attains a greater footprint in the post-acrosomal region; other sperm PLCs remain unchanged or reduced. Significantly and necessary as a possible sperm factor, PLCD4 is also retained in the head of the sperm post-acrosome reaction, which does not happen in WT sperm. Based on these results, a double KO mouse line was created. These males were infertile and unable to produce offspring, and their sperm failed to initiate Ca^{2+} oscillations. Together, these results suggest that upregulated PLCD4 in *Plcz*$^{-/-}$ sperm is the backup molecule responsible for the residual oscillations and subfertility of *Plcz*$^{-/-}$ males. Similar studies should be conducted in other mammals to determine the full scope of the egg-activating signal in this species.

2.3 Results

2.3.1 Impact of CRISPR Deletion of PLCZ1 and PLCD4 on Mouse Fertility

Despite the well-established importance of Ca^{2+} in the fertilization process across various species, the precise molecular mechanisms that regulate its influx and release remain elusive. To better understand these mechanisms, we developed knockout (KO) mice lacking two prevalent enzymes in mouse sperm, namely PLCZ1, and PLCD4, which are key players in the phosphoinositide pathway and in generating 1,4,5-inositol trisphosphate (IP_3), a crucial signaling molecule that triggers Ca^{2+} release from the endoplasmic reticulum (ER) in all cells, and here from both, the sperm and egg. This Ca^{2+} release, in turn, participates in acrosome reaction in the sperm, and events of activation in eggs.

Utilizing CRISPR Cas9 technology, we targeted exon 3 in the *Plcz1* and *Plcd4* genes to generate KO mice (**Figure 5 A & B**). Confirmation of protein abrogation in the sperm of these KO animals was accomplished through immunoblot analysis, as depicted in **Figure 5C**, where expression of PLCZ1 (left panel) and PLCD4 (right panel) are absent in respective KOs.

To comprehensively evaluate the impact of *Plcz1* and *Plcd4* deletion on male fertility, we extended our investigations to generate double KO mice lacking both proteins, leveraging individual KO strains of *Plcz1* and *Plcd4* that were crossed to obtain the combined deletions. We analyzed the sperm parameters of all these animals utilizing computer-assisted sperm analysis (CASA) and immunohistochemistry (IHC); our analysis revealed no discernible alterations in sperm and testicular parameters of the null lines (data not shown). Noteworthy, these deletions did not manifest any discernible effects on female fertility, as evidenced by the unaltered reproductive capabilities of homozygous females (5.8 ± 2.6 n.s.). This observation underscores the male-specific nature of PLCZ1 and PLCD4, with negligible roles in females or other tissues. Furthermore, we rigorously

assessed over six months the impact of *Plcz1* and *Plcd4* deletions on mouse fertility by mating these KO males with both wild-type (WT) and KO females. As expected and reported by others ((Hachem et al., 2017b; Nozawa et al., 2018), *Plcz* KO males exhibited subfertility, producing average litter sizes of 2.5 ± 0.8 compared to 7.2 ± 1.8 pups for WT males and 4.2 ± 2.0 for heterozygous crosses (ZzDd), while double KO males were infertile **(Figure 5D)**, emphasizing the indispensable roles of PLCZ1 and PLCD4 in sperm fertilization.

PLCZ1 and PLCD4 are known to be localized to the acrosome of the sperm and PLCZ1 is also found in the equatorial or post-equatorial region ((Young et al., 2009). We use immunofluorescence to localize these proteins in WT sperm and confirmed the antibodies' specificity using the null lines. Using confocal microscopy, we demonstrate the localization of PLCZ1 to the acrosome and post-equatorial regions **(Figure 6A),** whereas the localization of PLCD4 was restricted to the acrosome, which is consistent with results from our laboratories and those of others **(Figure 6B)** (Fukami et al., 2001). However, to delve deeper into the subcellular localization of PLCZ1 and PLCD4, we employed advanced high-resolution techniques. Our findings unequivocally confirmed the presence of PLCZ1 outside the outer acrosomal membrane (OAM) **(Figure 6C)** and PLCD4 seemingly within or partly overlapping with the inner and outer acrosomal membranes, IAM and OAM, respectively; the acrosomal membranes were unveiled using the peanut agglutinin (PNA) lectin **(Figure 6D)**, which is a common reagent widely used in the literature to localize this organelle (Cheng et al., 1996). These distinct localization patterns underscore the divergent functionalities of these proteins, with PLCZ1 serving as a pivotal

sperm factor orchestrating egg activation post-fertilization, while PLCD4 plays a pivotal role in the acrosome reaction.

2.3.2 Impact of PLCZ1 and PLCD4 Deletion on Fertilization-Induced Calcium Oscillations

Initially, it was thought that PLCZ1, a sperm-specific enzyme, was the exclusive trigger of the Ca^{2+} oscillations essential for fertilization. Mutations in *Plcz1* have been associated with infertility in humans (references). We predicted that deleting *Plcz1* gene would seriously diminish the Ca^{2+} oscillations of fertilization but not abolish them, as reported previously by Nozawa et al., (2018) and to a lesser extent by Hachem et al., (2017). These studies showed the deletion of *Plcz1* causes subfertility and leaves a few residual Ca^{2+} rises. To confirm this in our KO model, we fertilized eggs with sperm lacking *Plcz1* and monitored Ca^{2+}oscillations. We found that although the Ca^{2+} oscillations did occur, they were delayed and significantly reduced compared to normal sperm, similar to what was reported by Nozawa et al **(Figure 7A**, left two panels**)**.

The Ca^{2+} rises triggered by PLCZ1 were thought to be involved in preventing polyspermy, the entry of multiple sperm into an egg, by mechanism(s) not yet clearly defined, but suggested to include among others the "zinc sparks", which are the release of zinc in the from the cortical granules (Kim et al., 2011). In the absence of PLCZ1 and delayed Ca^{2+} oscillations, there is no effective block against polyspermy. Interestingly, we observed that the frequency of Ca^{2+} oscillations from sperm lacking PLCZ1 increased with the number of sperm penetrations (**Figure 7A,** right two panels), suggesting that the expression of this backup mechanism in the null sperm.

We also examined the ability of *Plcz1* null sperm to initiate Ca^{2+}oscillations after intracytoplasmic sperm injection (ICSI), as other groups had reportedly shown the inability of these sperm to induce oscillations following ICSI (References). Consistent with previous results, we noted that sperm lacking PLCZ1 failed to induce Ca^{2+} oscillations (**Figure 7B**). We also found following *in vitro* fertilization *Plcz1*-null fertilized zygotes resulted in reduced rates of blastocyst formation, with only 20% of fertilized embryos reaching the blastocyst stage (**Table 2**). This data implies that the few Ca^{2+} rises induced *Plcz1*$^{-/-}$ sperm can support reduced development, possibly due to the delayed oscillations and polyspermy. However, the molecular mechanism(s) that supports the residual Ca^{2+} oscillations is still unclear.

The second most abundant PLC enzyme in sperm is PLCD4. When we deleted *Plcd4* and monitored the Ca^{2+} responses, we observed two different patterns of Ca^{2+} oscillations, one with reduced frequency and the other with normal frequency as WT (**Figure 7C)**. The initiation of oscillations was always delayed, potentially because of the role of PLCD4 in the acrosome reaction (Fukami et al., 2001). Hence, *Plcd4*$^{-/-}$ sperm have difficulty penetrating. We performed ICSI to bypass the delay in sperm penetration and monitored Ca^{2+} oscillations. We observed *Plcd4*$^{-/-}$ induced Ca^{2+} responses displayed lower frequency and amplitude than WT sperm **(Figure 7D)**. This data showed that *Plcd4*$^{-/-}$ sperm can initiate Ca^{2+} oscillations, although the oscillations are not identical to those of WT sperm. However, the results suggest that PLCD4 may have a role in fertilization-induced Ca^{2+} oscillations in the mouse.

2.3.3 PLCD4 is upregulated in the Plcz1-null sperm and is retained in the sperm head after the post-acrosome reaction.

There are various phospholipase Cs (PLC) in mouse sperm that can potentially act as a backup mechanism for PLCZ1. Among these, PLCD4 stands out as the second most abundant protein in mouse sperm. We investigated the expression level of PLCD4 in *Plcz1*$^{-/-}$ sperm using immunoblotting and immunofluorescence microscopy. We found a significant upregulation of PLCD4 in *Plcz1* null sperm (**Figure 8A & B).** Additionally, immunofluorescence analysis confirmed the increased expression of PLCD4 in *Plcz1*$^{-/-}$ sperm as it displayed increased intensity and a wider signal distribution (arrow, lower panel) in comparison to WT sperm (arrow, lower panel). (**Figure 8C).**

We also scrutinized the expression levels of other PLCs present in sperm. We performed immunoblotting for PLCβ3 and PLCγ2, which are also expressed in sperm ((Fukami et al., 2001). Neither of these PLCs was upregulated, and, in fact, were downregulated in *Plcz1* (**Figure 8D & E).** These findings raise the possibility that PLCD4 may function as a backup molecule for PLCZ1.

During the acquisition of fertilizing ability, the sperm undergo capacitation followed by the acrosome reaction. During these processes, PLCs undergo re-location and achieve different distributions in acrosome-reacted sperm more suited for fertilization. During the acrosome reaction, PLCZ1 re-localizes strongly to the equatorial and post-equatorial regions, consistent with its delivery into the ooplasm post-fusion; PLCD4 is largely released from the acrosome-reacted sperm and its signal largely disappears from the sperm once the acrosome is shed.

The above results represented a challenge as if PLCD4 indeed serves as a backup molecule in the absence of PLCZ1, it should remain in the sperm head after the acrosome reaction. To investigate this, we induced the acrosome reaction in capacitated sperm using progesterone and monitored the localization of PLCZ1 and PLCD4 using immunofluorescence. In WT and *Plcd4*$^{-/-}$ non-capacitated sperm, PLCZ1 localized to both acrosome (arrow) and equatorial region (arrowhead), as expected (**Figure 9A,** upper and lower panel), whereas in acrosome reacted WT and *Plcd4*$^{-/-}$sperm, PLCZ1 re-localized to the post equatorial region (arrowhead). (**Figure 9B**, upper and lower panel**),** suggesting there is no effect of the deletion of Plcd4 in the redistribution of PLCZ1. In contrast, while in WT and *Plcz1*$^{-/-}$ non-capacitated sperm, acrosome-reacted WT lost PLCD4, as expected and reported ((Fukami et al., 2001), whereas in *Plcz1*$^{-/-}$ sperm, PLCD4 re-localized to the post acrosome region and it was retained (arrow). (**Figure 9C,** upper and lower panel) (**Figure 9D,** upper and lower panel**).** This suggests that not only does PLCD4 undergo upregulation, but it also undergoes relocation post-acrosome reaction in the absence of PLCZ and could serve as the backup Ca^{2+} signaling mechanism.

2.3.4 Deletion of Both PLCZ1 Abrogates Sperm's Ability to Generate Calcium Oscillations

To investigate whether residual PLCD4 in *Plcz1*$^{-/-}$ KO sperm plays a role in generating residual Ca^{2+} oscillations, we examined fertilization-induced Ca^{2+} oscillations in zzdd DKO sperm. Surprisingly, when both PLCs were deleted, the sperm mostly lost their ability to generate Ca^{2+} oscillations (**Figure 10A).** Only a few oocytes showed a single Ca^{2+} rise following fertilization with DKO sperm, but with a significantly reduced amplitude, which was inadequate to activate the egg. (**Figure 10A,** right panel).

During decondensation of the sperm head once in the ooplasm, sperm undergo a turnover of protamines that are replaced with histones. We utilized this exchange process to determine the penetration rates of the zzdd sperm and ensure that fertilization was achieved. We injected eggs with histone-2B (H2B) mRNA labeled with GFP to track sperm head penetration and decondensation. (**Figure 10B,** Green, H2B; F-female, pink arrow; M-male, blue arrow**).** After monitoring Ca^{2+} levels, we assessed all eggs for sperm penetration. Interestingly, approximately 53% of sperm failed to fertilize the eggs. Among those 46% fertilized, 21% showed monospermic fertilization, while 25% displayed polyspermic fertilization **(Figure 10B).** Upon analyzing fertilized oocytes for Ca^{2+} rise, only 47% of monospermic and 37.5% of polyspermic oocytes exhibited a single rise in (**Figure 10C**). This indicates that although zzdd sperm managed to successfully penetrate the eggs, they could not initiate Ca^{2+} oscillations. Subsequent IVF experiments and embryo development revealed that these sperm failed to activate the eggs and the embryo development (**Table 2**), further underscoring that the abnormal single Ca^{2+} rise observed in a significantly lower number of eggs was insufficient to activate them.

2.3.5 Higher Concentrations of Plcd4 mRNAs are required to Generate Ca^{2+} Oscillations.

Our results here strongly suggest that PLCD4 may serve as the backup mechanism of oscillations in the mouse and that its potential to initiate Ca^{2+} oscillations has been overlooked. To explore this further, we investigated whether PLCD4 alone could initiate the Ca^{2+} oscillations. For this, we microinjected varying concentrations of Plcz1 and Plcd4 mRNAs into eggs and observed the ensuing Ca^{2+} oscillations. Remarkably, we found that a concentration of 0.01µg/µl of *Plcz1* mRNA was adequate to induce Ca^{2+} oscillations

reminiscent of those seen during fertilization **(Figure 11A)**. Conversely, higher concentrations (ranging from 0.05-0.1µg/µL) of *Plcd4* mRNA were required to elicit similar Ca^{2+} oscillations **(Figure 11B)**.

This represents the first demonstration that *Plcd4* possesses the capacity to induce Ca^{2+} oscillations. However, these oscillations exhibited delayed onset and marked reduced frequency compared to typical fertilization-induced Ca^{2+} oscillations or those induced by *Plcz1* mRNA. Notably, the Ca^{2+} oscillations initiated by *Plcd4* mRNA were characterized by irregular spikes spaced out by almost one hour **(Figure 11B),** which is much longer than the 20-minute responses induced by *Plcz1* mRNA **(Figure 11A)**.

The atypical nature of these oscillations induced by *Plcd4* mRNA suggests that while *Plcd4* can indeed trigger Ca^{2+} oscillations, it does so at substantially higher concentrations than *Plcz1* mRNA. Furthermore, the observed oscillations with *Plcd4* mRNA deviate significantly from the conventional Ca^{2+} oscillations observed during fertilization. Hence, it is plausible that PLCD4 may not function as the primary sperm factor but rather compensates for the absence of PLCZ1 to some extent by increasing expression levels, which is the case for *Plcz1*$^{-/-}$ sperm.

2.4 Discussion

The elucidation of the precise signaling molecule(s) responsible for triggering egg activation remains a significant challenge in reproductive biology, despite extensive research efforts spanning various species. However, a pivotal advancement in this area was achieved within mammals with the discovery of phospholipase Cζ (PLCζ).(Saunders et al., 2002) PLCζ, an enzyme predominantly expressed in the testes, emerged as a key player due to its association with fractions of sperm extracts exhibiting Ca^{2+} activity. (Hachem et

al., 2017b) Remarkably, injection of PLCζ mRNA induced Ca^{2+} oscillations reminiscent of those occurring during fertilization, underscoring its pivotal role in this fundamental reproductive event. Subsequent investigations confirmed the widespread presence of PLCζ across mammalian species, with localization primarily to the equatorial/subacrosomal region of the sperm head, aligning with its function as the initiator of Ca^{2+} oscillations crucial for fertilization.

The pivotal association of PLCζ expression with fertility was firmly established in humans, with individuals displaying defective expression or mutations in PLCζ presenting infertility issues, that cannot be bypassed by intracytoplasmic sperm injection (ICSI)(Hachem et al., 2017b). Surprisingly, studies in mice revealed that males lacking PLCζ exhibited subfertility alongside aberrant and delayed Ca^{2+} responses(Hachem et al., 2017b; Nozawa et al., 2018). However, the identity of the molecule(s) responsible for inducing oscillations in PLCζ-deficient males, serving as a backup system, remains a critical knowledge gap that necessitates further exploration.

Multiple mechanisms have been proposed for generating Ca^{2+} oscillations in mouse eggs, including pathways independent of inositol trisphosphate (IP_3) production, such as the use of thimerosal and $SrCl_2$, albeit with inherent toxicity concerns. The sperm could induce oscillations in eggs by those mechanisms, however, it is unlikely to have the capacity to deliver the concentrations required to induce the delayed oscillations observed in *Plcz1* null males. Other hypothesized mechanisms involve molecules like NAADP, cADPR, PAWP, or citrate synthase proteins derived from sperm, but also these have failed to replicate fertilization-like Ca^{2+} oscillations (Kang et al., 2020). Although mouse eggs possess the capability to produce IP_3 through the stimulation of their own phospholipase C

(PLC) enzymes, and their stimulation results inCa^{2+} oscillations, the pattern of oscillations is unlike those observed during fertilization, indicating that this might not represent the acting mechanism. Lastly, another potential mechanism might be offered by other PLC isoforms expressed in sperm that might serve as backup systems for PLCζ.

In our current investigation, we generated *Plcz* KO mice using CRISPR technology, demonstrating that *Plcz*-deficient sperm not only exhibit reduced residual Ca^{2+} oscillations but also necessitate higher concentrations of the putative backup molecule(s) for generating repetitive, prolonged Ca^{2+} oscillations, that increased with increase in number of penetrated *Plcz*$^{-/-}$ sperm. Notably, we observed upregulation of PLCδ4 expression in the absence of PLCζ, suggesting a compensatory role. PLCδ4, abundantly expressed in the testes and sperm, primarily localizes to the acrosome, where it regulates the acrosome reaction crucial for sperm-egg fusion. Our findings indicate that *Plcz*-null sperm retained the expression of PLCD4 post-acrosome reaction, underscoring its potential role as the backup molecule of PLCZ1.

Plcd4 is an essential sperm protein present in the exocytotic vesicles of the acrosome and released during the acrosome reaction before the fusion of the sperm to the egg. *Plcδ4*- null males are infertile even after mating with WT females. PLCδ4, splice variant II, is abundantly expressed in the testes and sperm of mice and rats. (Fukami et al., 2001)(Fukami et al., 2003). *Plcδ4* null sperm have impaired acrosome reaction, which affects the fertilization and egg activation event. In this study we showed that *Plcd4* KO sperm displayed unaffected expression and localization of PLCZ1, suggesting mounting normal Ca^{2+} oscillations once penetrated. However, when we analyzed the Ca^{2+} oscillation post-ICSI, we found an abnormal pattern of oscillations compared to Ca^{2+} oscillations

induced by WT sperm, suggesting PLCD4 could participate in the generation of fertilization oscillations.

To investigate whether PLCδ4 serves as the backup molecule for PLCζ, we examined double knockout (DKO) mice lacking both proteins. Our findings revealed that DKO mice were sterile and unable to generate Ca^{2+} oscillations or activate eggs. Interestingly, DKO sperm could penetrate eggs following an induced acrosome reaction with an adequate concentration of progesterone. However, even when performing ICSI with DKO sperm, the absence of Ca^{2+} oscillations persisted, indicating the absence of compensatory molecules in the DKO. These results strongly implicate PLCδ4 and PLCζ as the crucial factors in sperm-mediated egg activation. Whether these proteins function independently warrants further investigation. Additionally, our study demonstrated that while *Plc*ζ mRNA injection induced Ca^{2+} oscillations at lower concentrations, *Plc*δ4 mRNA required significantly higher concentrations and produced non-conventional oscillations. This raises questions about PLCδ4's functional capacity in isolation and its ability to activate eggs. Further research is necessary to elucidate the interdependence of these proteins, their localization within eggs, downstream targets, and their presence in other species to determine if alternative backup molecules exist.

In summary, our study underscores the essential roles of PLCζ and PLCδ4 as key sperm factors in fertilization and egg activation. Future investigations are warranted to delineate the interplay between these proteins and determine their individual and cooperative functionalities. Additionally, exploring the downstream targets and destinations of PLCζ and PLCδ4 within eggs will provide further insights into their mechanisms of action. Comparative studies across species may also elucidate species-

specific mechanisms or identify alternative backup molecules for PLCζ, contributing to a deeper understanding of fertilization and potential therapeutic avenues for infertility.

2.6 Figures

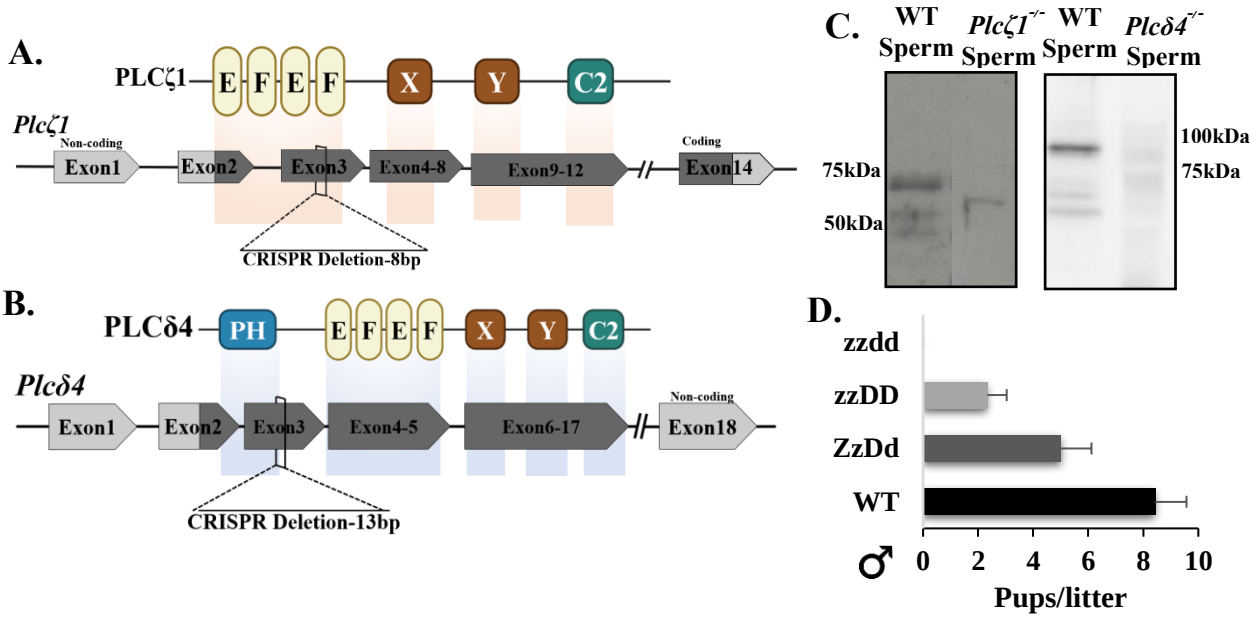

Figure 5. Schematic of knock out allele generation of **A.** *Plcζ1* and **B.** *Plcδ4* using CRISPR Cas9 technology. Exon 3 is targeted for the generation of KO animals which stalls the formation of respective proteins. Protein structure is upper panel, depicting respective exons. **C.** Western blot demonstrating the abrogation of the proteins PLCζ1 and PLCδ4 in their respective KO, whereas WT has reactivity, confirming the deletion of the gene. $1x10^6$ sperm are loaded in each lane. n=3. **D.** Bar graph depicting the pups per litter for WT, ZzDd, zzDD, and zzdd. There is significant reduction in pups/litter in ZzDD and zzDD in comparison to WT, whereas zzdd are infertile. Six pairs monitor for 6 months for fertility. * $p<0.05$, ***$p<0.001$, ‡ invalid comparison. One way ANOVA.

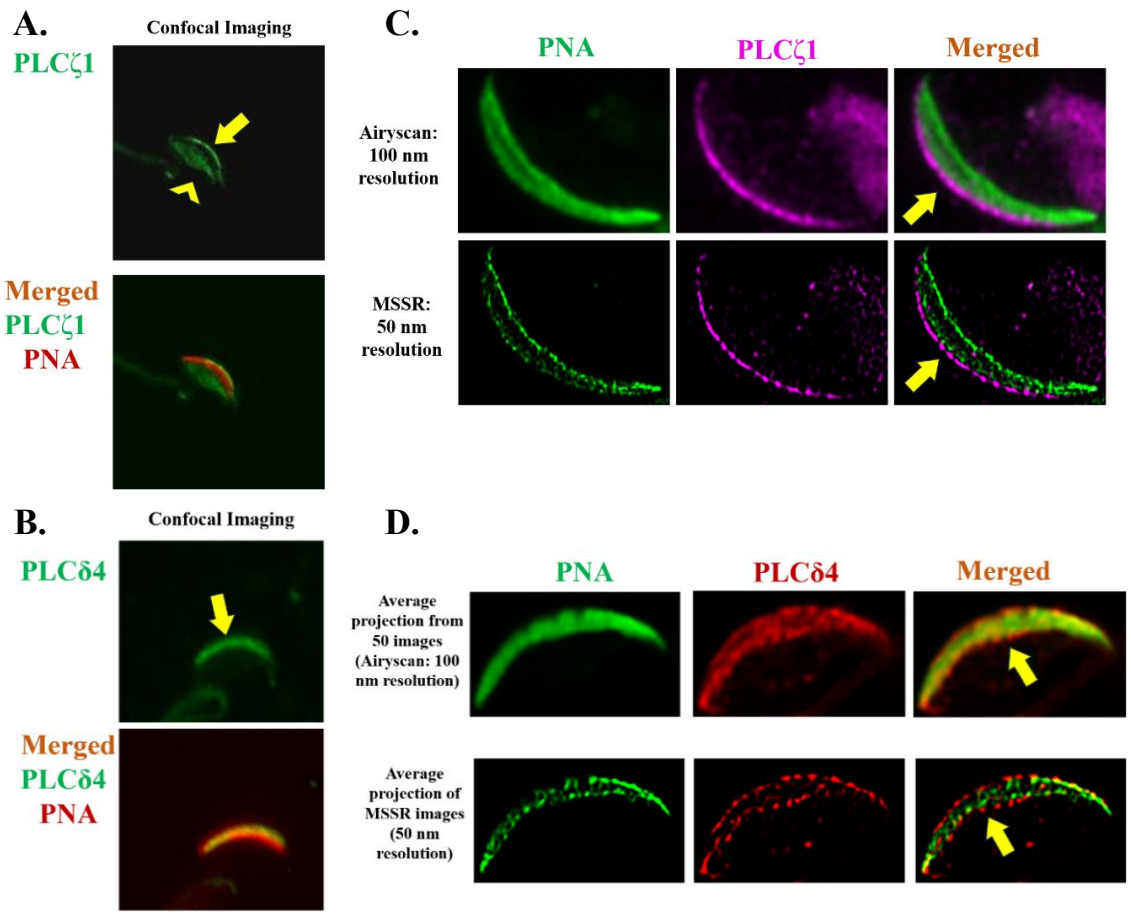

Figure 6. Localization of PLCζ1 **(A, C)** and PLCδ4 **(B, D)** in the WT sperm. **A.** Confocal imaging to demonstrate the localization of PLCζ1 in the acrosome (arrow) and post equatorial region (arrowhead) of the sperm. PLCζ1, green; PNA, red. **B.** Confocal imaging to demonstrate the localization of PLCδ4 in the acrosome of the sperm (arrow). PLCδ4, green; PNA, red. **C & D** Higher resolution images of sperm to demonstrate the localization of PLCζ1 outside acrosome (OAM, upper two panels, PLCζ1, pink; PNA, green) whereas PLCδ4 is in the acrosome (lower two panels, PLCδ4, pink; PNA, green). n=50

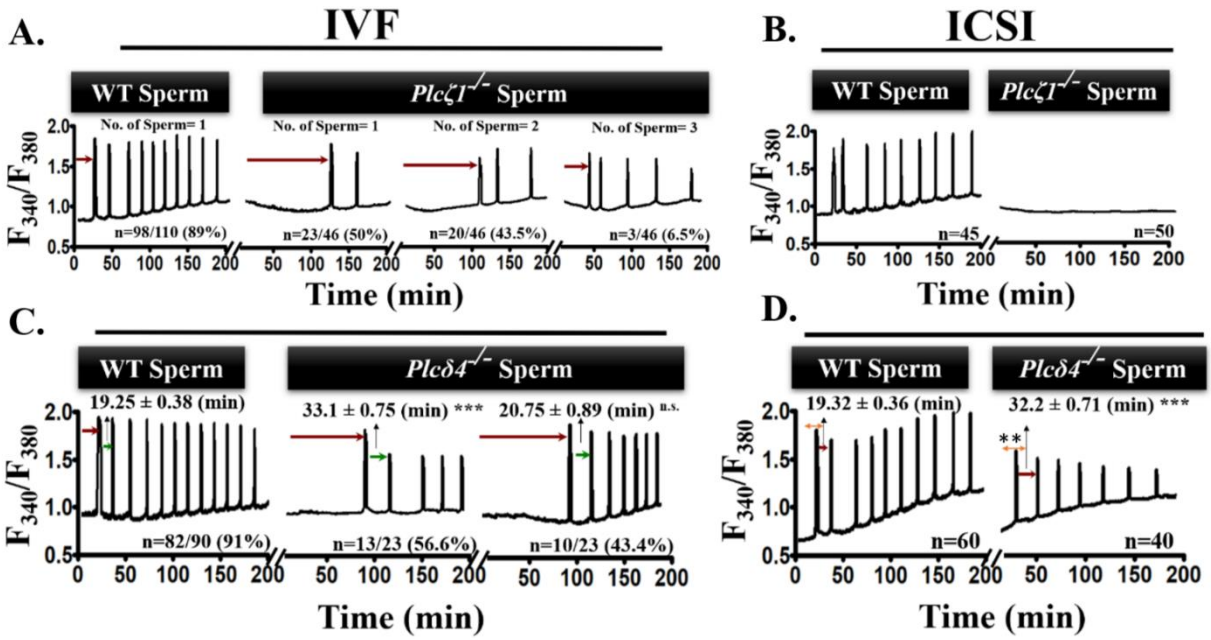

Figure 7. Fertilization induced Ca^{2+} oscillations in *Plcζ1*$^{-/-}$ **(A, B)** and *Plcδ4*$^{-/-}$ **(C, D)** sperm. **A.** Ca^{2+} oscillations during in vitro fertilization with WT sperm (left panel) and with *Plcζ1*$^{-/-}$ sperm (middle three panels). The frequency of oscillations in *Plcζ1*$^{-/-}$ sperm increase with increase in number of sperm. The oscillations by *Plcζ1*$^{-/-}$ sperm are delayed and less frequent than WT. **B.** Ca^{2+} oscillations after ICSI with WT sperm, (left panel) and *Plcζ1*$^{-/-}$ sperm (right panel). *Plcζ1*$^{-/-}$ sperm failed to induce any Ca^{2+} oscillations. **C.** Ca^{2+} oscillations during in vitro fertilization with WT sperm (left panel) and with *Plcδ4*$^{-/-}$ sperm (middle three panels). The oscillation by *Plcδ4*$^{-/-}$ sperm demonstrated two different patterns (middle two panels). **D.** Ca^{2+} oscillations after ICSI with WT sperm, (left panel) and *Plcδ4*$^{-/-}$ sperm (right panel). *Plcδ4*$^{-/-}$ sperm demonstrated abnormal oscillations with lower amplitude and frequency. Number of sperm is shown at top of each panel. n, number of oocytes monitored, is shown at the bottom of each graph. n.s., non-significant. **p<0.01, ***p<0.001. Student t-test.

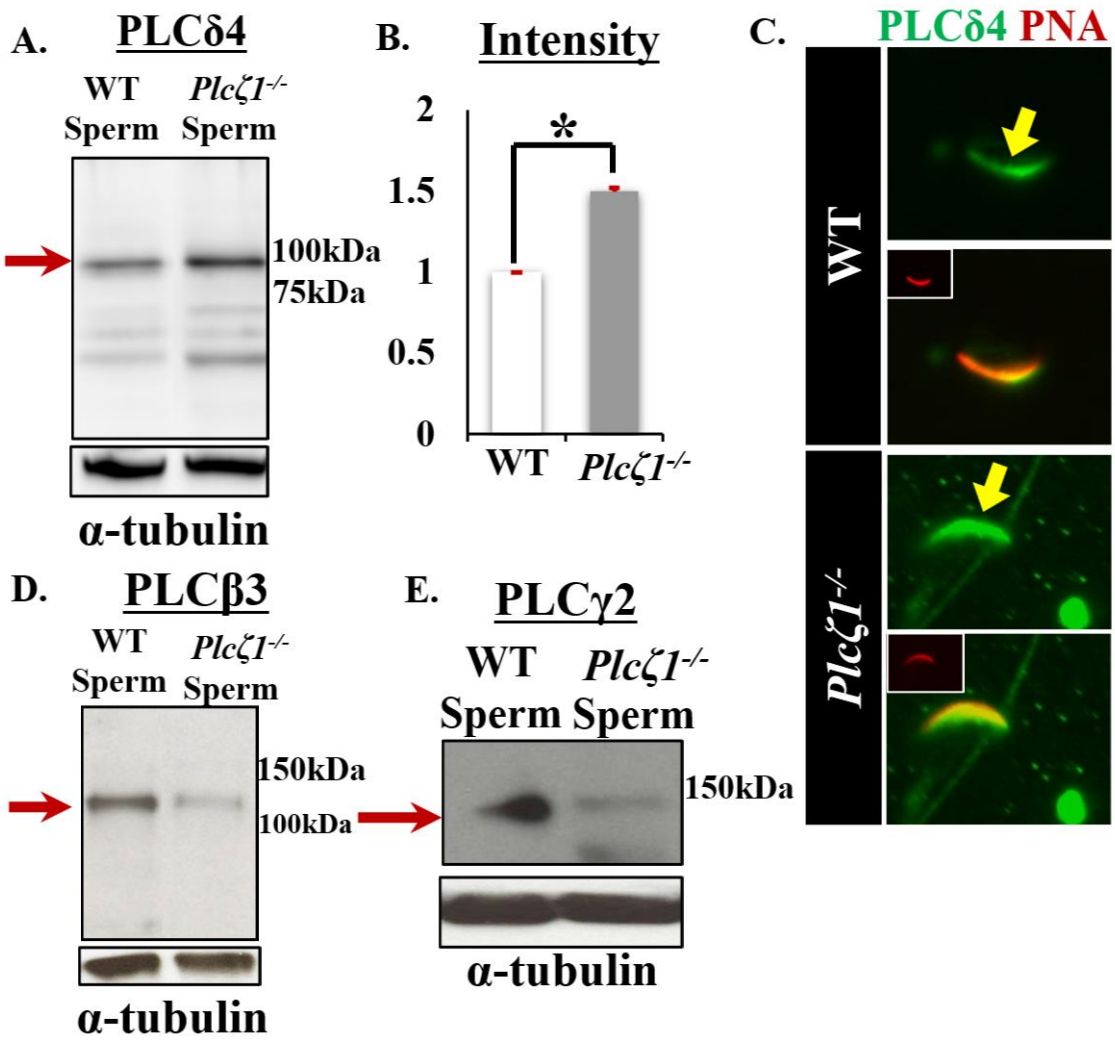
A.
PLCδ4
WT Sperm
Plcζ1-/- Sperm
100kDa
75kDa
α-tubulin
B.
Intensity
2
1.5
1
0.5
0
*
WT
Plcζ1-/-
C.
PLCδ4 PNA
WT
Plcζ1-/-
D.
PLCβ3
WT Sperm
Plcζ1-/- Sperm
150kDa
100kDa
α-tubulin
E.
PLCγ2
WT Sperm
Plcζ1-/- Sperm
150kDa
α-tubulin

Figure 8. Expression of different PLCs in *Plcζ1*$^{-/-}$ sperm. **A.** Western blot showing expression of PLCδ4 in WT and *Plcζ1*$^{-/-}$ sperm. **B.** Intensity of the PLCδ4 band was quantified and it showed significant increase in the expression of PLCδ4 in *Plcζ1*$^{-/-}$ sperm. **C.** Immunofluorescence showing PLCδ4 localization in WT sperm (arrow, upper panel) and *Plcζ1*$^{-/-}$ sperm (arrow, lower panel). PLCδ4 is upregulated and relocalized to the post acrosome region. Green, PLCδ4; red, PNA. **D & E.** Expression of PLCβ3 and PLCγ2 is shown using western blot. There is no significant upregulation of these proteins in *Plcζ1*$^{-/-}$ sperm. n=3. *$p<0.05$. Student t-test.

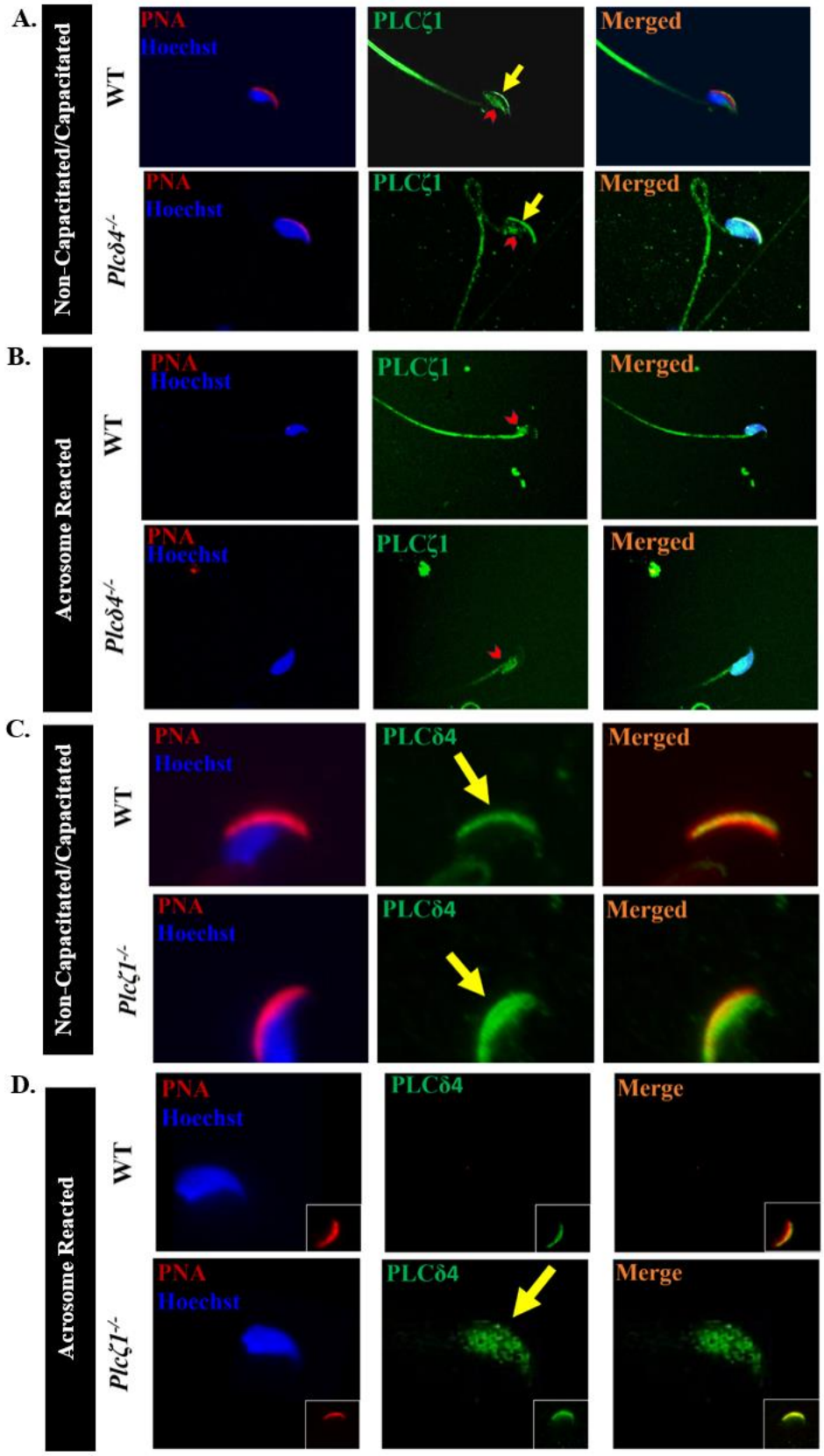
A.
Non-Capacitated/Capacitated
WT
Plcδ4-/-
PNA
Hoechst
PLCζ1
Merged
B.
Acrosome Reacted
WT
Plcδ4-/-
PNA
Hoechst
PLCζ1
Merged
C.
Non-Capacitated/Capacitated
WT
Plcζ1-/-
PNA
Hoechst
PLCδ4
Merged
D.
Acrosome Reacted
WT
Plcζ1-/-
PNA
Hoechst
PLCδ4
Merge

Figure 9. Acrosome reacted sperm display different localization of PLCs. **A.** Localization of PLCζ1 in non-capacitated and capacitated WT and *Plcδ4*$^{-/-}$ sperm (upper and lower panel respectively). **B.** Localization of PLCζ1 in acrosome reacted sperm induced by progesterone in WT and *Plcδ4*$^{-/-}$ sperm (upper and lower panel respectively). PLCζ1 redistributed to post equatorial region in both WT and *Plcδ4*$^{-/-}$ acrosome reacted sperm. PNA, red; DNA, blue; and PLCζ1, green. **C.** Localization of PLCδ4 in non-capacitated and capacitated WT and *Plcζ1*$^{-/-}$ sperm (upper and lower panel respectively). **D.** Localization of PLCδ4 in acrosome reacted sperm induced by progesterone in WT and *Plcζ1*$^{-/-}$ sperm (upper and lower panel respectively). All the WT acrosome reacted sperm display no expression of PLCδ4, whereas *Plcζ1*$^{-/-}$ acrosome reacted sperm displayed residual PLCδ4 protein in the head of the sperm. PNA, red; DNA, blue; and PLCδ4, green. n=50

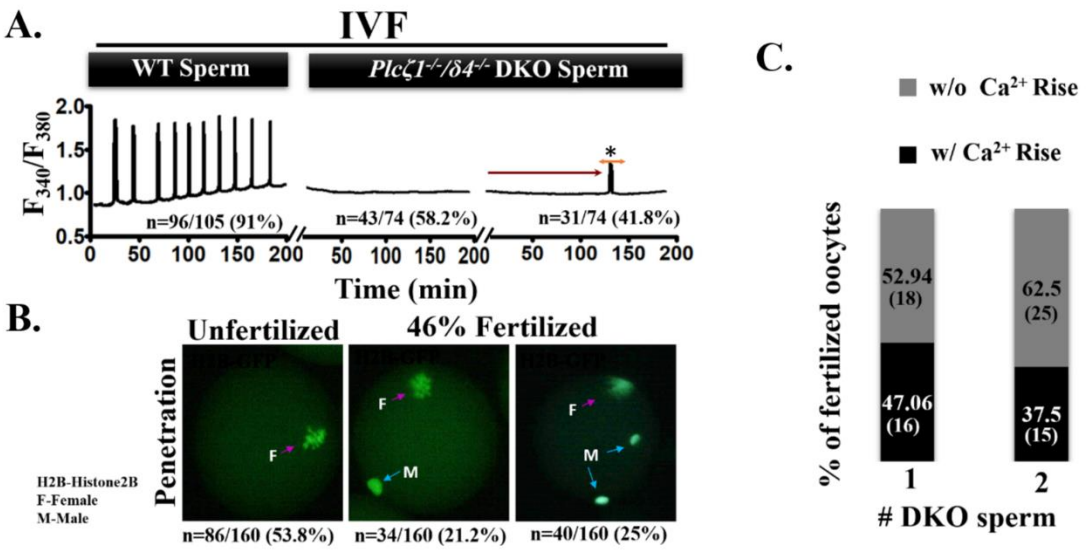

Figure 10. Fertilization induced Ca^{2+} oscillations in *Plcζ1*$^{-/-}$/*δ4*$^{-/-}$DKO **A.** Ca^{2+} oscillations during in vitro fertilization with WT sperm (left panel) and with *Plcζ1*$^{-/-}$/*δ4*$^{-/-}$ DKO sperm (right two panels). Deletion of both the PLCs abrogates the ability to generate Ca^{2+} oscillations. 41% of the oocyte displayed on abnormal single rise. **B.** H2B, green, displaying the penetration of the sperm. 46% of the oocytes fertilized with 21% monospermic (middle panel) and 25% polyspermic (right panel). Pink arrow, female, oocyte spindle; blue arrow, penetrated sperm. **C.** Bar graph showing % of oocytes that had 1 or 2 sperm are with (w/) or without(w/o) Ca^{2+} rise. 52% and 62% of monospermic and polyspermic respectively are without Ca^{2+} rise. n, number of oocytes monitored, is shown at the bottom of each graph. n.s., non-significant. *p<0.05. Student t-test.

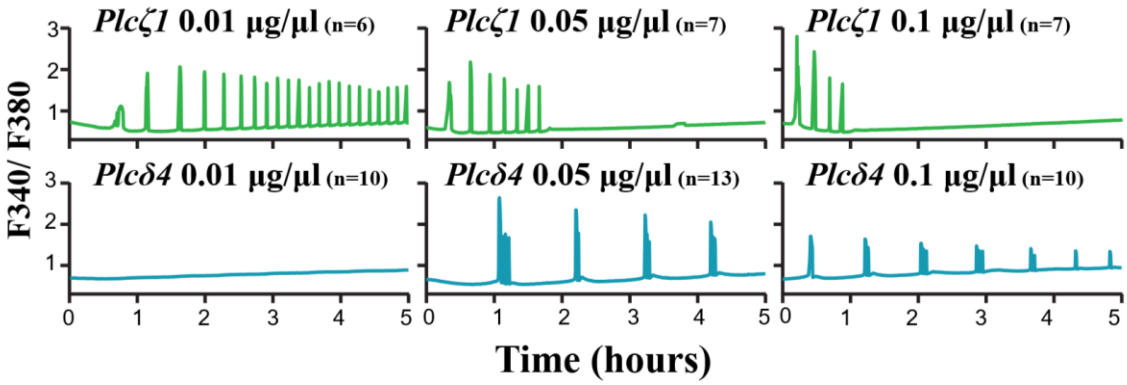

Figure 11. Ca^{2+} oscillations with *Plcζ1* and *Plcδ4* mRNA, upper and lower panels respectively. Different concentration of mRNA showed different pattern of Ca^{2+} oscillations. Lower concentration of *Plcζ1* mRNA displayed continuous and long lasting Ca^{2+} oscillations, mimicking fertilization. Whereas *Plcδ4* mRNA required in higher concentration to induce Ca^{2+} oscillations. However, they are reduced in frequency and has different patter than fertilization induced Ca^{2+} oscillations. n, number of oocytes monitored, is shown at the top of each graph.

Table 2. In vitro fertilization and embryo development

Genotype	Fertilized/N	2C	4C	8C	Morula	Bls
WT	**98/110 (89.09%)**	**90/98 (91.8%)**	**88/98 (89.8%)**	**88/98 (89.8%)**	**85/98 (86.7%)**	**85/98 (86.7%)**
ZzDd	**65/100 (65%)**	**40/65 (61.5%)**	**38/65 (58.5%)**	**35/65 (53.8%)**	**35/65 (53.8%)**	**35/65 (53.8%)**
zzDD	**60/105 (57.14%)**	**15/60 (25%)**	**14/60 (23.3%)**	**14/60 (23.3%)**	**13/60 (21.7%)**	**13/60 (21.7%)**
ZZdd	**59/112 (52.68%)**	**22/59 (37.3%)**	**20/59 (33.9%)**	**20/59 (33.9%)**	**18/59 (30.5%)**	**18/59 (30.5%)**
zzdd	**49/120 (40.83%)**	**0**	**0**	**0**	**0**	**0**

CHAPTER 3

TRPM7 IS ESSENTIAL FOR MG^{2+} HOMEOSTASIS AND MOUSE EMBRYO DEVELOPMENT

(Published: Cell Rep. 2023 Oct 31;42(10):113232. doi: 10.1016/j.celrep.2023.113232. Epub 2023 Oct 11.)

3.1 Abstract

TRPM7 (transient receptor potential cation channel subfamily M member 7) is a chanzyme with channel and kinase domains essential for embryo development. Using gamete-specific *Trpm7*-null lines, we report that TRPM7-mediated Mg^{2+} influx is indispensable for reaching the blastocyst stage. TRPM7 is expressed dynamically from gametes to blastocysts, displays stage-specific localization on the plasma membrane, cytoplasm, and nucleus, and undergoes cleavage that produces C-terminal kinase fragments. TRPM7 underpins Mg^{2+} homeostasis, and excess Mg^{2+} but not Zn^{2+} or Ca^{2+} overcomes the arrest of *Trpm7-null* embryos; expressing *Trpm7 mRNA restores development, but mutant versions fail or partially rescue*. Transcriptomic analyses of *Trpm7-null* embryos reveal an abundance of oxidative stress-pathway genes, confirmed by mitochondrial dysfunction, and a reduction of transcription factor networks essential for proliferation; Mg^{2+} supplementation corrects these defects. Hence, TRPM7 underpins Mg^{2+} homeostasis in preimplantation embryos, prevents oxidative stress, and promotes gene expression patterns necessary for developmental progression and cell lineage specification.

3.2 Introduction

Divalent cations play essential functions in fertilization and early embryo development, including events associated with egg activation, implantation, and gastrulation(Komiya et al., 2014; Krauchunas & Wolfner, 2013; Stein et al., 2020; Wozniak & Carlson, 2020). The role of calcium (Ca^{2+}) in egg activation is universal, but the pattern of Ca^{2+} release changes across species. In mammals, the signal consists of repeated, brief rises in intracellular concentration lasting for several hours (h) and is known as Ca^{2+} oscillations(Stein et al., 2020; Stricker, 1999; Wakai & Fissore, 2019). The realization that Zn^{2+} contributes to fertilization is more recent, and the full scope of its effects remains incomplete(Kim et al., 2011; Kim et al., 2010). Zn^{2+} undergoes exocytosis during fertilization, generating the Zn^{2+} sparks, and participates in the molecular control of meiosis exit post-fertilization and the polyspermy block(Burkart et al., 2012; Suzuki et al., 2010; Tokuhiro & Dean, 2018). Lastly, the precise role of Mg^{2+} in early development is unknown, despite the content of extracellular Mg^{2+} influencing the periodicity of Ca^{2+} oscillations and impacting embryo development(Bernhardt et al., 2018; Ozil et al., 2017). Thus, divalent cations play essential roles in the initiation and progression of embryo development.

Gametes and embryos uptake divalent cations from their environment using multiple specific and non-specific plasma membrane (PM) channels and transporters that remain incompletely characterized. Mammalian eggs and embryos express a complete Ca^{2+} toolkit(Stein et al., 2020; Wakai et al., 2011), but the molecules mediating Ca^{2+} influx have been investigated only in mouse eggs and early embryos (Carvacho et al., 2016). Mouse eggs functionally express three Ca^{2+}-permeating channels, $Ca_V3.2$, a T-type voltage-gated

channel (*Canah1h*)(Bernhardt et al., 2015; Peres, 1987), and two transient receptor potential (TRP) family members, vanilloid-3(Carvacho et al., 2013) and melastatin-7 (TRPV3 and TRPM7, respectively)(Bernhardt et al., 2017; Carvacho et al., 2016). Eggs null for any of these channels (conditional knockout (cKO) for *Trpm7*) mount somewhat altered Ca^{2+} responses after fertilization, and if paired with WT males, KO females display varying degrees of subfertility. *Trpv3*- or *Cacna1h*-null females are subfertile even after homozygous mating or combined deletion(Mehregan et al., 2021), contrasting with the early development arrest caused by the homozygous deletion of *Trpm7*(Jin et al., 2008). A host of members of the solute carrier family 39 (*Slc39a1-14 or Zip1-14*) and family 30 (*Slc30a1-10 or ZnT1-10*) combine in a cell-specific manner to control the intracellular levels of Zn^{2+} (Kambe et al., 2015; Lichten & Cousins, 2009). However, their assortment and role in early development are untested. Oocytes highly express *Zip6* and *Zip10*(Kong et al., 2014) and embryos *Zip4*(Dufner-Beattie et al., 2007), but thus far, only homozygous deletion of *Zip4* causes embryonic death by mid-gestation (for review, see(Dufner-Beattie et al., 2007; Hara et al., 2022)). Several molecular transporters and buffering systems regulate the concentrations of free basal Mg^{2+} (~mM) in somatic cells(Romani, 2011). However, hitherto, only genetic deletion of TRPM6 and TRPM7, which also conduct Mg^{2+}, impairs fertility and causes early embryonic death(Chubanov et al., 2016; Jin et al., 2008; Jin et al., 2012; Schütz et al., 2021). TRPM7 is notable among all the mentioned channels because of its widespread expression and permeability to Zn^{2+}, Mg^{2+}, and, to a lesser extent, Ca^{2+}(Li et al., 2006; Monteilh-Zoller et al., 2003; Nadler et al., 2001). It is unknown if the absence of TRPM7 affects the transport of a combination of these cations in gametes and zygotes.

TRPM7 is a unique bifunctional molecule that, besides the channel domain, is outfitted on its intracellular-C-terminal end with an active α-type serine-threonine kinase(Schmitz et al., 2003). It is a cationic, non-selective channel with a permeability sequence favoring divalent cations that physiologically supports small inward currents(Monteilh-Zoller et al., 2003; Nadler et al., 2001). TRPM7 forms active homomeric complexes and undergoes cleavage in a cell type-specific manner that releases a C-terminal kinase (C-kinase) capable of nuclear translocation and histone phosphorylation(Krapivinsky et al., 2014). Whether this occurs in gametes and embryos is unknown. The function of TRPM7 is essential for embryogenesis. TRPM7 ablation causes developmental arrest before embryonic day 7 (ED 7)(Jin et al., 2008; Jin et al., 2012), and a recent investigation found earlier demise of KO embryos, ED 5, and failure of trophectoderm differentiation and implantation(Schütz et al., 2021). Neither study pinpointed the underlying molecular mechanism(s). Remarkably, the *Trpm7*-null embryos used in those studies resulted from heterozygous pairings, raising the possibility that due to the oocyte's ability to synthesize and store mRNA and protein from the WT allele(Wu & Dean, 2020), they may retain levels of maternal TRPM7 post-fertilization, delaying KO embryos from acquiring null status. In support of this view, the pharmacological inhibitor of TRPM7 NS8593 caused embryonic arrest during cleavage stages(Carvacho et al., 2016), suggesting that TRPM7 is essential at earlier stages of development than reported thus far by genetic studies. However, the expression, distribution, and function of TRPM7 in mammalian gametes and early embryos are unknown.

In this study, we examined the expression and role of TRPM7 in mouse gametes and preimplantation embryos. In oocytes, eggs, sperm, and cleaving embryos, TRPM7

expression is distinct and dynamic, and null gametes and embryos failed to accumulate TRPM7, with *Trpm7*-null zygotes failing to advance to the blastocyst stage. The absence of TRPM7 lowered Zn^{2+} and Mg^{2+} basal levels in eggs and embryos but not of Ca^{2+} and did not prevent the initiation of Ca^{2+} oscillations. We further show that extracellular Mg^{2+} supplementation overcame the embryo development arrest and reversed the abnormal transcriptome of *Trpm7*-null embryos dominated by the expression of oxidative stress genes, dysfunctional mitochondria, and the downregulation of transcription factor networks involved in cell proliferation. *Trpm7* mRNA expression also rescued development in null zygotes, but a pore-deficient version did not, and a "kinase-dead" mutant, only partially. Our results demonstrate the essential role of Mg^{2+} and TRPM7 for mammalian preimplantation development.

3.3 Results

3.3.1 *Conditional deletion prevents TRPM7 expression in gametes.*

Despite the essential role of TRPM7 in development, the stage of embryonic arrest and the molecular mechanism(s) underpinning it remain unresolved(Jin et al., 2008; Jin et al., 2012; Schütz et al., 2021). To address this question, we generated zygotes devoid of TRPM7. To this end, we produced a male-specific *Trpm7* cKO model using the *Hspa2*-cre transgene, which is expressed in spermatocytes(Inselman et al., 2010). We employed a previously used *loxP* strain $Trpm7^{fl/fl}$(Bernhardt et al., 2018; Govin et al., 2006), and crossed it with *Hspa2-Cre* or *Gdf9*-Cre lines to produce sperm- (*Trpm7*-Sp cKO) or oocyte-specific (*Trpm7*-Oo cKO) lines, respectively(Bernhardt et al., 2018). The deletion of *Trpm7* was confirmed by real-time PCR, as previously reported in eggs(Bernhardt et al., 2018), and as shown here for sperm (**Figure 12**).

We also confirmed the lack of protein expression in *Trpm7-null gametes and investigated* the presently unknown expression and distribution of TRPM7 in gametes and embryos. We produced a monoclonal antibody to accomplish this *because* available antibodies had low affinity and recognized TRPM6 and TRPM7(Ardestani et al., 2020). We raised it against a fusion protein corresponding to a portion of the intracellular, C-terminal domain of mTRPM7. Western blotting (WB) showed that GV oocytes displayed strong reactivity at ~210kDa **(Figure 13A**, left lane, red arrow), consistent with the molecular weight (MW) of TRPM7 in cells(Schmitz et al., 2003) and with our results in oocytes(Ardestani et al., 2020). MII eggs also showed reactivity at this approximate MW but with less intensity and shifted upwards, possibly reflecting phosphorylation **(Figure 13A**, middle lane), a common modification of TRPM7(Cai et al., 2017). The ~210 kDa signal was absent in *Trpm7*-Oo cKO GV oocytes (**Figure 13A**, right lane). GV oocytes also showed lower MW bands consistent with earlier findings that TRPM7 undergoes cell-specific cleavage upstream of the kinase domain, generating C-terminal products(Desai et al., 2012; Krapivinsky et al., 2014). We observed three prominent bands of ~115-, 70-, and 45-kDa (**Figure 13A**, arrowheads), which were not detected or of lower intensity in MII eggs and were absent in null oocytes. Brain, testes, and sperm also expressed TRPM7 and displayed a ~210kDa band corresponding to full-length TRPM7 (**Figure 13B**, middle lanes). The testes of *Trpm7*-Sp cKO males showed lesser TRPM7 reactivity, congruent with TRPM7 expression in testicular cells other than sperm (**Figure 13B**, third lane), but sperm lacked reactivity altogether (**Figure 13B**, right lane). Further, testes and sperm also displayed C-term products with distinct MWs (**Figure 13D**, arrowheads).

We next examined the location of TRPM7 in *Trpm7*$^{fl/fl}$ gametes using immunofluorescence (IF). At threshold intensities, TRPM7 adopts a uniform PM localization in GV oocytes (**Figure 13C**, upper row, left and center panels; arrow), while MII eggs display an uneven PM distribution punctuated by a few clusters and increased cortical and cytoplasmic reactivity (**Figure 13C**, middle row, left and center panels; arrows). Besides the change in distribution, the signal in MII eggs was less intense, as evidenced by the negligible fluorescence when these cells were exposed to the GV's threshold intensity (**Figures 14A and 14B,** upper panels), and vice versa, the additional appearance of a cytosolic signal in GVs when exposed to the threshold intensity of MII eggs (**Figures 14A and 14B,** lower panels). These results are consistent with our electrophysiological characterization of TRPM7 function in these cells(Carvacho et al., 2016).

TRPM7's cytosolic reactivity in somatic cells does not colocalize with markers of known cellular compartments(Abiria et al., 2017). To determine if the cytosolic distribution of TRPM7 in eggs corresponded with the location of the ER or internal lipid vesicles that are present throughout the ooplasm, we expressed the D1-ER construct(Palmer et al., 2004) or stained eggs with BODIPY (500/510), respectively, and examined their fluorescent signals. We did not observe a significant overlap between TRPM7 and these structures, indicating that they are not TRPM7's hosting organelle(s) in eggs, whose determination will require additional studies (**Figure 14C**). We also tested our antibody's specificity by examining if *Trpm7*-Oo cKO oocytes and eggs lacked TRPM7 reactivity **(Figure 13D**), which was indeed the case. Granulosa cells from *Trpm7*-Oo cKO cumulus displayed staining **(Figure 13D**, arrowhead), as did granulosa cells of *Trpm7*$^{fl/fl}$ females (**Figure 13C**,

arrowhead), consistent with the presence of *Trpm7* transcripts in these cells(Wathlet et al., 2011). Lastly, sperm showed diffuse reactivity in the head but not in the tail; this reactivity was absent in *Trpm7*-Sp cKO sperm (**Figure 13E**-lower row panels, arrow). Our data confirm that the conditional deletion approach of *Trpm7* effectively depletes the protein from gametes and shows that gametes distinctively express TRPM7.

3.3.2 *TRPM7 is indispensable for preimplantation embryo development and fertility.*

We first examined the fertility of the gamete-specific *Trpm7* cKO lines by pairing them with the corresponding male/female $Trpm7^{fl/fl}$ counterparts that express normal levels of TRPM7 and recorded their fecundity parameters. $Trpm7^{fl/fl}$ homozygous crosses produced a mean litter size of 6.5±1.8 pups comparable to pairs using *Trpm7*-Sp cKO sires, consistent with sperm analyses demonstrating the *Hspa2-Cre* transgene had negligible effects on sperm production or function (**Tables 3 and 4**; P>0.05). In contrast, consistent with previous findings(Bernhardt et al., 2018), mating pairs using *Trpm7*-Oo cKO dams produced smaller litters (**Figure 15A-**left panel; ****P<0.0001). Additionally, both *Trpm7*-gamete specific lines generated less than half of the total number of pups and parturitions than $Trpm7^{fl/fl}$ pairs, reinforcing the requirement of TRPM7 for embryo development **(Figure 4A-**center, and right panels, respectively; P<0.05**)**. Expectedly, crossing *Trpm7*-Oo females and *Trpm7*-Sp cKO males failed to produce offspring (**Figure 15A-**left panel; P<0.05).

To discover the timing of the arrest of *Trpm7*-Embryo (Em) KOs during development, we monitored every 24h the progression of zygotes to the blastocyst stage (BL). Zygotes produced after mating or *in vitro* fertilization (IVF) were cultured *in vitro*

for the study (**Figure 15B-D**). Regardless of origin, *Trpm7*-Em KO zygotes were unsuccessful in becoming BLs, with only a fraction of *in vivo*-produced zygotes developing into BLs (**Figure 15B-D;** $P<0.05$). We parsed this data to establish if the developmental block displayed a stage preference. Nearly all zygotes, defined as those with identifiable PNs at 8-h post-fertilization, cleaved to the 2-cell (2C) stage, but successive cleavages showed attrition that was most evident between the 2C to 4-cell (4C) and the 4- to 8-cell (8C) stage transitions, with most of the few morulae failing to advance to BLs (**Figure 15B-D**; $P<0.05$). Lastly, the few embryos that became BLs had abnormally low cell numbers (**Figure 15C**; $P<0.05$), unlike *Trpm7*$^{fl/fl}$ zygotes that developed to BLs at high rates (**Figure 15B-D**) and displayed the expected number of cells (**Figure 15C**; $P<0.05$). We next examined if higher rates of cellular apoptosis could at least partly explain the lower cell numbers in null BLs. It was the case, as whereas the majority of *Trpm7*-Em KO BLs had TUNEL-positive cells, this was not the case for control BLs **(Figures 15E and 15F),** suggesting that cell death may compromise the development of *Trpm7*-Em KO BLs.

To confirm the preimplantation *in vitro* results, we collected embryos from females at different times post-mating. We flushed oviducts at 36 h and 60 h post ovulation, ~1.5 and 2.5 dpc, to collect 2C and 8C embryos, respectively(Brinster, 1967). Our *in vivo* results confirm the *in vitro* data, as besides retrieving approximately the same number of embryos per female, *Trpm7*$^{fl/fl}$ *and Trpm7* cKO pairs produced similar numbers of 2C embryos, but *Trpm7* cKO pairs had fewer 8Cs along with higher numbers of 4Cs (**Figure 16A and 16B**), demonstrating developmental delay. Additional *in vitro* culture of the *in vivo* generated 2C and 8C embryos failed to produce BLs (**Figure 16C**). Together, these results

indicate that TRPM7 plays an essential role in mammalian development starting at the early cleavage stages and is indispensable beyond the 8C stage.

3.3.3 *TRPM7 displays stage-specific expression and distribution during preimplantation embryo development.*

To elucidate the basis of the essential role of TRPM7 in embryos, we first investigated the expression and cellular localization of the chanzyme in preimplantation embryos. We confirmed that GV oocytes express the ~210kDa band corresponding to the full-length TRPM7 (M7-FL), whose intensity declined in MII eggs. In zygotes (PN), the 210kDa band remained low, as displayed in the blot where all embryo stages were handled concurrently (**Figure 17A**, first three left lanes, red arrow). The intensity of the M7-FL band remained low in 2C embryos but increased in 4C and 8C stage embryos, consistent with the onset of the zygotic transcription at the 2C stage (**Figure 17A,** first three center lanes, **Figure 17B**; $P<0.05$). Morula stage embryos experienced a marked decline in the reactivity of the M7-FL band, which rebounded in BLs (**Figure 17A**, two-most right lanes; red arrow, $P<0.05$). The C-terminal products of TRPM7 (M7-CTs) also showed pronounced changes in expression throughout the preimplantation stages (**Figure 17A**, red arrowheads, **Figure 17B**), suggesting TRPM7 undergoes targeted cleavages. Given their estimated sizes, these fragments likely contain the kinase domain of the chanzyme.

We next examined the cellular localization of TRPM7 on *in vivo* fertilized zygotes cultured *in vitro* to the specified stage. We also located other cellular landmarks by DNA staining, the nucleus, and actin staining, the cortical area near the PM. The rightmost column displays the integrated profiles of these signals (**Figure 17C**). Like in MII eggs, the presence of TRPM7 in zygotes was predominantly cytosolic (**Figure 17C**-upper row).

In 2C embryos, despite retaining cytoplasmic staining, the distribution of TRPM7 noticeably changed. In the PM/cortex, TRPM7 appeared in regularly spaced clusters-like accumulations (**Figure 17C-**second row; yellow circle in the zoomed-in image), whereas a nascent aggregation became evident in the nucleus (**Figure 17C-**second row; yellow arrowhead in the zoomed-in image). TRPM7 reactivity of any kind was absent in 2- and 4C *Trpm7*-Em KO embryos, confirming the specificity of our antibody (**Figure 18A**). Four-cell stage embryos showed larger PM/cortical clusters accompanied by increased nuclear localization and decreased cytoplasmic reactivity (**Figure 17C-**third row of panels and **17D**, $P < 0.05$). As in the previous stage, 8C embryos displayed larger PM/cortical clusters and nuclear distribution (**Figure 17C-**fourth row). The intensity of TRPM7 reactivity seemed lowest at the morula stage, without distinct PM clusters, and regained diffuse cytoplasmic staining while maintaining nuclear localization (**Figure 17C-**fifth row). In BLs, the distribution of TRPM7 also seemed to be nuclear and cytoplasmic, with the outer cells part of the trophoblast showing an almost homogeneous distribution of TRPM7 between the nucleus and cytoplasm (**Figure 17C-** sixth-row panels), while the internal cells that likely correspond to the ICM appear more intensively reactive on the cytoplasm/cortex **(Figure 18B)**. Collectively, the dynamic expression and localization of TRPM7 throughout preimplantation development with the concurrence of PM and nuclear localizations in specific stages is consistent with TRPM7's vital role in preimplantation embryo development and differential contributions of its channel and kinase domains.

3.3.4 *Loss of TRPM7 impairs divalent cation homeostasis in eggs*.

The widespread expression and distinct distribution of TRPM7 in gametes and embryos and its preferred permeability for divalent cations(Monteilh-Zoller et al., 2003)

predict a pivotal role in their homeostasis in early development. We used cation-specific fluorescent dyes first to estimate their intracellular concentrations in MII eggs. Ca^{2+} and Sr^{2+} were unchanged in *Trpm7*$^{fl/fl}$ control eggs and in *Trpm7*-Oo cKO eggs (**Figure 20A**, left two panels; P>0.05), consistent with the ability of *Trpm7*-Em KO zygotes to initiate Ca^{2+} oscillations in response to fertilization with normal individual Ca^{2+} rises parameters (**Figures 19A-C** and data not shown); the reduced frequency is consistent with a previous report showing lower periodicity responses when using eggs from this null line(Bernhardt et al., 2018) (**Figures 19A-C;** P<0.05). Remarkably, Zn^{2+} and Mg^{2+} were significantly lower in *Trpm7*-Oo cKO eggs (**Figure 20A;** P<0.05). These results extend previous electrophysiological demonstrations that TRPM7 is functionally active in oocytes and eggs(Bernhardt et al., 2018; Carvacho et al., 2016) and suggest pivotal contributions to Zn^{2+} and Mg^{2+} homeostasis in these cells.

The unchanged levels of Ca^{2+} in *Trpm7*-Oo cKO eggs contrast with results by others that showed that *Trpm7*-null 2C embryos displayed lower basal Ca^{2+} in addition to reduced Mg^{2+} concentrations(Schütz et al., 2021). To ascertain if the levels of Ca^{2+} progressively changed during embryo progression and if other divalent cations remained low, we evaluated their intracellular levels in *Trpm7*-Em KO 4C embryos. We selected this stage because blastomeres are amenable to individual monitoring, TRPM7 adopts distinct positioning, and the development of many *Trpm7-null* embryos stalls at this stage. The Ca^{2+} levels were undisturbed in 4C *Trpm7*-Em KOs (**Figure 20B**, left panel), but Mg^{2+} and Zn^{2+} concentrations remained low, especially the former (**Figure 20B-**center and right panel, respectively; P<0.05). These results suggest that TRPM7 is mainly responsible for Mg^{2+} homeostasis in eggs and preimplantation embryos. In this vein, we evaluated if Mg^{2+}

concentrations spontaneously changed in *Trpm7*$^{fl/fl}$ embryos during the first divisions. We found that Mg^{2+} levels remained steady throughout the early cellular divisions despite the changes in cellular distribution that TRPM7 experiences in these embryos (**Figure 21).**

3.3.5 *Mg^{2+} but not Zn^{2+} supplementation rescues the arrest of Trpm7-Em KO zygotes.*

Given that the absence of TRPM7 expression significantly lowered the intracellular concentrations of Mg^{2+} and Zn^{2+} in eggs and embryos, we examined if supplementing these cations could overcome the developmental arrest that *Trpm7*-Em KO embryos experience. *In vivo*-produced zygotes were cultured from the 2C stage until the BLs stage in media with 10-mM $MgCl_2$, 10-μM $ZnCl_2$, or a combination of these ions (**Figure 22A)**. Supplementing external Mg^{2+} restored BLs rates but increasing Zn^{2+} did not (**Figures 22B-D**; $P<0.05$), and together rescued development but at lower rates than Mg^{2+} alone (**Figures 22D and 22E**; $P<0.05$), possibly reflecting competition among these cations for influx or, alternatively, Zn^{2+} inhibition of the putative Mg^{2+} influx molecule(s). Mg^{2+} supplementation also increased BLs' cell numbers without reaching the numbers of the supplemented controls (**Figure 22D**; $P<0.01$). These results suggest that TRPM7 is essential for Mg^{2+} homeostasis in preimplantation embryos.

We next investigated when the demands for Mg^{2+} increased in preimplantation embryos. We delayed supplementation until the 4C or 8C stage **(Figure 23A)** and monitored *in vitro* development as above. Adding Mg^{2+} at the 4C stage rescued BLs development rates but not cell numbers (**Figures 23B and 23C**; $P>0.05$, $P<0.0001$, respectively), and at the 8C stage did not recover either parameter but still supported development to the BLs stage (**Figures 23D and 23E**; $P<0.01$, $P<0.0001$, respectively).

These results suggest that the demand for Mg^{2+} increases from the 2C onwards, which is when expression of *Trpm7* increases in preimplantation embryos to remain at high levels after that(Park et al., 2015; Zeng et al., 2004) (KOMP-sponsored website-https://blogs.umass.edu/jmager/early-gene-expression/); it also coincides with the activation of transcription and the major zygotic gene activation (ZGA) milestone in 2C mouse embryos.

We performed a BL outgrowth assay to determine if the Mg^{2+} requirement extended past the BL stage. *Trpm7*$^{fl/fl}$ and *Trpm7*-Em KO zygotes were cultured in 10-mM Mg^{2+} until the BL stage. Then, BLs were transferred to conditions with different extracellular Mg^{2+} concentrations (mM), 0.8, 1.8, and 10, which are the concentrations in DMEM media, uterus, and required for rescue, respectively. While *Trpm7*$^{fl/fl}$ BLs hatched and expanded at all Mg^{2+} concentrations, almost none of the *Trpm7*-Em KO BLs hatched in 0.8 mM Mg^{2+}, but most did at 1.8 mM Mg^{2+} although without expansion, and 10-mM Mg^{2+} was necessary for *Trpm7*-Em KO BLs to behave as controls (**Figures 22F and 22G;** $P<0.05$). These results demonstrate the continuous Mg^{2+} and TRPM7 requirement during preimplantation and initial implantation stages.

3.3.6 *Trpm7*^{wt} *mRNA but not mutant versions fully rescue the development of Trpm7-Em KO zygotes without* Mg^{2+} *supplementation.*

To demonstrate that TRPM7 underpinned the arrest of *Trpm7*-Em KO zygotes, we injected *Trpm7* ^{wt}*-Venus* mRNA into *in vivo* fertilized *Trpm7*-Em KO zygotes (**Figures 24A**) to assess the ability to promote development to the BL stage without Mg^{2+} supplementation. We confirmed mRNA translation by live fluorescence and VENUS visualization **(Figure 25)**. The heterologous protein successfully restored cleavage rates

and BLs cell numbers to the levels of control embryos (**Figures 24A-C**; P>0.05). TRPM7^{wt}-VENUS achieved similar distribution to the endogenous protein in 2C and 4C embryos, although with minor differences such as accumulation on the nuclear membrane, lesser concentration in the nucleus, and PM localization but with less conspicuous clusters, possibly due to the VENUS tag on the C-terminal end of the molecule (**Figure 25**).

To examine in detail if only the channel portion of the TRPM7 was required for embryo development, we mutated it to generate a channel pore mutant, *Trpm7*^{P1040R}, a truncated molecule without the kinase domain *Trpm7*^{1570Stop}, or a kinase-dead version *Trpm7*^{K1646R}(Chubanov et al., 2007; Desai et al., 2012; Ryazanova et al., 2014; Ryazanova et al., 2010). mRNAs for all mutants were injected as above, and embryo development followed; the injection of *Trpm7*^{wt} mRNA expression served as the positive control. The *Trpm7*^{P1040R} pore mutant and the kinase-less chanzyme failed to rescue embryo development, and the channel pore mutant also prevented the development of wild-type embryos, acting in a dominant-negative-like manner (**Figures 24D and 24E**), confirming findings by others of inactivation of native channels by expression of the pore mutant form(Chubanov et al., 2007). Expression of the *Trpm7*^{K1646R} mRNA rescued embryo development but not to the same extent as *Trpm7*^{wt} mRNA, ~40% less (**Figure 24F**). Collectively, these results validate the essential role of TRPM7 in embryo development and Mg^{2+} homeostasis and suggest that both domains of the chanzyme contribute to promoting the optimal function of the chanzyme.

3.3.7 *Trpm7-Em KO embryos experience oxidative stress and have abnormal transcriptome profiles rescued by Mg^{2+} supplementation.*

We performed transcriptome profiling of MII eggs and embryos through the morula stage to identify the molecules and pathways undermining the development of *Trpm7*-Em KO zygotes. There were few differentially expressed genes (DEGs) in MII eggs (153) and 2C embryos (17), but these numbers progressively increased from the 4C to the morula stage (**Figure 26A; Table 5**). We applied Ingenuity Pathway Analysis (IPA) to evaluate canonical pathways and upstream regulators that could explain the developmental differences between control and *Trpm7*-Em KO embryos. At the 4C stage, too few DEGs were available to carry out a pathway analysis, but IGF1 signaling was among the activated upstream regulators (**Figure 26B**). Notably, 50% (6/12) of the DEGs driving the identification of IGF1 have roles in mitochondrial function, inflammation, or oxidative stress. In 8C embryos, almost all the significant canonical pathways identified showed an association with oxidative stress (**Figure 26C**; **Table 6**). This theme persisted in the morula stage, although canonical pathways involved in cell proliferation and embryo development were also identified here (**Figure 26D; Table 6**). We confirmed the transcriptomic changes by qPCR assessment of nine genes selected from the RNAseq datasets and involved in oxidative and ER stress, gene expression, and TRPM7 channel regulation (**Figure 27A**). In addition, to test physiological evidence of oxidative stress, we examined mitochondrial membrane potential (MMP). MMP was similar in MII eggs of both groups, but in *Trpm7*-Em KO embryos, starting at the 2C stage, MMP progressively declined through the 8C relative to stage-matched controls (**Figure 26E; Figure 27B**). These results are consistent with oxidative stress underlying the continuous decline of embryo development in cleaving *Trpm7*-null embryos.

We next tested if Mg^{2+} supplementation could rescue the abnormal transcriptome of *Trpm7*-Em KO embryos, as it did embryo development. Two-cell *Trpm7*-Em KO and control embryos were supplemented or not with 10-mM Mg^{2+} and collected 24- and 48 h later. After 24 h culture, RNAseq revealed 295 DEGs when comparing controls to *Trpm7*-Em KO embryos, but Mg^{2+} supplementation almost returned the transcriptome to normal in 24 h because only 19 DEGs remained in the $+Mg^{2+}$ group (**Figure 26G; Table 7**). By 48 h, there were 830 DEGs when comparing controls to *Trpm7*-Em KO embryos but only 5 DEGs in the $+Mg^{2+}$ group. Indeed, unsupervised hierarchical clustering no longer sorted the Mg^{2+}- supplemented separately from control embryos (**Figure 26H**). Consistent with these results, we show that Mg^{2+} supplementation rescued intracellular levels of Mg^{2+} (**Figure 27C**) and MMP values (**Figure 26F; Figure 27D)**. These results highlight the determinant role of TRPM7 during preimplantation embryo development in regulating Mg^{2+} homeostasis, which is vital for gene expression and developmental competence of early embryos. It also suggests that the Mg^{2+} imbalance is responsible for the oxidative stress undermining *Trpm7-Em* KO development.

3.4 Discussion

Here, we showed that TRPM7-mediated Mg^{2+} influx is required for early embryo development because *Trpm7*-null zygotes displayed diminished Mg^{2+} levels and failed to progress to the BL stage. This arrest is significantly earlier than previous reports that paired *Trpm7*-heterozygous mice. TRPM7 adopts distinct and dynamic localization in oocytes, eggs, and early embryos. Ablating it, besides affecting Mg^{2+}, reduced the intracellular levels of Zn^{2+} and caused widespread alteration of the transcriptome and oxidative stress. Mg^{2+} supplementation alone entirely rescued embryo development, as did *Trpm7* ^{wt}*-Venus*

mRNA expression. These results establish that aberrant Mg^{2+} homeostasis underlies the inability of *Trpm7*-Em KO embryos to complete development, providing a mechanistic understanding of the vital role of TRPM7 in preimplantation embryo development and defining the timing of the arrest. The coexistence of TRPM7 in distinct cellular compartments in specific embryo stages suggests varied contributions of the chanzyme to underpin embryo development in mammals.

The role of TRPM7 in divalent cation homeostasis is well documented(Nadler et al., 2001; Schmitz et al., 2003), but the ion(s) regulated vary widely among cell types and systems. Earlier studies showed TRPM7 participated in Mg^{2+} homeostasis because B-lymphocytes and other cell types without *Trpm7* failed to proliferate, a defect rescued by Mg^{2+} supplementation(Chubanov et al., 2016; Sahni et al., 2010; Schmitz et al., 2003). However, Mg^{2+} did not rescue all *Trpm7*-mutant cell lines, some of which showed altered levels of Zn^{2+} or Ca^{2+} and not Mg^{2+}(Abiria et al., 2017; Hanano et al., 2004; Krapivinsky et al., 2014; Middelbeek et al., 2012; Mittermeier et al., 2019). Here, we found that TRPM7 is the essential Mg^{2+} conducting channel in preimplantation mouse embryos beyond the 4C stage, as without it, embryonic arrest and developmental failure ensue. The mechanistic insights into the role of TRPM7 gleaned from our studies may extend to the embryo development of other vertebrates(Elizondo et al., 2005; Liu et al., 2011).

It is unknown why TRPM7 is essential for some cells and tissues and not for others. Gametes and zygotes are endowed with robust and alternate systems that ensure the steady supply of Ca^{2+} and Zn^{2+} even in the event of loss or malfunction of a channel(s) because of their indispensable roles in meiosis, fertilization, and early development(Bernhardt et al., 2018; Bernhardt et al., 2015; Carvacho et al., 2013). The expression of Mg^{2+} transporters

in mammalian oocytes, eggs, and embryos remains unexamined, despite transcriptomic information revealing that several of the common Mg^{2+} transporters and antiporters(Franken et al., 2022) are detectable in mouse zygotes and embryos, such as *Trpm6* and two members of the cyclin, and CBS domain divalent metal cation transport mediator family (CNNM), *Cnnm1 and 4*(Park et al., 2015). Based on our results in oocytes and early embryos, these molecules are unable to compensate for the absence of TRPM7, at least at the physiological levels of external Mg^{2+} and during ~ the first two-thirds of the pregnancy, because deletion of *Trpm7* after E14 does not appear to affect litter size(Jin et al., 2008). Given the role of Zn^{2+} in gene expression and the lower levels of Zn^{2+} in *Trpm7*-Em KO embryos, we cannot rule out a role in diminishing the developmental competence of these embryos despite its supplementation being unable to rescue development.

The low levels of Mg^{2+} in *Trpm7*-null eggs remained so in 4C embryos and through the BL stage, congruent with a previous report showing lower Mg^{2+} levels in *Trpm7*-null 2C embryos from heterozygous crosses(Schütz et al., 2021). It is unclear when TRPM7 becomes essential for Mg^{2+} homeostasis during oogenesis and folliculogenesis. *Trpm7*-Oo KO females produce the expected number of functional oocytes and eggs after hormonal stimulation, implying that Mg^{2+} demands are lower during this process or met by other channels or transporters until ovulation. Granulosa cells, the nurse cells of the ovary, are in intimate contact with oocytes throughout folliculogenesis, allowing the exchange of metabolites and cell products during this process(Jaffe & Egbert, 2017). Analyses of transcriptomic profiles reveal the expression of *Trpm7* in granulosa cells (UniProtKB-Q96QT4; Q923J1)(Mishieva et al., 2020), which we confirmed by IF studies. Noteworthy, RNA-Seq and micro-array studies suggest an association between the expression of *Trpm7*

in cumulus cells and pregnancy rates in ART patients(Wathlet et al., 2012). Therefore, the cumulus-oocyte complex organization may support folliculogenesis in *Trpm7*-Oo cKO females. We also show spermatozoa express TRPM7 but did not examine the functional expression and possible role(s) in these cells. The localization in the sperm head and absence in the tail suggests TRPM7 is not involved in the regulation of motility and its role in cation homeostasis(Desai et al., 2012), if any, may occur earlier during spermatogenesis.

TRPM7 expression is widespread and detected in almost every tissue and cell type(Kunert-Keil et al., 2006; Nadler et al., 2001; Runnels et al., 2001). Its subcellular localization runs the gamut of PM, cytoplasmic, and nuclear(Abiria et al., 2017; Clark et al., 2008; Krapivinsky et al., 2014). The expression and localization of TRPM7 in gametes and embryos were unknown until this study. We discovered it is expressed with remarkable precision and distinct localization throughout the preimplantation stages. Further, we observed a decline in the reactivity of the full-length protein from the GV stage to the end of maturation at the MII stage, remaining low until the 4C stage; this is consistent with our IF results. We are uncertain if the reduced reactivity is due to TRPM7's degradation or post-translational modifications that interfere with epitope recognition. The section of TRPM7 used to raise the antibody is the target of post-translational changes(Cai et al., 2017), which may obstruct antibody recognition. Further, the C-terminal products of TRPM7 resulting from its proteolytic processing detected in somatic cells(Desai et al., 2012; Krapivinsky et al., 2014) are also recognized in GVs and embryos and displayed stage-specific differential expression that follows that of the full-length protein. Future studies should examine the enzyme(s) and proteases(s) that modify the chanzyme and their functional consequences.

In MII eggs and zygotes, TRPM7 shows predominant cytoplasmic accumulation. TRPM7 also displays cytoplasmic localization in somatic cells and associates with glutathione-rich internal vesicles(Abiria et al., 2017). It is unknown if this happens in eggs and zygotes and whether the cytoplasmic expression represents the full-length TRPM7 or its C-terminal fragments. From the 2C to the 8C stage, TRPM7 in the PM/cortex becomes organized in prominent clusters, achieving a "pearls-on-a-string" appearance. This organization may have functional consequences and impact TRPM7's whole-cell currents, which rebound in 2C following inactivation in MII eggs(Carvacho et al., 2016) despite TRPM7's apparent expression remaining unchanged. Future studies will investigate if clustering and size impact the permeability and ion selectivity of TRPM7 and elucidate the other components of this likely complex. It will be interesting to discover if TRPM7's expression and function contribute to the *de novo* polarization that unfolds in 8C embryos(Johnson & Ziomek, 1983; Zhu et al., 2017). This step requires cortical recruitment of actomyosin(Zhu et al., 2017) and depends on myosin IIA phosphorylation, a substrate of TRPM7(Clark et al., 2008). Finally, the nuclear accumulation of TRPM7 is first evident at the 2C stage, increases in 4C and 8C blastomeres, and is retained in morulae and BLs' blastomeres. The role of TRPM7 in the nucleus of blastomeres is unknown, but in somatic cells, the C-terminal kinase products bind chromatin-remodeling complexes and phosphorylate histone H3 serine residues(Krapivinsky et al., 2014). The zygotic genome becomes activated following fertilization, and remodeling of the parental genomes ensures normal development. DNA and protein modifications, DNA accessibility, and transcription factors instruct this closely regulated transition(Messerschmidt et al., 2014; Rivera & Ross, 2013; Xu et al., 2021). Therefore, the nuclear localization of TRPM7 in preimplantation

embryos may influence the remodeling of the genome and gene expression during embryogenesis. The reduced expression of transcription factors and associated regulatory networks in *Trpm7*-Em KO embryos supports this possibility.

The demonstration that only Mg^{2+} supplementation restored *Trpm7*-Em KO's developmental rates and BLs composition confirmed TRPM7's essential role in Mg^{2+} homeostasis. Mg^{2+} demands increase sharply between the late zygote- and 4C stage because, after this time, supplementation does not recover embryo development or BLs' cell numbers. Mg^{2+} supports the function of hundreds of enzymes and is synonymous with cellular growth and metabolism(de Baaij, 2015; Ryazanova et al., 2010). Consequently, these early embryos, which require new gene expression and activation of the embryonic genome, and where timely cell division and differentiation are necessary for forming a new organism, are susceptible to Mg^{2+} deficiency, which promptly interrupts developmental progression. Cancer cells display similar demands and dependency for Mg^{2+}(Trapani & Wolf, 2019) and routinely show enriched expression of molecules that favor its transport(Sun et al., 2012; Wolf et al., 2007). Mg^{2+} deficiency is a common cause of oxidative stress and inflammation-induced oxidative stress that underlies the development of many cancers(Mazur et al., 2007; Trapani & Wolf, 2019). Congruent with this, IPA analysis of DEGs in *Trpm7*-Em KO 4C and 8C embryos showed an overrepresentation of canonical oxidative stress pathways. These changes translated into metabolic consequences indicative of oxidative stress and compromised mitochondrial function, confirmed by decreasing JC-1 fluorescence ratios in *Trpm7*-Em KO embryos. Remarkably, transcriptomic analyses of liver samples from *Trpm6* KO mice and intestinal samples from organ-specific-*Trpm7* KO 5-day-old pups also displayed gene expression changes

consistent with oxidative stress, suggesting this might be the prototypical gene response to hypomagnesemia(Chubanov et al., 2016; Mittermeier et al., 2019). Mg^{2+} supplementation at the 2C stage also reversed the transcriptomic changes of *Trpm7*-Em KO embryos, indicating that aberrant Mg^{2+} homeostasis underlies most of the transcriptomic, metabolic, and developmental changes that prevent these embryos' progress. These results imply that the channel, not the kinase activity of TRPM7, is essential for embryo development. Nevertheless, we cannot rule out altered gene expression or epigenome in *Trpm7*-Em KO embryos or offspring, mainly because Mg^{2+} supplementation does not fully restore *Trpm7*-Em KO BL's cell numbers. Furthermore, we show that whereas injection of *Trpm7*^{wt}*-Venus* mRNA rescued the development of *Trpm7*-null embryos, expression of the *Trpm7*^{K1646R} kinase-dead mutant was far less successful, pointing to a possible contribution of the kinase domain to embryo development. Future studies will examine whether it accomplishes this by modifying the channel's function or impacting gene expression. Collectively, these results validate the essential role of TRPM7 in embryo development and Mg^{2+} homeostasis and suggest that all domains contribute to promoting the optimal function of the chanzyme.

In summary, TRPM7 is essential for Mg^{2+} homeostasis in preimplantation embryos. Our results add a third divalent cation, besides Ca^{2+} and Zn^{2+}, whose regulated availability is indispensable for the successful initiation of development. Its insufficiency causes oxidative stress and transcriptional aberrations. Besides being expressed in both gametes and embryos, we show that TRPM7 adopts dynamic and stage-specific expression and localizations that enable its ionic and molecular functions. Elucidation of the partners and regulators that underpin its pervasive presence in preimplantation embryos will provide

insights into factors that buttress cell proliferation, differentiation, and embryonic development.

3.5 Figures

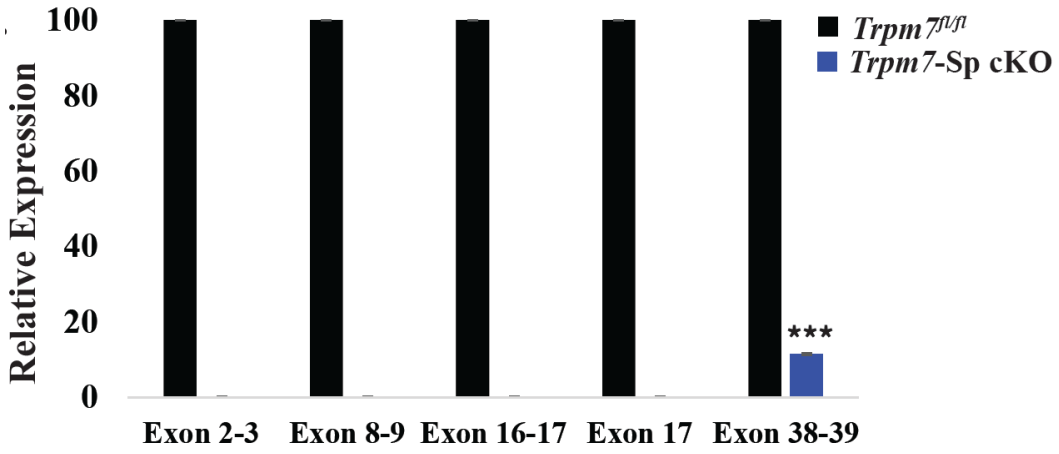

Figure 12. *The conditional deletion of Trpm7 prevents expression of Trpm7 mRNA in spermatozoa, while* TRPM7 *intensity and distribution changes during oocyte maturation with minimal colocalization with two intracellular organelles.* Sperm-specific deletion of *Trpm7, Trpm7*-Sp cKO, was performed in mice carrying *loxP* sites flanking exon 17, *Trpm7*$^{fl/fl}$, followed by mating with transgenic males expressing a *Hspa2-Cre* recombinase. Primers to detect the gene mutation bound to exons 2-3, 8-9, 16-17, and 38-39 of *Trpm7*. Real-time PCR using total RNA extracted from *Trpm7*$^{fl/fl}$ sperm (controls) or sperm of Sp-cKO males showed absence or reduced *Trpm7* expression in KOs vs. controls.

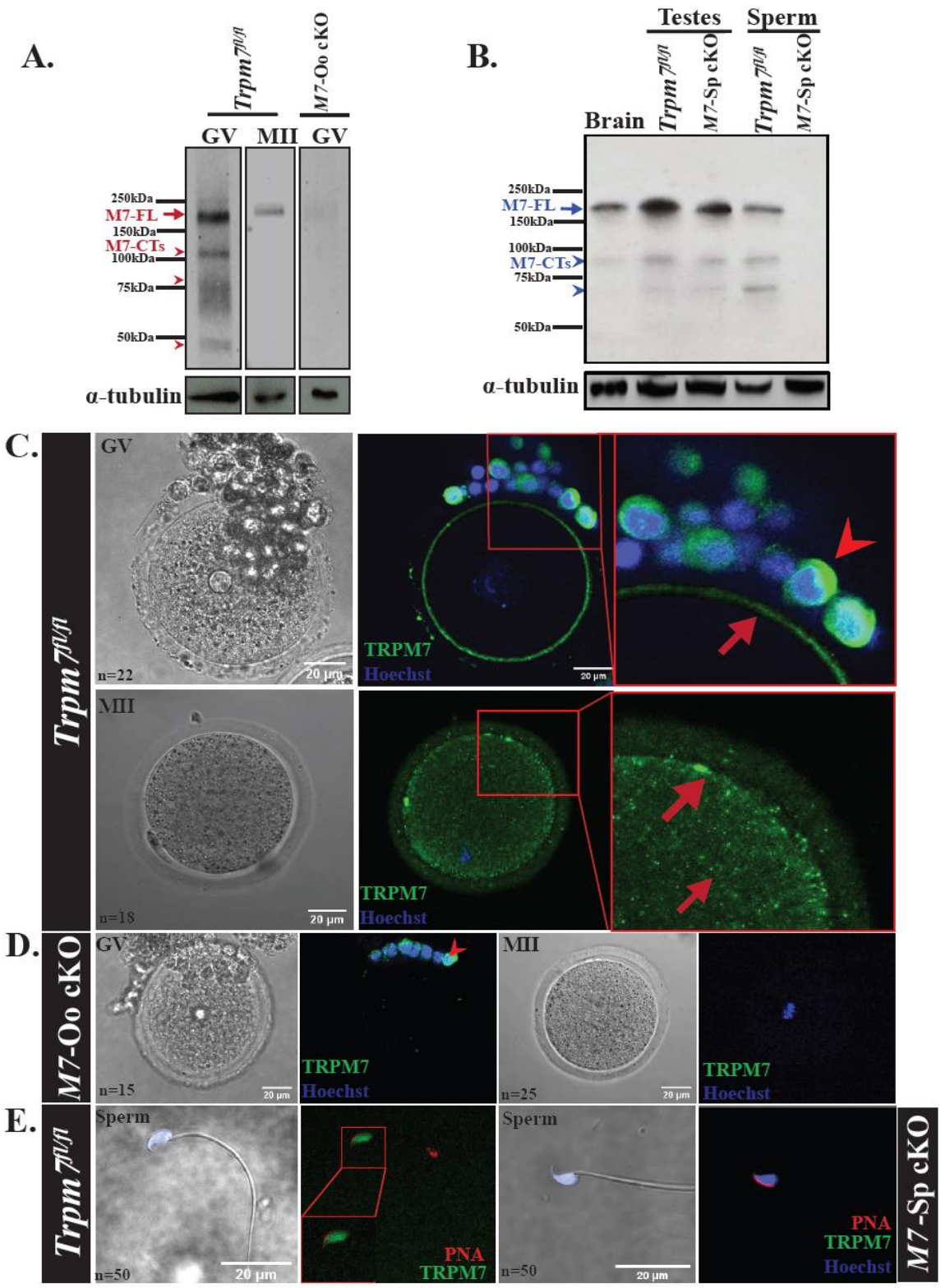
A.
Trpm7fl/fl
M7-Oo cKO
GV
MII
GV
250kDa
M7-FL
150kDa
M7-CTs
100kDa
75kDa
50kDa
α-tubulin
B.
Testes
Sperm
Brain
Trpm7fl/fl
M7-Sp cKO
Trpm7fl/fl
M7-Sp cKO
250kDa
M7-FL
150kDa
100kDa
M7-CTs
75kDa
50kDa
α-tubulin
C.
Trpm7fl/fl
GV
n=22
20 μm
TRPM7
Hoechst
20 μm
MII
n=18
20 μm
TRPM7
Hoechst
D.
M7-Oo cKO
GV
n=15
20 μm
TRPM7
Hoechst
MII
n=25
20 μm
TRPM7
Hoechst
E.
Trpm7fl/fl
Sperm
n=50
20 μm
PNA
TRPM7
Sperm
n=50
20 μm
PNA
TRPM7
Hoechst
M7-Sp cKO

Figure 13. *Mouse gametes express TRPM7, and Trpm7 conditional deletion prevents it.* **(A)** Images of western blotting (WB) of GVs and MIIs denoting expression of full-length TRPM7, M7-FL (red arrow) in *Trpm7*$^{fl/fl}$ oocytes and eggs, and lack of it in the adjacent lane in GVs of *Trpm7*-Oo cKO (M7-Oo cKO) females. M7-CTs (red arrowheads) below correspond to C-terminal fragments of the chanzyme. The images below the TRPM7 blots corresponds to α-tubulin and were used to normalize TRPM7 expression here and elsewhere. **(B)** WB of brain tissue, testes, and sperm extracts from *Trpm7*$^{fl/fl}$ and *Trpm7*-Sp cKO (*M7*-Sp cKO) lines showing TRPM7-FL reactivity (blue arrow) and lack of it in the cKO sperm line (right-most lane). Tissues and sperm also contain M7-CTs (blue arrowheads). **(C-E)** Bright-field (left column) and immunofluorescence (IF) images of TRPM7 in oocytes and eggs of *Trpm7*$^{fl/fl}$ and *M7*-Oo cKO lines (**C** and **D**, respectively), and sperm (**E**) from *Trpm7*$^{fl/fl}$ and *M7*-Sp cKO line (two left and right panels, respectively). TRPM7 reactivity (green), DNA (blue), and PNA (red), marking the acrosome. Square red insets in the upper two rows, center panels, are enlarged in the right panels; red arrows denote the TRPM7 position in oocytes/eggs and arrowheads in granulosa cells. **D** and **E** show the absence of TRPM7 reactivity in *M7*-Oo cKO oocytes and eggs and *M7*-Sp cKO sperm, respectively. The white bars represent distance in μm here, and for the rest of the study, n= represents the number of observations per panel here and elsewhere.

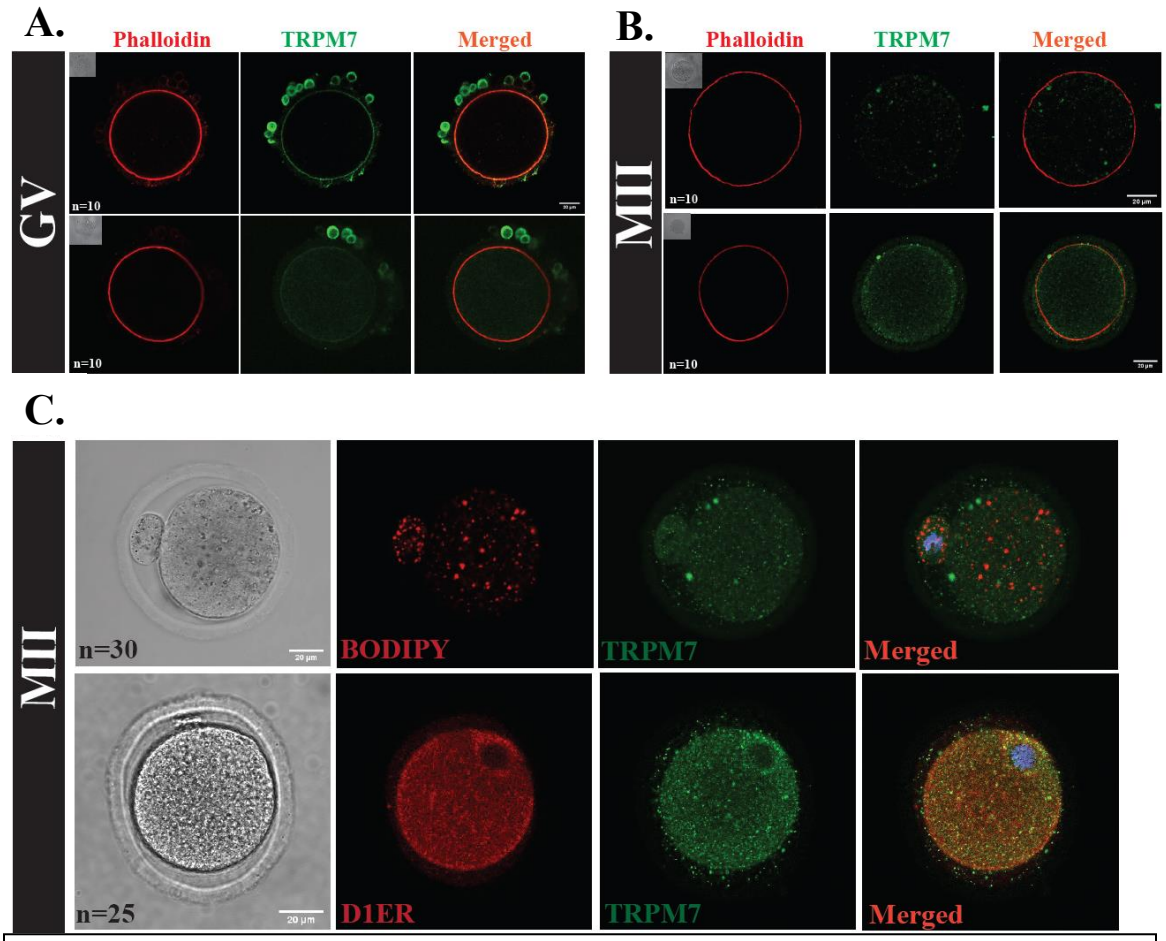

Figure 14. TRPM7 *intensity and distribution changes during oocyte maturation with minimal colocalization with two intracellular organelles.* **A.** IF images of *Trpm7*$^{fl/fl}$ oocytes and **(B)** eggs displaying phalloidin (actin-red- left panels) and TRPM7 signals (green-center panels); merged images are shown in the right panels. The upper panels were captured with the threshold intensity used for GV oocytes, whereas the lower panels were captured using the threshold intensity used for MII eggs. **C.** IF image of *Trpm7*$^{fl/fl}$ eggs displaying staining of lipid vesicles (BODIPY, red-upper panels) and ER (endoplasmic reticulum) staining (D1ER, red-lower panels). The right panels are the merged images showing minimal colocalization of TRPM7 with the identified organelles. Bright-field images are shown as insets in the left columns. Data are presented as control mean ± SEM; ***P<0.001 (*Student's t-test*). n= oocytes and eggs examined for each condition

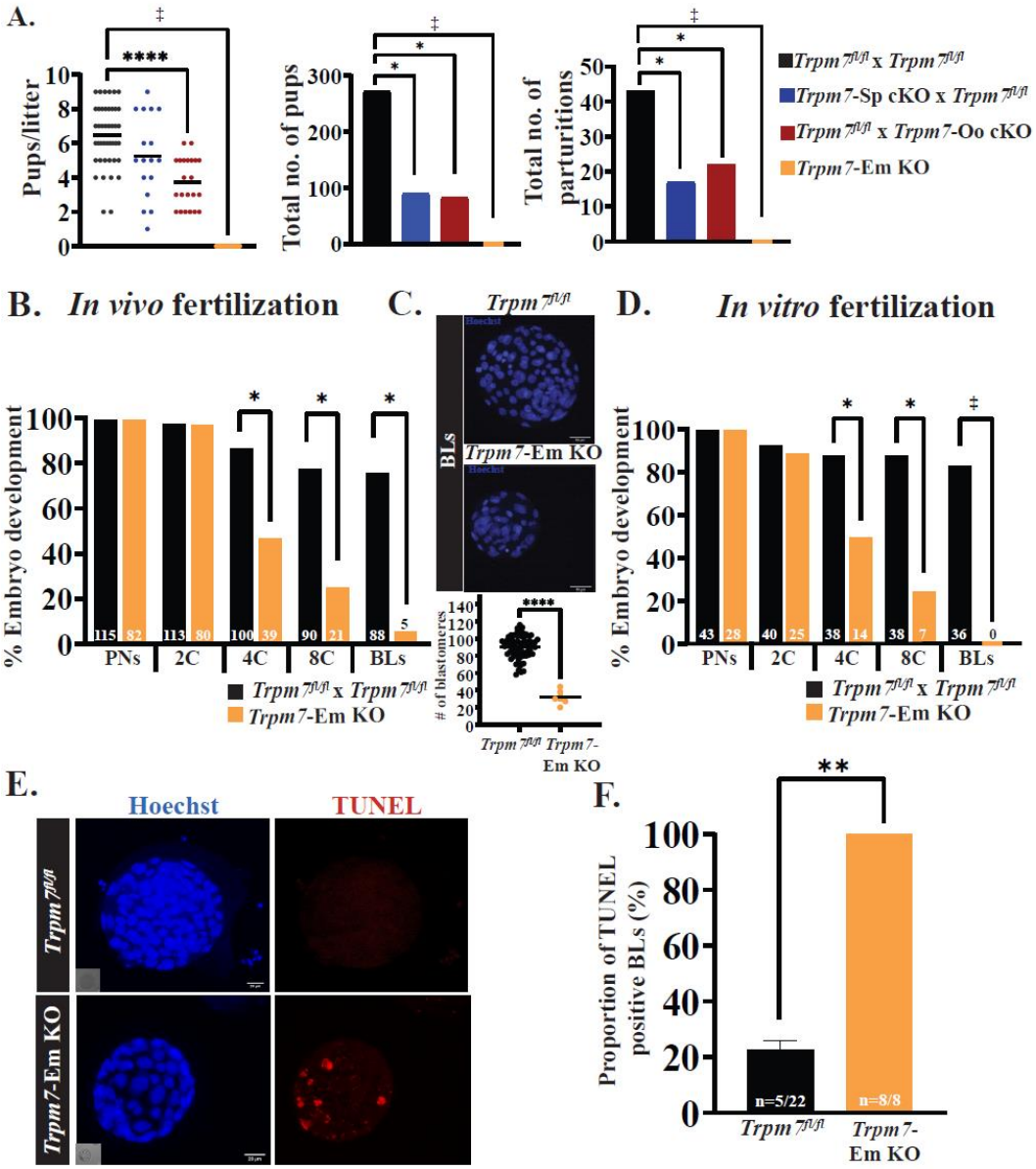
A.
Pups/litter
Total no. of pups
Total no. of parturitions
Trpm7fl/fl x Trpm7fl/fl
Trpm7-Sp cKO x Trpm7fl/fl
Trpm7fl/fl x Trpm7-Oo cKO
Trpm7-Em KO
B. In vivo fertilization
% Embryo development
PNs
2C
4C
8C
BLs
C.
Trpm7fl/fl
Trpm7-Em KO
BLs
# of blastomeres
D. In vitro fertilization
E.
Hoechst
TUNEL
F.
Proportion of TUNEL positive BLs (%)
n=5/22
n=8/8

Figure 15. *Trpm7 is a requisite for fertility and preimplantation embryo development*. **A.** A dot plot and bar graphs depicting the mating outcomes between crosses of *Trpm7*$^{fl/fl}$ mice and breeder lines expressing gamete-specific *Cre's*. Six pairs per group were observed for six months, and the number of litters, pups, and pups/litter were recorded and statistically compared. Differences between groups were assessed by ANOVA followed by Tukey's posthoc test. Asterisks (*) above columns indicate significance between columns/groups here and elsewhere (*P<0.05; ****P<0.0001). **B-D**. Rates of preimplantation development of *Trpm7*$^{fl/fl}$ and *Trpm7*-Em KO zygotes collected after *in vivo* mating (**B**) or *in vitro* fertilization (**D**) and cultured *in vitro*. Bar graphs illustrate the embryo stages examined during culture. Data are % of embryos reaching each successive stage from PN to BL and the precise numbers noted in the columns. The number of zygotes was the reference (100%). **C.** BLs were stained with Hoechst, and nuclei were counted to estimate the number of blastomeres per BL (****P<0.0001). **E.** The TUNEL assay was used to determine the presence of apoptotic cell in BLs from *Trpm7*$^{fl/fl}$ and *Trpm7*-Em KO zygotes (red internal fluorescence-right lower panel). **F.** Bar graph depicts the proportion of apoptotic BLs in *Trpm7*$^{fl/fl}$ vs. *Trpm7*-Em KO zygotes. Student's *t-tests* were applied for comparisons (*P<0.05-P<0.0001). The ‡ symbol denotes crosses that did not produce offspring or BLs here and elsewhere.

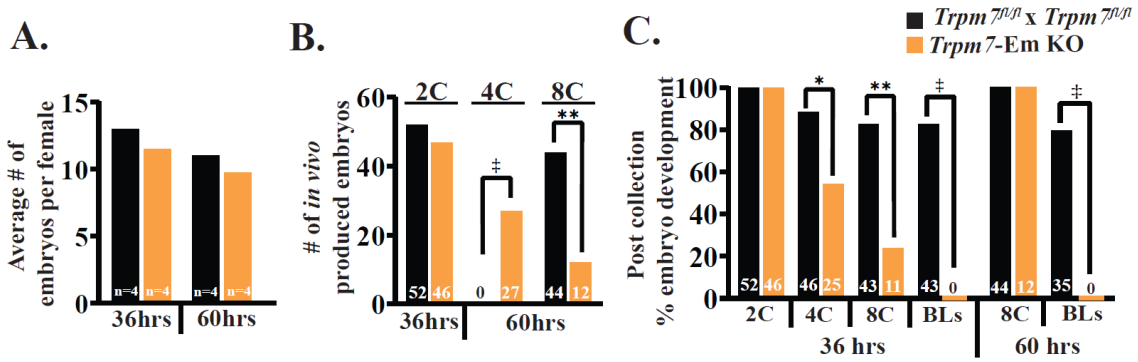

Figure 16. *Trpm7*-Em KO *embryos in vivo undergo development arrest between the 4C and 8C stages.* **A-C** Bar graphs depicting the average number of embryos collected per female **(A)**, number of *in vivo* produced embryos collected 36 h post-mating (2C) or after 60 h (8C) **(B),** and % of *in vivo* development post-collection of embryos collected 36 and 60h post-mating from *Trpm7*$^{fl/fl}$ and *Trpm7*-Em KO pairing. *P<0.05; **P<0.01 (*Student's t-test*) (**C**). n= embryos examined for each condition.

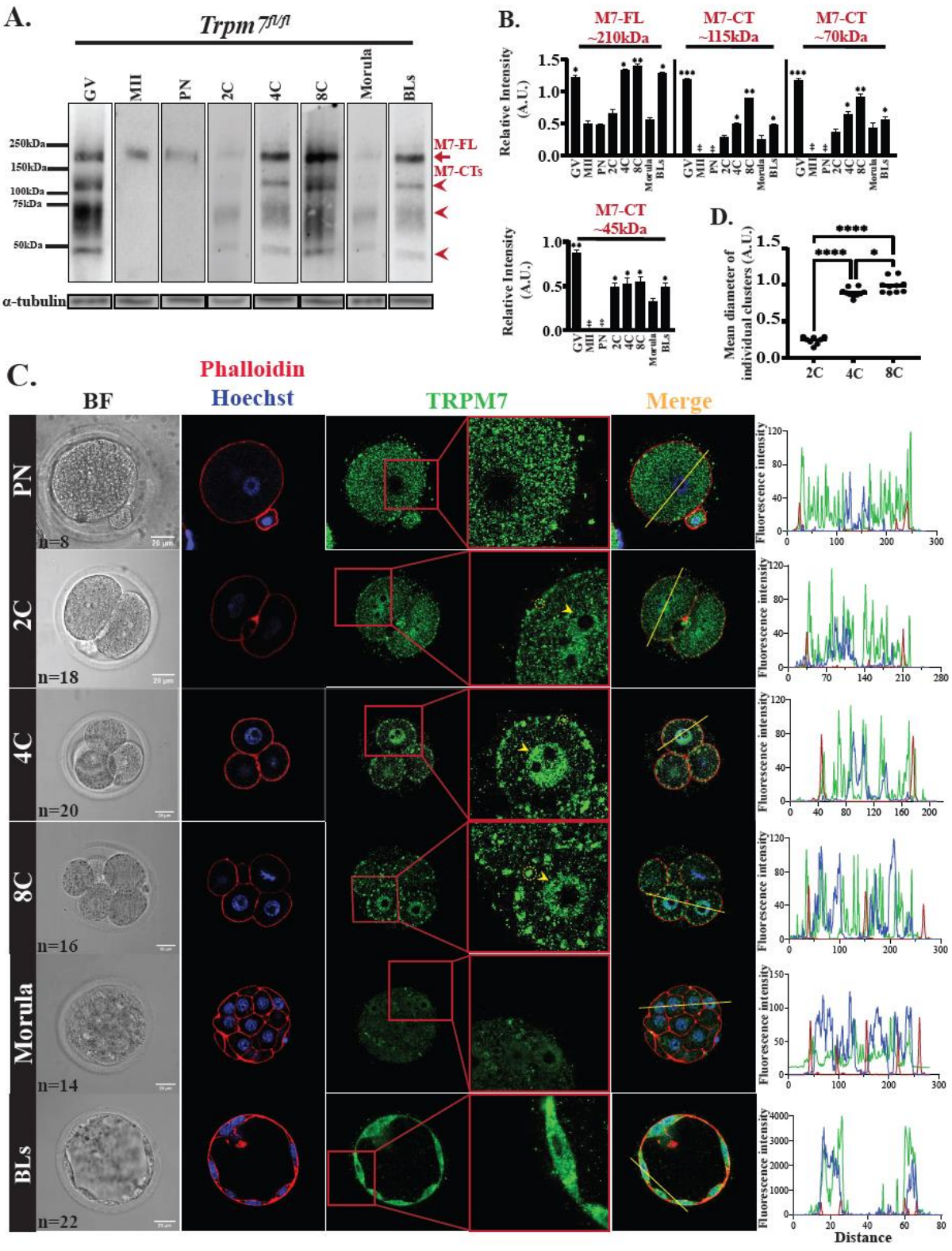
A.
Trpm7fl/fl
GV
MII
PN
2C
4C
8C
Morula
BLs
250kDa
150kDa
100kDa
75kDa
50kDa
M7-FL
M7-CTs
α-tubulin
B.
M7-FL ~210kDa
M7-CT ~115kDa
M7-CT ~70kDa
Relative Intensity (A.U.)
M7-CT ~45kDa
C.
BF
Phalloidin
Hoechst
TRPM7
Merge
PN
2C
4C
8C
Morula
BLs
n=8
n=18
n=20
n=16
n=14
n=22
Fluorescence intensity
Distance
D.
Mean diameter of individual clusters (A.U.)
2C
4C
8C

Figure 17. *TRPM7 displays stage-specific expression and distinct distributions in preimplantation embryos.* **A.** WB of TRPM7 reactivity in oocytes, eggs, and preimplantation embryos (n=50). The red arrow denotes the full-length protein, M7-FL, and the arrowheads below the three most abundant C-terminal fragments. α-tubulin reactivity is shown below each lane and used to normalize TRPM7 quantifications. **B.** The relative intensities of M7-FL and M7-CTs between oocytes, eggs, and embryos were quantified from three replicates, statistically compared, and represented by bar graphs. Columns without asterisks are stages with lower and statistically significant expression than those with asterisks ($P<0.05$ or $P<0.01$) whereas, bars with asterisks, a different number of them indicate differences between groups ($P<0.01$) **C.** Bright field (left column) and IF images of PN, 2C, 4C, 8C, morula, and BLs stage embryos (remaining columns) displaying actin distribution by phalloidin labeling (red) and nuclear DNA by Hoechst staining (blue) (second column) and TRPM7 distribution (green; three most right columns). A yellow trace in the Merged column denotes the line where the fluorescence was estimated for the three probes. At the right of this column, the line plots display the intensity of the fluorescent signals across the embryos. The number of cells and embryos examined per stage is indicated in the bright field panels (n=), and the white bars represent distance in μm. **D.** Comparison of the size of the TRPM7 PM clusters observed at the 2C, 4C, and 8C stage embryos (*$P<0.05$, ****$P<0.0001$). Comparisons were carried-out using ANOVA followed by Tukey's post hoc tests**.**

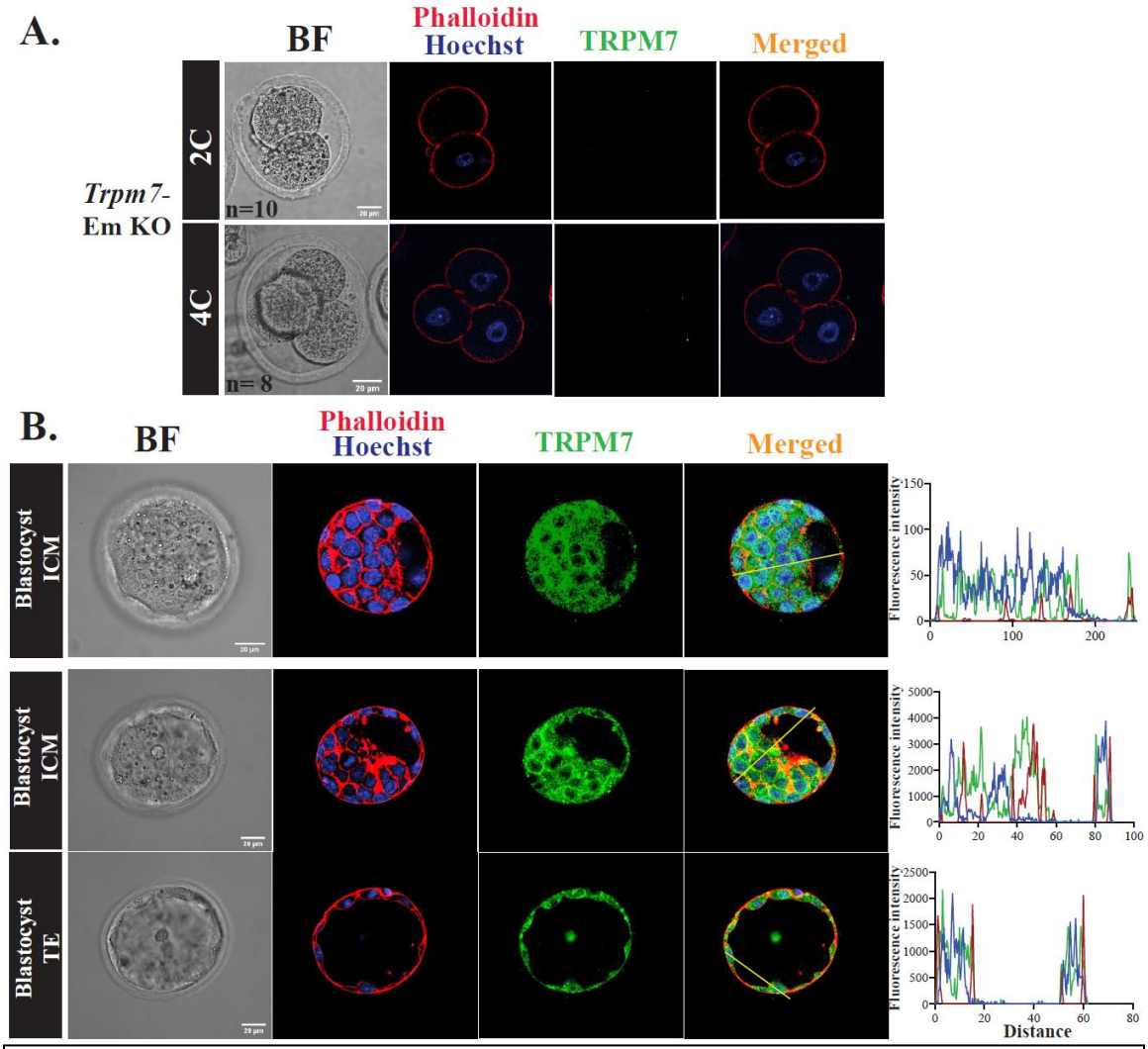

Figure 18. *Conditional deletion of Trpm7 abolishes expression of the chanzyme in 2C and 4C embryos and expression in inner cell mass (ICM) and trophectoderm (TE) of BLs.* **A.** Bright-field (left column) and IF images, Phalloidin (actin-red), Hoechst (DNA-blue) (center left column), TRPM7 (green) (center right column), and Merged (right column), are shown. **B.** Representative confocal images of a BL section that includes ICM and TE cells; two BLs assessed and ICM in the top row corresponds to the BL in **Figure 6**. Left column, BF, bright-field images, first center column, IF images of Phalloidin (red-actin) and Hoechst (blue-DNA). The center-right column shows TRPM7 (green). The rightmost column shows the merged images. A yellow trace in the merged column denotes the region of interest where the fluorescent signals were assessed and displayed in line plots to the right. The white bars represent distance in µm. n= represents the number of embryos examined.

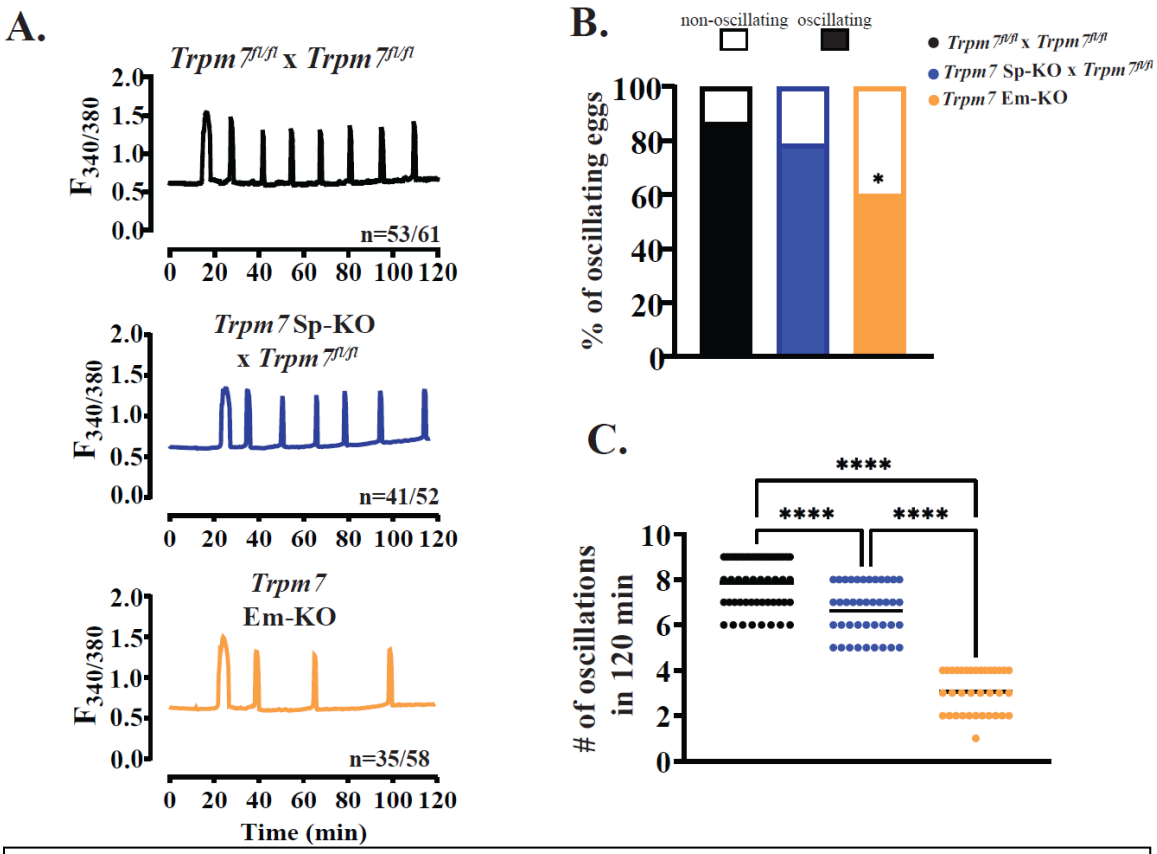

Figure 19. *Trpm7 null sperm initiates lower frequency but persistent fertilization* Ca^{2+} *oscillations.* **A**. Traces shown correspond, top to bottom, to *Trpm7*$^{fl/fl}$, *Trpm7*-Sp cKO x *Trpm7*$^{fl/fl}$, *Trpm7*-Sp cKO x *Trpm7*-Oo cKO zygotes. Oscillations were monitored for 120 min for all gamete combinations and parameters quantified. N= represents the number of oscillating zygotes over the total number of monitored eggs for each strain combination. **B**. Stacked bar graph depicting the number of oscillating eggs in all groups (*P<0.05). **C**. Dot plot showing mean and distribution of the number of Ca^{2+} oscillations in 120 min in groups examined (ANOVA followed by Tukey's posthoc test; ****P<0.0001).

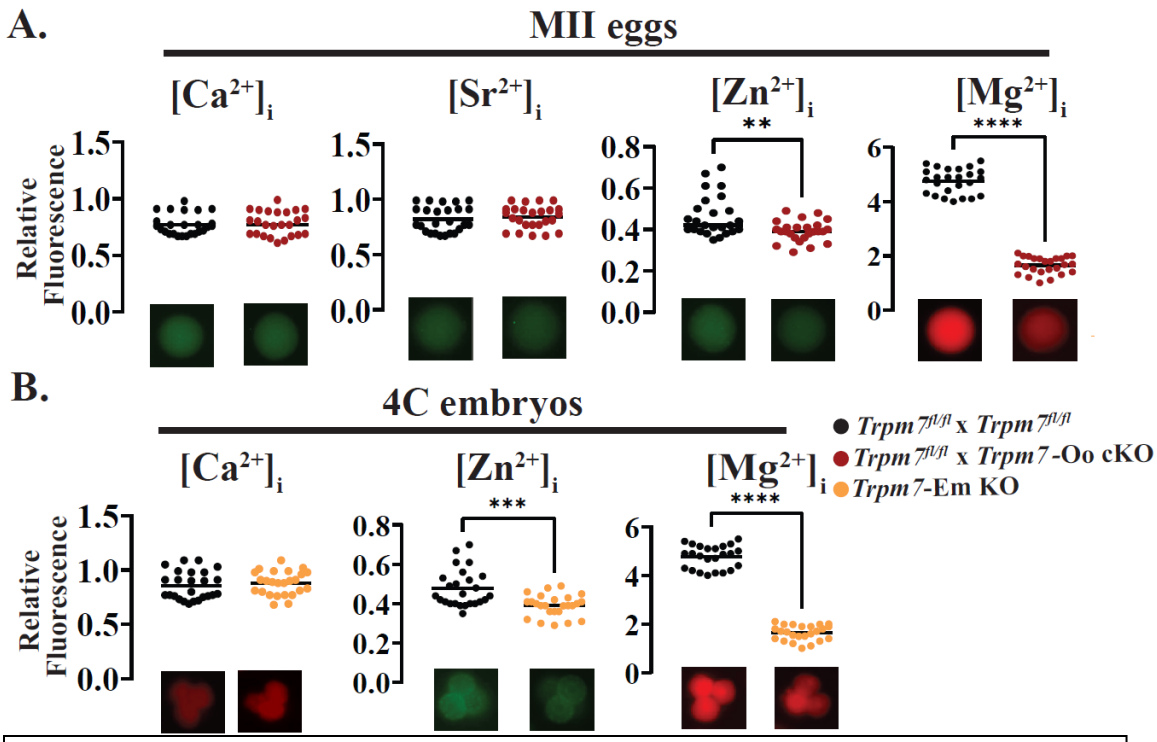

Figure 20. *TRPM7 is essential for divalent cation homeostasis in eggs and early embryos*. **A.** Dot plots displaying normalized intracellular concentrations of divalent cations, Ca^{2+}, Sr^{2+}, Zn^{2+}, and Mg^{2+} (left to right panels, respectively) in MII eggs from *Trpm7*$^{fl/fl}$ (black) and *Trpm7*-Oo *c*KO (red) lines (**P<0.01; ****P<0.0001) **B.** Dot charts displaying normalized intracellular concentrations of divalent cations in 4C stage embryos, from left to right, Ca^{2+}, Zn^{2+}, and Mg^{2+} from *Trpm7*$^{fl/fl}$ and *Trpm7*-Em KO lines. Representative images are shown below the dot plots to depict differences in fluorescence intensities. Data were compared from at least three experiments using the Student's *t-test* (***P<0.001, ****P<0.0001).

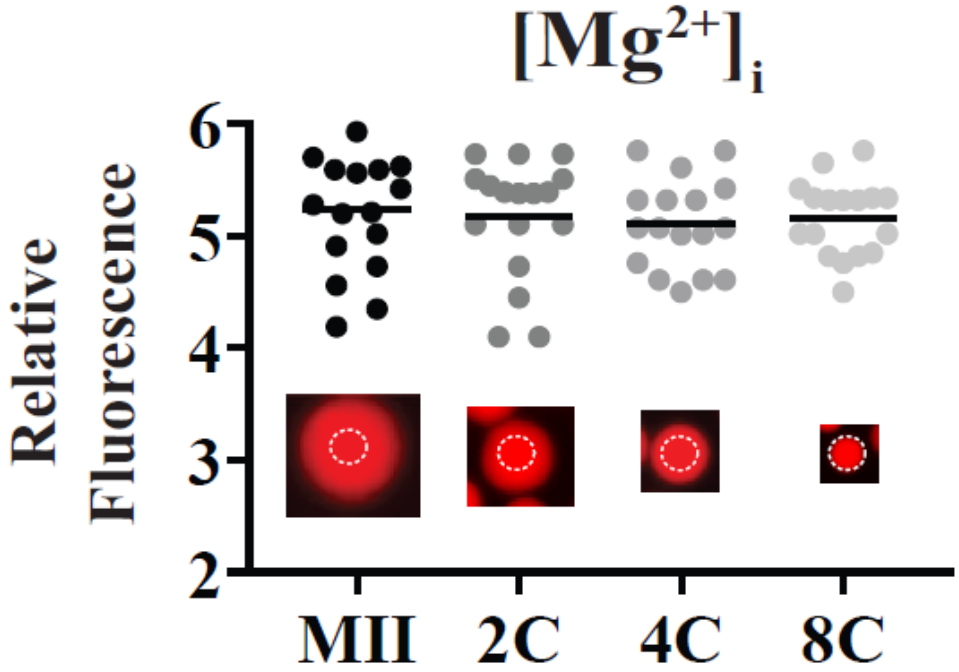

Figure 21. *Intracellular Mg^{2+} concentration remains consistent from eggs and through the 8C stage. A* dot plot graph showing normalized intracellular Mg^{2+} concentrations in *Trpm7*$^{fl/fl}$ eggs and early embryo stages until the 8C stage, where cells from these embryos could be assessed individually. Representative images are shown below the dot plots displaying fluorescence intensities. Intracellular Mg^{2+} levels remained steady, and the broken circles within cells or blastomeres represent the ROI used to assess fluorescence. (ANOVA; *P>0.05).

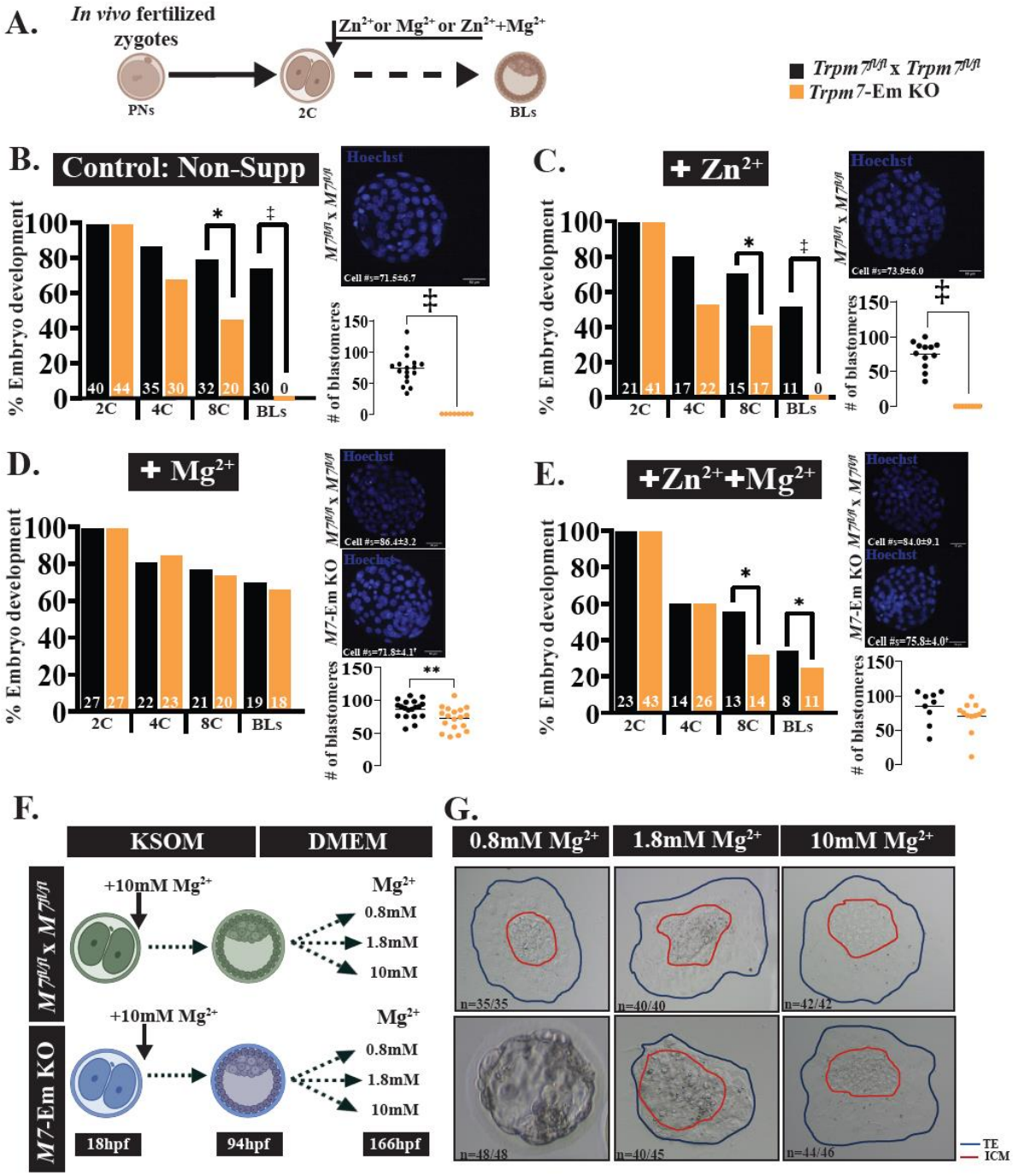
A.
In vivo fertilized zygotes
Zn2+or Mg2+ or Zn2+ +Mg2+
PNs
2C
BLs
Trpm7fl/fl x Trpm7fl/fl
Trpm7-Em KO
B.
Control: Non-Supp
% Embryo development
40 44 35 30 32 20 30 0
2C 4C 8C BLs
Hoechst
Cell #s=71.5±6.7
# of blastomeres
C.
+ Zn2+
21 41 17 22 15 17 11 0
Cell #s=73.9±6.0
D.
+ Mg2+
27 27 22 23 21 20 19 18
Cell #s=86.4±3.2
Cell #s=71.8±4.1
E.
+Zn2+ +Mg2+
23 43 14 26 13 14 8 11
Cell #s=84.0±9.1
Cell #s=75.8±4.0
F.
KSOM
DMEM
+10mM Mg2+
Mg2+
0.8mM
1.8mM
10mM
18hpf
94hpf
166hpf
G.
0.8mM Mg2+
1.8mM Mg2+
10mM Mg2+
n=35/35
n=40/40
n=42/42
n=48/48
n=40/45
n=44/46
TE
ICM

Figure 22. *Mg^{2+} supplementation rescues Trpm7-Em KO preimplantation embryo development*. **A.** Schematic of Mg^{2+} supplementation strategy. The extra divalent cations were added at the 2C stage and remained throughout the culture period. **B-E.** Bar graphs depicting rates of *in vitro* preimplantation development of zygotes from *Trpm7$^{fl/fl}$* and *Trpm7*-Em KO mice in not supplemented media **(B)** or supplemented with Zn^{2+} (**C**), Mg^{2+} (**D**), or both ions (**E**). Representative images of BLs stained with Hoechst and BLs cell number means are displayed in dot charts for each condition to the right of the graphs. **F.** Schematic of outgrowth assay strategy. *Trpm7$^{fl/fl}$* and *Trpm7*-Em KO embryos were cultured to the BL stage (94hpf; hours post fertilization) in KSOM supplemented with 10mM Mg^{2+}. After this time, BLs from both groups were transferred to DMEM media containing 0.8mM, 1.8mM and 10mM Mg^{2+} and cultured until 166hpf. **G.** Representative images of expanded Bls with different concentrations of Mg^{2+} in control and *M7*-Em KOs. Statistical comparisons were performed using the Student's *t-test* (P>0.05). The ‡ symbol denotes groups that did not produce BLs and were not statistically compared.

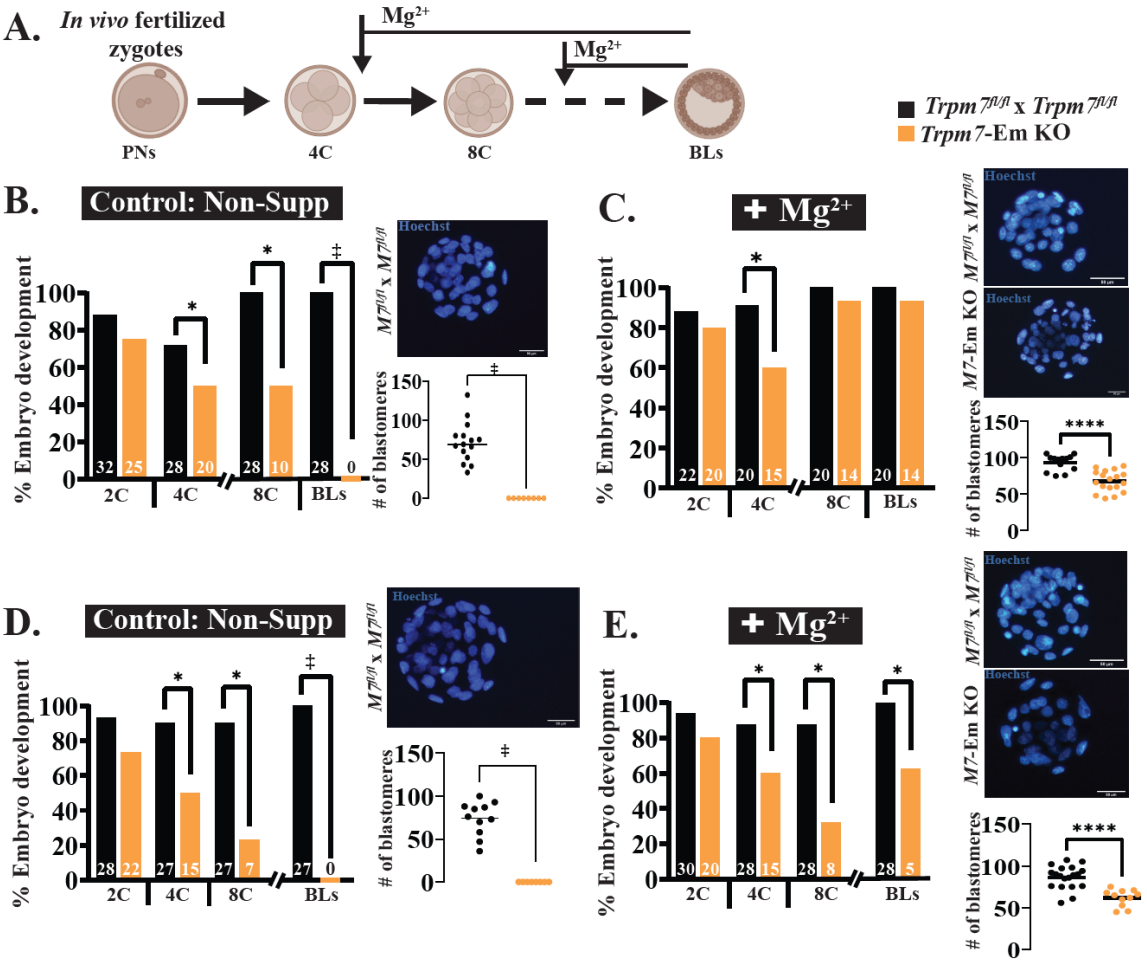
A.
In vivo fertilized zygotes
Mg2+
Mg2+
PNs
4C
8C
BLs
Trpm7fl/fl x Trpm7fl/fl
Trpm7-Em KO
B.
Control: Non-Supp
% Embryo development
100
80
60
40
20
0
32 25 28 20 28 10 28 0
2C 4C 8C BLs
M7fl/fl x M7fl/fl
Hoechst
# of blastomeres
150
100
50
0
C.
+ Mg2+
22 20 20 15 20 14 20 14
M7-Em KO
****
D.
Control: Non-Supp
28 22 27 15 27 7 27 0
E.
+ Mg2+
30 20 28 15 28 8 28 5

Figure 23. *Mg^{2+} supplementation of 4C- or 8-C embryos differentially rescues their development.* **A.** Schematic showing supplementation of Mg^{2+} at 4C- or 8C embryos followed by culture to the BL stage in supplemented media. **B-E.** Bar graphs depicting development rates of *in vivo* fertilized zygotes from *Trpm7$^{fl/fl}$* (controls) and *Trpm7*-Em KO mice. **B** and **C**, data for 2C- and 4C embryos are % of embryos reaching each stage relative to the number of PNs that was 100% ($P<0.05$), whereas, for development to the 8C and BL stages, marked by a break in the X-axis, the %s reflect the numbers of embryos that reached each stage relative to the number of 4C embryos at the time of supplementation. **D** and **E**, as B and C, but rates of BL development were calculated from the number of 8C embryos, which was the stage of supplementation. Representative images of BLs derived from 4C- or 8C *Trpm7$^{fl/fl}$* and *Trpm7*-Em KO embryos supplemented with Mg^{2+} and stained with Hoechst are displayed to the right of each bar graph. Dot plots comparing BL mean cell counts and distribution between strains and treatments are below the DNA images for all groups. (Student's *t-test*; **P <0.01 or ****P<0.0001).

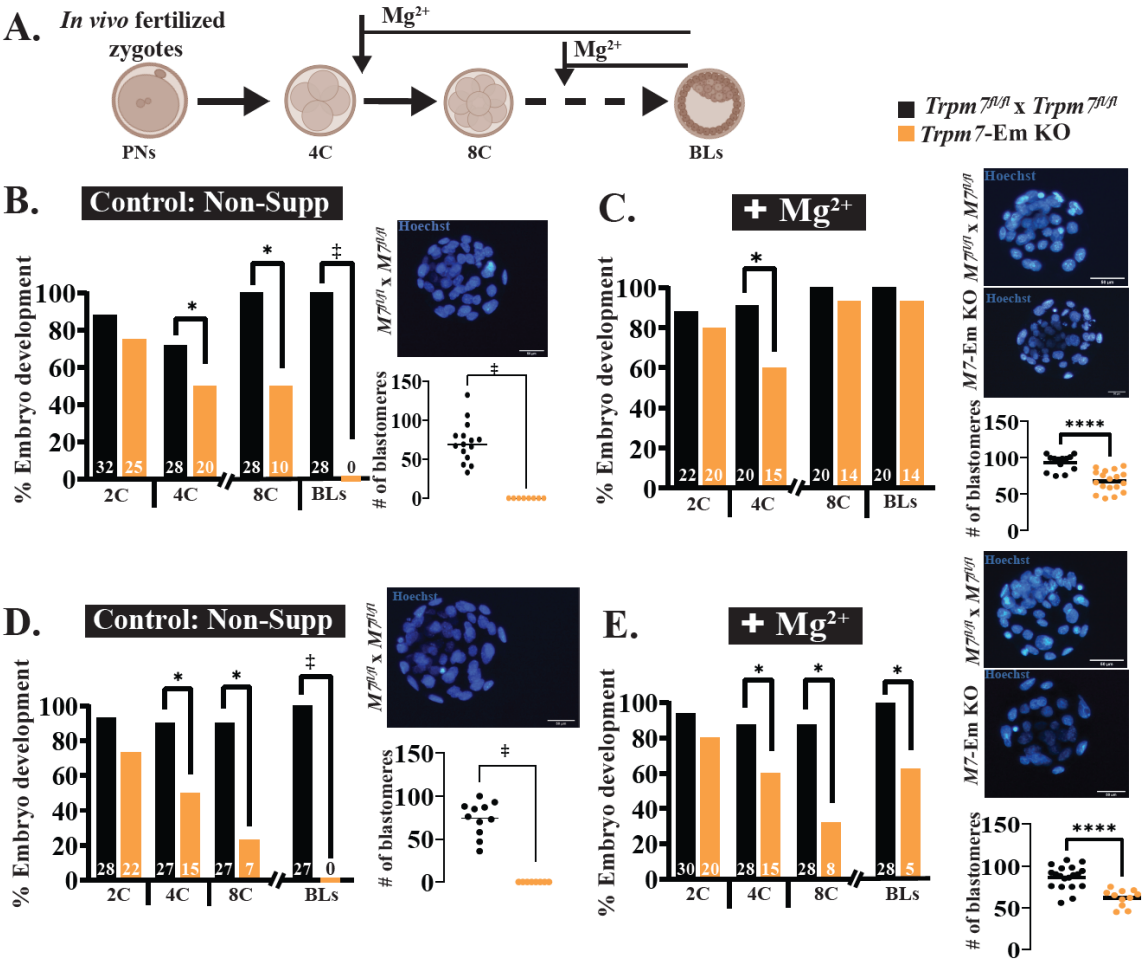

Figure 24. *TRPM7^{wt} mRNA rescues Trpm7-Em KO embryo development, but mutant versions are not as effective.* **A.** Schematic of the *Trpm7* mRNAs rescue strategy. mRNA injections were always performed into *Trpm7*-Em KO zygotes, after which they were cultured in media not supplemented with Mg^{2+}. **B-F.** Bar graphs depicting rates of preimplantation embryo development of *Trpm7$^{fl/fl}$* and *Trpm7*-Em KO non-injected embryos and used as controls (P<0.05) (**B**) or injected with *Trpm7^{wt}* **(C)**, *Trpm7^{p1040R}* **(D)**, *Trpm7^{K1646R}* **(E)**, and *Trpm7^{1570Stop}* mRNA (P>0.05-0.01). Representative images of BLs stained with Hoechst and cell number quantifications are shown to the right of each graph. Statistical comparisons were performed using the Student's *t-tests* (P>0.05). The ‡ symbol denotes groups that did not produce BLs and were not statistically compared.

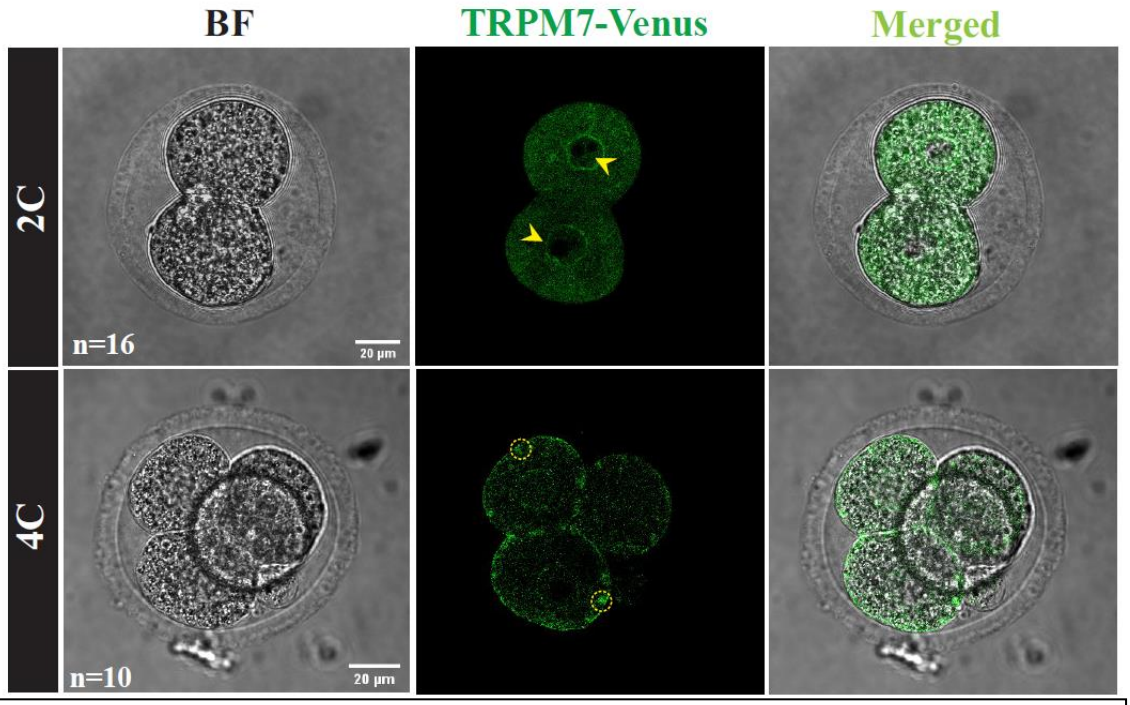

Figure 25. Heterologous **e***xpression of Trpm7-Venus mRNA attains distribution of TRPM7 analogous to the endogenous protein in 2C and 4C embryos. In vivo*-produced zygotes were injected with *Trpm7-Venus* mRNA, and live-confocal imaging was performed 24- and 48-h later. The left column portrays bright-field (BF) images, the center column displays their fluorescent signals, and the right column shows the merged images. The yellow arrowheads point at the nuclear presence of TRPM7-Venus in 2C embryos, which also showed distinct accumulation in the nuclear membrane. The broken circles in the 4C images denote the presence of cortical/PM accumulations of TRPM7-Venus.

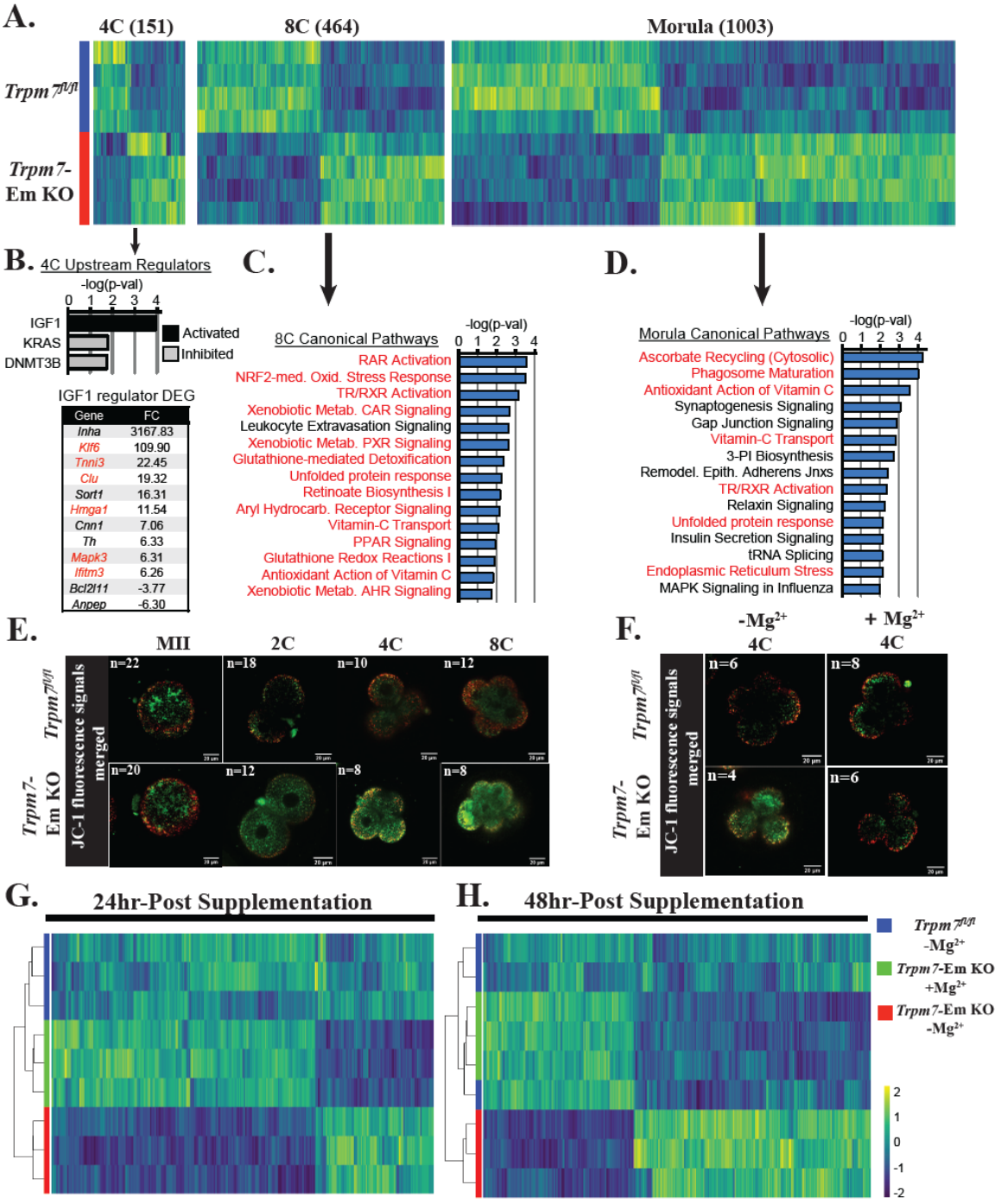
A.
4C (151)
8C (464)
Morula (1003)
Trpm7fl/fl
Trpm7-Em KO
B. 4C Upstream Regulators
-log(p-val)
0 1 2 3 4
IGF1
KRAS
DNMT3B
Activated
Inhibited
IGF1 regulator DEG
Gene FC
Inha 3167.83
Klf6 109.90
Tnni3 22.45
Clu 19.32
Sort1 16.31
Hmga1 11.54
Cnn1 7.06
Th 6.33
Mapk3 6.31
Ifitm3 6.26
Bcl2l11 -3.77
Anpep -6.30
C.
8C Canonical Pathways
-log(p-val)
0 1 2 3 4
RAR Activation
NRF2-med. Oxid. Stress Response
TR/RXR Activation
Xenobiotic Metab. CAR Signaling
Leukocyte Extravasation Signaling
Xenobiotic Metab. PXR Signaling
Glutathione-mediated Detoxification
Unfolded protein response
Retinoate Biosynthesis I
Aryl Hydrocarb. Receptor Signaling
Vitamin-C Transport
PPAR Signaling
Glutathione Redox Reactions I
Antioxidant Action of Vitamin C
Xenobiotic Metab. AHR Signaling
D.
Morula Canonical Pathways
-log(p-val)
0 1 2 3 4
Ascorbate Recycling (Cytosolic)
Phagosome Maturation
Antioxidant Action of Vitamin C
Synaptogenesis Signaling
Gap Junction Signaling
Vitamin-C Transport
3-PI Biosynthesis
Remodel. Epith. Adherens Jnxs
TR/RXR Activation
Relaxin Signaling
Unfolded protein response
Insulin Secretion Signaling
tRNA Splicing
Endoplasmic Reticulum Stress
MAPK Signaling in Influenza
E.
MII
2C
4C
8C
Trpm7fl/fl
Trpm7-Em KO
JC-1 fluorescence signals merged
n=22
n=18
n=10
n=12
n=20
n=12
n=8
n=8
F.
-Mg2+
+ Mg2+
4C
4C
Trpm7fl/fl
Trpm7-Em KO
JC-1 fluorescence signals merged
n=6
n=8
n=4
n=6
G.
24hr-Post Supplementation
H.
48hr-Post Supplementation
Trpm7fl/fl -Mg2+
Trpm7-Em KO +Mg2+
Trpm7-Em KO -Mg2+
2
1
0
-1
-2

Figure 26. *TRPM7 expression prevents oxidative stress in preimplantation embryos by promoting Mg^{2+}influx.* **A.** Heat map representation of the comparison of differentially expressed genes (DEG) identified by RNAseq in *Trpm7*$^{fl/fl}$ control embryos relative to *Trpm7*-Em KO embryos at the 4-cell (4C), 8-cell (8C), and morula stages. The number of DEGs at each stage is indicated in parentheses above each group. **B.** Ingenuity Pathway Analysis (IPA) of upstream regulators predicted as activated or inhibited in 4C embryos; $P<0.05$. DEG present in IGF1 upstream regulator dataset and fold-change (FC) shown; red font indicates a role in mitochondrial function, inflammation, or oxidative stress. **C-D.** IPA of canonical pathways in 8C embryos **(C)** and morulae **(D);** the 15 most significant pathways relevant to the two embryo stages are shown. The red font indicates oxidative stress-related pathways. **E-F.** Mitochondrial membrane potential as indicated by merged ratio images of JC-1 staining of MII eggs and embryos of the indicated genotypes and cellular stages. Representative images of all embryo stages examined **(E)**. Embryos of both strains were handled as before but supplemented or not with Mg^{2+} at the 2C and cultured to the 4C stage **(F)**. **G.** Unsupervised hierarchical clustering of DEG identified by RNAseq at the indicated time points in *Trpm7*$^{fl/fl}$, *Trpm7*-Em KO, and *Trpm7*-Em KO embryos cultured with and without added Mg^{2+}.

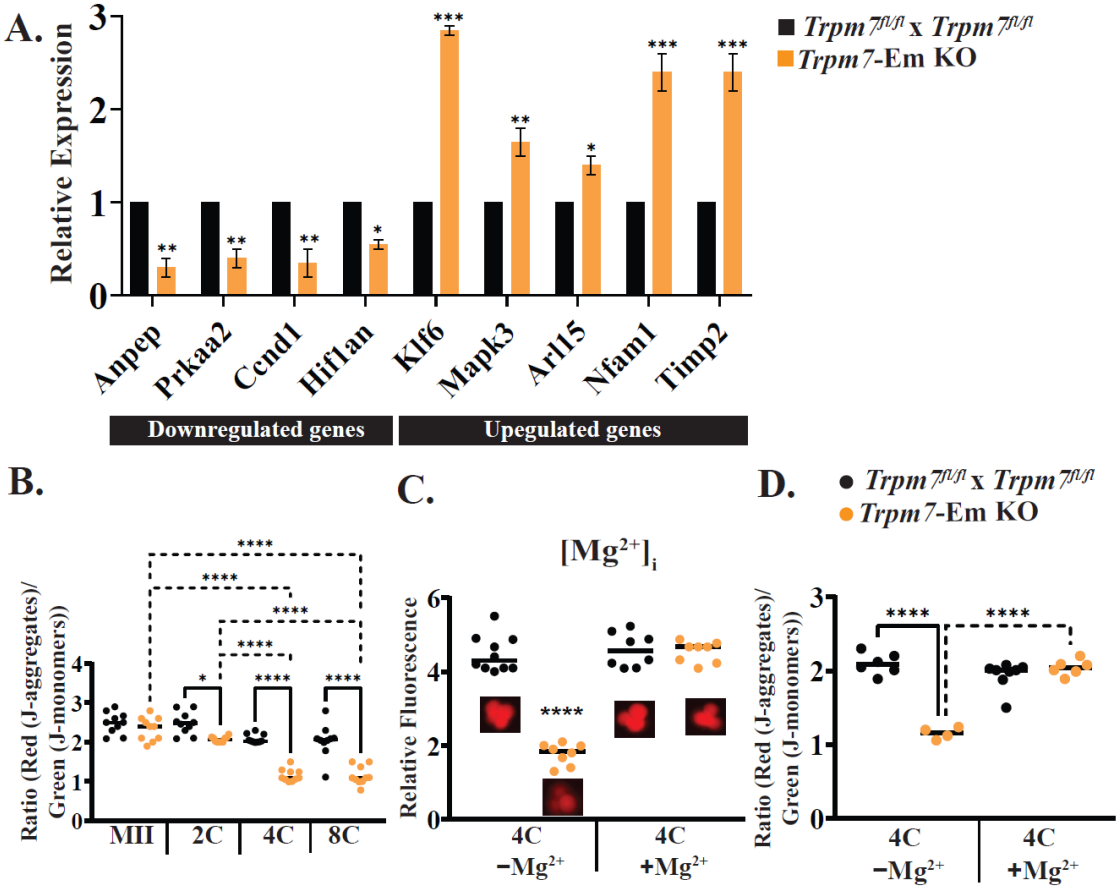
A.
Relative Expression
Trpm7fl/fl x Trpm7fl/fl
Trpm7-Em KO
Anpep
Prka2
Ccnd1
Hif1an
Klf6
Mapk3
Arl15
Nfam1
Timp2
Downregulated genes
Upegulated genes
B.
Ratio (Red (J-aggregates)/ Green (J-monomers))
MII
2C
4C
8C
C.
[Mg2+]i
Relative Fluorescence
4C −Mg2+
4C +Mg2+
D.
Trpm7fl/fl x Trpm7fl/fl
Trpm7-Em KO
Ratio (Red (J-aggregates)/ Green (J-monomers))
4C −Mg2+
4C +Mg2+

Figure 27. *Reversal of the increased cellular oxidation and decreased JC-1 ratios in Trpm7-Em KO embryos by Mg^{2+} supplementation, which restored intracellular Mg^{2+} levels in these embryos.* **A.** Relative expression of genes shown to be upregulated or downregulated in 4C *Trpm7*-Em KO relative to controls *$Trpm7^{fl/fl}$ embryos*; the selected genes are involved in functions associated with or affected by the absence of TRPM7 and/or Mg^{2+}, which includes oxidative stress pathways (*Anpep, Klf6, Mapk3, Nfam, Prkaa2, Timp2*), gene regulation (*Cnnd1, Hif1an*) and channel function (*Arl15*). The examined genes were selected from the differential expression in two Datasets (Supplementary Tables 3 and 5). Following total RNA extraction, gene expression comparisons were done using *qPCR* and *Actb* as the reference transcript (n=25 embryos per replicate and strain, two replicates). The results were normalized to the C_t values of the reference transcript and plotted in bar graphs. **(**$*P \leq 0.05$; $**P \leq 0.01$; $***P \leq 0.001$; *Student's t test*s). **B, C.** Quantification and mean comparisons of JC-1 ratios performed in MII eggs and embryos examined in **Figure 7E** from *$Trpm7^{fl/fl}$* and *Trpm7*-Em KO lines following *in vitro* culture without (**B**) or with Mg^{2+} supplementation (**C**). Following staining with JC-1 and acquiring of equivalent red and green images in eggs and embryos, ratios of red (JC-1 aggregates)/green (JC-monomers) fluorescence intensities were calculated and displayed in a dot chart. The solid connecting lines denote comparisons within stages between the two strains, whereas broken lines show comparisons within a strain (ANOVA followed by Tukey's post hoc test; *P<0.05-****P<0.0001). **(D)** *In vivo* produced *$Trpm7^{fl/fl}$* and *Trpm7*-Em KO zygotes were cultured to the 2C stage, supplemented or not with 10-mM Mg^{2+}, and cultured to the 4C. At this point, the levels of Mg^{2+} were quantified, normalized using the fluorescent dye Mag-Fura 2, and values were displayed in dot plots for all embryos examined; representative images of the relative fluorescent intensity of each cohort are also shown. Non-supplemented *Trpm7*-Em KO embryos displayed lower values than all other groups (ANOVA followed by Tukey's post hoc test; P<0.0001).

Table 3. *Trpm7*$^{fl/fl}$ and *Trpm7*-Sp cKO lines have comparable sperm counts and morphology

Male genotype	Concentration (x 10^6 spermatozoa/ml)	Normal morphology (%)
Trpm7$^{fl/fl}$	13.7±1.9	93.7±0.7
***Trpm7*-Sp cKO**	17.1±3.9$^{n.s.}$	92.7±0.9$^{n.s.}$

Statistical comparisons were done using t-test (middle column) and chi-square ($p>0.05$)

Table 4. *Trpm7*$^{fl/fl}$ and *Trpm7*-Sp cKO lines display normal and equivalent acrosome status and sperm motility parameters before and after capacitation.

	Male genotype	Intact acrosome (%)	Mot (%)	ProMot (%)	VCL (µm/s)	VSL (µm/s)	VAP (µm/s)	LIN (%)
NCAP	***Trpm7***$^{fl/fl}$	79.6±2.3	14.9±3.4	12.2±3.1	187.1±8.0	70.4±3.8	90.1±3.9	36.7±1.8
	***Trpm7*-Sp cKO**	75.1±1.6$^{n.s.}$	12.2±3.9$^{n.s.}$	9.4±3.3$^{n.s.}$	181.2±10.0$^{n.s.}$	72.1±5.9$^{n.s.}$	92.3±5.7$^{n.s.}$	38.9±3.1$^{n.s.}$
CAP	***Trpm7***$^{fl/fl}$	59.7±2.5	19.7±2.1	14.0±2.3	189.4±10.7	87.9±5.0	109.1±5.0	46.1±3.3
	***Trpm7*-Sp cKO**	59.4±0.8$^{n.s.}$	20.5±2.9$^{n.s.}$	14.8±2.0$^{n.s.}$	192.1±9.5$^{n.s.}$	95.5±2.4$^{n.s.}$	114.6±2.8$^{n.s}$	49.3±2.4$^{n.s.}$

NCAP-Non-Capacitated, CAP-Capacitated

Mot-Motility, ProMot-Progressive motility

VCL-Curvilinear velocity, VSL-Straight line velocity, VAP-Average path velocity, LIN-Linearity

Statistical comparisons were done using t-test and chi-square, as indicated by the type of data analyzed ($p>0.05$)

CHAPTER 4

CONCLUSION

Elucidating the precise signaling molecule(s) responsible for triggering egg activation remains a significant challenge in reproductive biology, despite extensive research efforts spanning various species, elucidating the precise signaling molecule(s) responsible for triggering egg activation remains a significant challenge in reproductive biology. However, a pivotal advancement was achieved in mammals with the discovery of phospholipase C ζ (PLCζ) and the transient receptor potential cation channel subfamily M member 7 (TRPM7). PLCζ, primarily expressed in the testes, emerged as a key player due to its association with fractions of sperm extracts exhibiting Ca^{2+} activity, inducing Ca^{2+} oscillations similar to those during fertilization upon injection. Meanwhile, TRPM7, expressed ubiquitously and present in almost every tissue and cell type, has been identified as essential for Mg^{2+} homeostasis during preimplantation embryo development.

Despite PLCζ's pivotal role, studies in mice lacking PLCζ revealed subfertility alongside aberrant Ca^{2+} responses, suggesting the existence of additional factors triggering sufficient Ca^{2+} responses for embryo development. Our investigation identified PLCδ4 as a potential backup molecule, upregulated in the absence of PLCζ, suggesting a compensatory role in sperm-mediated egg activation. Furthermore, our findings underscored the essential roles of PLCζ and PLCδ4 in fertilization and egg activation, with PLCδ4 primarily regulating the acrosome reaction crucial for sperm-egg fusion and potentially bifunctional in the absence of PLCζ1 by activating the eggs.

On the other hand, TRPM7-mediated Mg^{2+} influx was found to be indispensable for early embryo development, with *Trpm7*-null embryos displaying diminished Mg^{2+}

levels and developmental arrest during cleavage stages. TRPM7's dynamic and stage-specific expression and localizations throughout preimplantation stages underscore its essential role in ionic and molecular functions crucial for embryo development.

In conclusion, the discovery of PLCζ and TRPM7 as key players in sperm-mediated egg activation and preimplantation embryo development, respectively, sheds light on the intricate molecular mechanisms underlying these critical reproductive events. Further investigation into the interplay between these molecules and their downstream targets will provide deeper insights into fertilization and embryo development, with potential diagnostic and therapeutic implications for infertility and reproductive management in both humans and animals.

CHAPTER 5

MATERIAL AND METHODS

Animal husbandry

This study only used mouse models of the strains listed below. Females used to collect oocytes and, embryos were between 6 to 10 weeks old. When embryos were collected and mating was required, the age of males was between 8 to 10 weeks. The University of Massachusetts Institutional Animal Care and Use Committee (IACUC) approved all animal experiments and protocols. Balbc, *Trpm7*$^{fl/fl}$, *Hspa2-Cre*, and *Gdf9-Cre* mice, generated from a mixed background of C57BL6/J and 129s4/SvJae, were gifts from Dr. Carmen Williams (NIEHS, USA) or purchased from The Jackson Laboratory (Jackson Labs, Bar Harbor, ME), and bred at our facility. *Trpm7*-floxed (*Trpm7*$^{fl/fl}$) mice were crossed with *Trpm7*$^{fl/fl}$*-Hspa2-Cre* and *Trpm7*$^{fl/fl}$*-Gdf9-Cre* breeders to produce sperm-specific (*Trpm7*-Sp conditional knockout (cKO)) and oocyte-specific (*Trpm7*-Oo cKO) *Trpm7* cKO mouse lines, respectively. Whole KO embryos (*Trpm7*-Em KO) were obtained by crossing gametes from the *Trpm7*-gamete specific KO lines and controls from mating *Trpm7*$^{fl/fl}$ breeders.

Mice, genotyping, and PCR analysis

Mice were genotyped using tissue from an ear clip collected and lysed using tail lysis buffer (50 mM Tris-HCl pH 8.8, 1 mM EDTA pH 8, 0.5% Tween 20, 0.3 mg/ml proteinase K). Genomic DNA was stored at −20°C and used later for PCR analysis. PCR products were used to determine genotypes following their separation on a 1.2% agarose gel following standard procedures, as previously performed in our laboratory(Ardestani et al., 2020).

In vivo fertility of *Trpm7*-modified genetic lines

The fertility of gamete-specific and embryo-deleted *Trpm7* lines was evaluated by mating six pairs per genetic line for six months and recording the outcomes of these pairings. The following parameters were considered, the number of total parturitions, total number of pups, and pups per litter. The following crosses were evaluated (male x female): *Trpm7*$^{fl/fl}$ x *Trpm7*$^{fl/fl}$, *Trpm7*-Sp KO x *Trpm7*$^{fl/fl}$, *Trpm7*$^{fl/fl}$ x *Trpm7*-Oo KO, and *Trpm7*-Sp KO x *Trpm7*-Oo KO.

RNA isolation and RT-PCR

Total RNA was extracted from the sperm of *Trpm7*$^{fl/fl}$ and *Trpm7*-Sp cKO males using the High Pure RNA isolation kit (Roche, Cambridge, MA) and following the manufacturer's instructions. $1x10^6$ sperm were used to extract total RNA, 1μg of which was used for the additional procedures. For embryos, total RNA was extracted from 25 *Trpm7*$^{fl/fl}$ and *Trpm7*-Em KO 4C embryos. Reverse transcription was performed using an iScript cDNA synthesis kit (Bio-Rad, Hercules, CA). Real-time PCR was performed using the Power SYBR^{TM} Green PCR Master Mix (Thermo Fisher, Agawam, MA). *Actb* was used as an internal control for normalization. The Mx3000 Real-Time PCR System (Agilent Technologies, Santa Clara, CA) was used to amplify the products of the reaction, and quantification of these RNA products' was performed by normalizing to *Actb* using the comparative C_T methodology, as described.(Akizawa et al., 2021)

Gametes, zygotes, and preimplantation embryo culture and collection

Gametes and zygotes were collected and processed as previously described.(Ardestani et al., 2020; Mehregan et al., 2021) Briefly, 6- to 10-week-old females were intraperitoneally (IP) injected with pregnant mare's serum gonadotropin (PMSG, 10

IU., Biovendor, Asheville, NC) and with human chorionic gonadotrophin 48h later if collecting eggs/zygotes (hCG, 10 IU., Sigma-Aldrich, St. Louis, MO). Cumulus-enclosed, GV oocytes (COCs) were obtained 40h after the PMSG injection following removal and mincing of the ovaries and piercing the large antral follicles; MII eggs were recovered from the oviducts 12h after the hCG injection. GV oocytes and eggs were handled in HEPES-buffered Tyrode's lactate solution (TL-HEPES). To procure *in vivo* zygotes, after the hCG injection, females were paired with males overnight. A vaginal plug 14h after hCG was evidence of successful mating. Putative zygotes were collected from the oviducts of females 20h post-hCG administration and briefly incubated with hyaluronidase and transferred into micro drops of KSOM (MilliporeSigma) covered with light mineral oil (Fisher Scientific, Hampton, NH) in an incubator under a humidified atmosphere in air containing 5% CO_2 and at 37ºC. PN formation was evaluated at 24h post-hCG and cleavage to 2C at 40h.

For flushing *in vivo*-produced embryos from the oviduct, a 32 gauge needle (the end cut and ground to blunt the tip) is attached to a 1ml syringe filled with media. The embryos were flushed at 36h (2C) and 60h (8C) post-ovulation. Flushed embryos were cultured as mentioned above.

Zygotes were also produced by *in vitro* fertilization (IVF), and egg collection was performed as described above. For IVF, eggs were placed in 90 µL drops of Toyoda-Yokoyama-Hosi medium (TYH;(Y, 1971)) supplemented with 4 mg mL^{-1} of BSA (TYH-BSA; Sigma-Aldrich) covered with mineral oil and incubated under standard conditions. Sperm were recovered from 2- to 6-month-old male's cauda epididymis and placed in 1 mL TYH-BSA and allowed to swim out for 10 min. Additional sperm incubation,

capacitation, and insemination were performed as described(Ducibella & Matson, 2007; Navarrete et al., 2019). After 4 h, eggs were gently pipetted, washed, and incubated for 20 h in fresh TYH-BSA micro drops covered with mineral oil. After this time, zygotes were washed, placed into KSOM medium (MilliporeSigma), and cultured in standard conditions for variable intervals according to the experimental design.

Zygotes from all groups were washed and transferred to KSOM micro drops covered with mineral oil and cultured for 24-96 h according to experimental design. Their progression through development was evaluated every 24 h and until 120 h post-hCG, and embryos were scored (2-cell (2C), 4-cell (4C), 8-cell (8C) embryo, morula, or blastocysts (BLs). To assess cell numbers, BLs were fixed in 4% paraformaldehyde (PFA), stained with 1% (w/v) Hoechst 33342 (Thermo Fisher), and mounted on slides under coverslips using 1% glycerol. The cell counts were performed in BLs at 400x under an epifluorescence microscope (Eclipse TE300, Nikon, Japan). The culture media for rescue experiments was supplemented with 10μM $ZnCl_2$, or 10mM $MgSO_4 \cdot 7H_2O$ or their combination, at the 2C-, 4C-, or 8C stages. Embryo development and cell numbers were scored or counted as described. Eggs and embryos used for RNA isolation and sequencing studies, see procedures below, were collected following identical procedures and timelines.

For the outgrowth assay, BLs were cultured as mentioned in Miao et al. 2020(Miao et al., 2020). Briefly, BLs were cultured for 3 days in Dulbecco's modified Eagle's medium (DMEM, Lonza, MD, USA), supplemented with 10% fetal bovine serum (FBS, R&D systems, Minneapolis, MN) and 1X Glutamax (Fisher scientific) on glass slides, and several different external concentrations of Mg^{2+} with the purpose to establish the need of

Mg^{2+} post-BL stage. Individual outgrowths were imaged and manually marked the boundaries of ICM and TE cells.

Intracellular divalent cation imaging

Imaging for divalent cations in eggs and embryos was done as reported by our group(Ardestani et al., 2020) or following procedures published by others.(Kim et al., 2010; Tashiro et al., 2014) Eggs were pre-loaded with 1.25μM Ca^{2+} sensitive dye Fura-2-acetoxymethyl ester (Fura 2-AM; Invitrogen, Waltham, MA) in the presence of 0.02% pluronic acid (Thermo Fisher) for 10 min. Intracellular Zn^{2+} levels were measured using 1.25μM FluoZin^{TM}-3 AM and loaded for 20 min (Invitrogen), while Mg^{2+} was assessed using 0.6μM Mag-Fura-2 AM (Invitrogen) loaded for 5 min following the above procedures. The dye-loaded eggs were placed onto the bottom of glass-bottom dishes and given time to settle (Mat-Tek Corp., Ashland, MA). A group of eggs was monitored simultaneously using an inverted microscope (Nikon, Melville, NY) outfitted for fluorescence measurements. Fura-2 and Mag-Fura-2 were excited at 340 and 380 nm wavelengths, whereas FluoZin was at 480 nm, every 20s, and the light source was a 75-W Xenon arc lamp (Ludl Electronic Products Ltd., Hawthorne, NY). A cooled Photometrics SenSys CCD camera (Roper Scientific, Artisan Technology Group, Champaign, IL) collected the emitted light above 510 nm, and images were captured and processed using the Nikon NIS-Elements software.

Data analyses and plotting were performed using GraphPad Prism (GraphPad Software, San Diego, CA). F340/380 ratios were used to compare basal Ca^{2+} and Sr^{2+} concentrations among embryos from different genetic lines. Estimation of Zn^{2+} and Mg^{2+} levels between strains was carried out following normalization using the initial values of

each recorded egg/embryo (F_0), F_1/F_0 (Zn^{2+}), or the following the formula $(F_0-F_{max})/(F_{max}-F_{min})$ (Mg^{2+}).(Tashiro et al., 2014) The duration of the monitoring period depended on the experimental design but was as brief as 15 min and as long as 120 min for fertilization-induced responses. To assess sperm-induced Ca^{2+} oscillations, we used ZP-free eggs that reduced the time to fertilization. The ZP was removed following a short exposure to acid Tyrode's solution (pH=2.5). For these experiments, Fura 2-AM staining was as above, but Cell-Tak was used to coat the monitoring dishes and hold eggs in place during monitoring (Corning, Corning. NY). Sperm were added to final concentrations of ~$1.5x10^5$ mL^{-1} a few min after monitoring basal Ca^{2+}.

To compare intracellular Mg^{2+} concentrations among different embryo stages, we used two approaches to obtain embryos. At first, we collected *in vivo* fertilized embryos, cultured them for varied amounts of time until the 2, 4, and 8C stages, and monitored along freshly collected MIIs, which served as controls. In the second approach, *in vivo*, fertilized embryos following mating females at different times were flushed together, and we measured all embryo stages simultaneously, including MII eggs. Both approaches yielded the same results. Mg^{2+} was measured with the methods described above and in single blastomeres; blastomeres were isolated from others by 1h incubation in Ca^{2+}-free media supplemented with 500 μM of EDTA. Previously, the ZP was removed using Tyrode's acid.

Sperm analysis

Spermatozoa of *Trpm7*$^{fl/fl}$, *Trpm7*-Sp cKO and *Plcz*$^{-/-}$, *Plcd4*$^{-/-}$ and DKO were examined and compared following standard methods.(Tourzani et al., 2018) Sperm concentration and morphology were evaluated in non-capacitated (NCAP) spermatozoa

fixed after swimming out. After washing, they were resuspended in PBS, and 200 were analyzed per sample using contrast-phase microscopy at 400X. Sperm motility was determined in NCAP and in capacitated spermatozoa (CAP) by loading 35 µL into a pre-warmed chamber slide (Leja, 100 µm in depth) at 37 ºC. CEROS computer-assisted sperm analysis system, CASA (Hamilton Thorne Research, Beverly, MA), was used with the default setting to analyze at least five microscopy fields. The acrosome status in NCAP and CAP sperm was examined using fixed samples spread on poly-L-lysine treated slides and air-dried. Following permeabilization and washes, sperm were incubated with Alexa Fluor 488-conjugated PNA lectin (Invitrogen) 1:100 in PBS at RT and protected from light for one h. Slides were treated with mounting medium (Vectashield, Vector Laboratories, Newark, CA) and permanently mounted with coverslips sealed with nail polish.

Production of anti-TRPM7 monoclonal antibody

A monoclonal antibody, DA5C7-TRPM7, was produced in-house and generated against a bacterial fusion protein corresponding to the C-term portion of the cytoplasmic domain of mTRPM7 (amino acids 1159-1413). We followed standard hybridoma procedures and techniques described in the noted reference(Horr et al., 2023). Briefly, BalbC mice (Jackson Laboratories) were immunized with the TRPM7 protein. Following the production of hybridomas via electrofusion, these were screened by immunofluorescence using fixed *Xenopus*-XTC cells expressing *mTrpm7-GFP* (a kind gift from Dr. V. Chubanov, Ludwig-Maximilians-University of Munich, Germany). After the identification of candidate hybridomas, cells were subcloned and frozen. Identification and validation of the DA5C7-TRPM7 antibody were performed by Western blotting and immunofluorescence on XTC cells, followed by additional testing on mouse eggs and

sperm (WT, *Trpm7*-Oo cKO, and *Trpm7*-Sp cKO). The clones producing the DA5C7-TRPM7 antibody were further expanded and stored for future production.

Western blotting

Cell lysates from GV oocytes, MII eggs, and embryos (n=50 per lane and sample) from *Trpm7*$^{fl/fl}$ and *Trpm7*-null females and crosses were prepared by adding 2X-Laemmli sample buffer immediately after collection and frozen until use. Sperm proteins were extracted as described(Tourzani et al., 2018). Briefly, after swim-out, the sperm were centrifuged and washed in cold 1X PBS, centrifuged, resuspended in SDS-Laemmli buffer supplemented with β-mercaptoethanol, boiled for 4 min, and frozen until use. Whole tissue lysates were prepared as published by us(Wu et al., 1998). Upon thawing, samples were boiled, mixed well, separated on 6% SDS-PAGE gels, and transferred for 2 h to PVDF membranes (Millipore Sigma). After blocking with 5% fat-free milk in TPBS, the membranes were incubated overnight at 4°C with a monoclonal DA5C7-TRPM7 antibody. A goat anti-mouse IgG (Invitrogen) was used as the secondary antibody. After thoroughly washing the membranes, chemiluminescence detection was accomplished using ECL Prime (Sigma-Aldrich) and 1–5 min exposure to maximum sensitivity Kodak Biomax film (VWR, Radnor, PA), which was developed in an X-ray film processor (Optimax Protech Processor Technology, Germany). Noteworthy, to avoid substrate competition between gametes and embryos with widely different reactivities, after exposure to the secondary antibody, the membrane was divided into individual strips cut along vertical lines corresponding to the width of each well, incubated separately for 1 min in aliquots of an equal volume of the same ECL Prime master mix. The strips were reassembled as loaded in the gel and simultaneously exposed to the film. This approach enhanced signal detection

in all samples and stages. Broad-range pre-stained SDS–PAGE molecular weight markers (Bio-Rad) were run in parallel to estimate the molecular weight of the immunoreactive bands. These membranes were stripped at 50°C for 30 min (62.5 mM Tris, 2% SDS, and 100 mM 2-beta mercaptoethanol) and re-probed with anti-α-tubulin monoclonal antibody (Sigma-Aldrich, T9026, 1:1000), which was used as a loading control and to normalize the quantification procedures.

Preparation and microinjection of mRNA

pcDNA6-D1ER-KDEL, pcDNA6-*mTrpm7*^{wt}*-Gfp,* pcDNA6-*mTrpm7*^{K1646R}*-Gfp,* pcDNA6-*mTrpm7*^{P1040R}*-Gfp,* pcDNA6-*mTrpm7*^{1570Stop}*-Gfp, Plcz1-eGfp* and *Plcd4-eGfp* were linearized with the restriction enzyme *Pme1* and *in vitro* transcribed using the T7 mMESSAGE mMACHINE kit (Invitrogen) following procedures described in our previous studies.(Ardestani et al., 2020) A poly(A) tail was added to the *in vitro* synthesized RNA (mRNA) using a Tailing Kit, followed by quantification and dilution in nuclease-free water and stored at -80°C until use. Before microinjection, *mTrpm7-Gfp* mRNA was diluted in nuclease-free water to 1.0 μg/μl, heated at 95°C for 3 min, and centrifuged at 13,400×*g* for 10 min at 4°C. Cytoplasmic injection of mRNA was performed under a microscope equipped with micromanipulators (Narishige, Japan). The ZP and PM of zygotes were breached by applying small pulses generated by the piezo micromanipulator (Primetech, Ibaraki, Japan). Injections were performed with ICSI pipettes(Kurokawa & Fissore, 2003) but with a tip diameter of ~1 μm, and injected zygotes were monitored for development until the BL stage.

Immunostaining of gametes and embryos and confocal microscopy

Immunostaining was performed according to published protocols.(Akizawa et al., 2021; Paudel et al., 2019) Oocytes, eggs, and embryos were fixed with 4% (w/v) PFA in phosphate-buffered saline (PBS) for 20 min at RT and permeabilized for 60 min with 0.2% (v/v) Triton X-100 in PBS. Sperm were handled as above, but upon fixation, were placed onto poly-lysine coated coverslips and air dried for 15 min. The samples were blocked for 45 min in a buffer containing 0.2% (w/v) skim milk, 2% (v/v) fetal bovine serum, 1% (w/v) bovine serum albumin, 0.1% (v/v) TritonX-100, 0.75% (w/v) glycine in PBS. Gametes and embryos were incubated overnight at 4°C with mouse anti-TRPM7 antibody (1:1000) diluted in blocking buffer, followed by washes in 3X blocking buffer for 10 min, incubation at RT for 30 min with the secondary antibody Alexa Fluor 488 goat anti-mouse IgG (H + L) (1:400; (Invitrogen) diluted in blocking buffer that contained rhodamine-Phalloidin (1:100, Invitrogen) and Hoechst 33342 (1:100, Thermo Fisher). The secondary antibody mixture for sperm included Lectin-PNA (Invitrogen, L32458, 1:100) instead of rhodamine phalloidin, was incubated for one h and followed by mounting on coverslips using Vectashield mounting solution (Vector Laboratories). For lipid vesicle staining, fixed and permeabilized BLs were incubated with 10 μg/ml BODIPY (Invitrogen) for 30min. For the detection of apoptotic cells, we used the TUNEL Assay Apoptosis Detection Kit (30074, Biotium) following the manufacturer's protocol and instructions. Briefly, fixed and permeabilized BLs were incubated with the TUNEL reaction buffer and TdT enzyme for 1 h at 37°C, washed 3X 5min followed by 10min staining with Hoechst 33342 (1:100, Thermo Fisher). A laser-scanning confocal microscope (Nikon A1 Resonant Confocal with six-color TIRF) fitted with a 63X 1.4 NA oil-immersion objective lens was used to visualize the fluorescence signals.

Determination of mitochondrial membrane potential

To assess the status of the mitochondria as an estimation of the embryos' oxidative stress, we evaluated their membrane potential using the JC-1 assay (Abcam, Cambridge, UK). The procedure was carried out as per the manufacturer's instructions. Briefly, eggs and embryos were incubated with JC-1 (10 μM) in KSOM for 30 min at 37°C in the dark. Eggs and embryos were then washed and imaged immediately using confocal microscopy, as described above. The red-to-green fluorescence ratio was averaged for ten z-sections and quantified using ImageJ.

Egg and embryo RNA isolation and sequencing

RNA was sequenced from eggs or embryos from zygotes to BLs. Four biological replicates at each stage for each group were sequenced. Each biological replicate consisted of five eggs or embryos. Following collection as described, eggs and embryos were washed in sterile PBS and snap-frozen on dry ice. RNA was prepared using the SMART-Seq v4 Ultra Low Input RNA Kit (Takara Bio, Japan), and cDNA was purified using the Agencourt AMPure XP kit (Beckman Coulter). RNA quality and yield were measured using the Agilent 2100 Bioanalyzer (Agilent Technologies). Library preparation was carried out on 100-150 pg amplified cDNA using the Illumina DNA Prep kit (Illumina, San Diego, CA). Sequencing was performed on a NovaSeq 6000 Sequencing System (Illumina).

RNA-seq data processing and analysis

Adapter and low-quality tails were removed from sequenced reads using Cutadapt (v3.7)(M, 2011) prior to alignment to the reference genome using STAR (v2.6.0c).(Dobin et al., 2013) RNA abundance was quantified using uniquely mapped reads only with feature Counts (v1.6.3)(Liao et al., 2014) and GENCODE mouse reference GRCm38 vM17. For

each set of replicates, the sample with the lowest number of gene-associated reads was removed from downstream analysis. The sequencing data generated in this study have been deposited in the Gene Expression Omnibus database and will be publicly available as of the date of publication.

Differential expression between experimental groups was carried out using DESeq2 (v1.34.0),(Love et al., 2014). Hierarchical clustering was performed using the R function Hclust with Euclidean distances between variance-stabilizing transformed count data. Visualization was carried out by transforming this data to z-scores within comparison sets prior to heatmap generation. DEGs were analyzed using Ingenuity Pathway Analysis (Qiagen, Germantown, MD). Canonical pathways and upstream regulators were filtered for $p<0.05$ and >2 molecules.

Quantification and statistical analysis

Comparisons for statistical significance of experimental values between treatments and experiments were performed with at least three experiments on different batches of gametes or embryos. Data were compared using SPSS Statistics (v.20) or GraphPad software packages, including *Student's t-test*, One-Way ANOVA followed by multiple comparisons Tukey post-hoc test, or Fisher's exact Chi-Square test, depending on the experiment and type of data analyzed. In addition, the number of replicates and statistical analyses used are indicated in the figure and table legends. The numerical data are presented as mean ± s.d. Significant differences were considered when *P<0.05, **P<0.01, ***P<0.001, or ****P<0.0001.

REFERENCES

Abiria, S. A., Krapivinsky, G., Sah, R., Santa-Cruz, A. G., Chaudhuri, D., Zhang, J., Adstamongkonkul, P., DeCaen, P. G., & Clapham, D. E. (2017). TRPM7 senses oxidative stress to release Zn(2+) from unique intracellular vesicles. *Proc Natl Acad Sci U S A*, *114*(30), E6079-e6088. https://doi.org/10.1073/pnas.1707380114

Akizawa, H., Saito, S., Kohri, N., Furukawa, E., Hayashi, Y., Bai, H., Nagano, M., Yanagawa, Y., Tsukahara, H., Takahashi, M., Kagawa, S., Kawahara-Miki, R., Kobayashi, H., Kono, T., & Kawahara, M. (2021). Deciphering two rounds of cell lineage segregations during bovine preimplantation development. *Faseb j*, *35*(10), e21904. https://doi.org/10.1096/fj.202002762RR

Ardestani, G., Mehregan, A., Fleig, A., Horgen, F. D., Carvacho, I., & Fissore, R. A. (2020). Divalent cation influx and calcium homeostasis in germinal vesicle mouse oocytes. *Cell Calcium*, *87*, 102181. https://doi.org/10.1016/j.ceca.2020.102181

Bernhardt, M. L., Padilla-Banks, E., Stein, P., Zhang, Y., & Williams, C. J. (2017). Store-operated Ca(2+) entry is not required for fertilization-induced Ca(2+) signaling in mouse eggs. *Cell Calcium*, *65*, 63-72. https://doi.org/10.1016/j.ceca.2017.02.004

Bernhardt, M. L., Stein, P., Carvacho, I., Krapp, C., Ardestani, G., Mehregan, A., Umbach, D. M., Bartolomei, M. S., Fissore, R. A., & Williams, C. J. (2018). TRPM7 and Ca(V)3.2 channels mediate Ca(2+) influx required for egg activation at fertilization. *Proc Natl Acad Sci U S A*, *115*(44), E10370-e10378. https://doi.org/10.1073/pnas.1810422115

Bernhardt, M. L., Zhang, Y., Erxleben, C. F., Padilla-Banks, E., McDonough, C. E., Miao, Y. L., Armstrong, D. L., & Williams, C. J. (2015). CaV3.2 T-type channels mediate Ca^{2+} entry during oocyte maturation and following fertilization. *J Cell Sci*, *128*(23), 4442-4452. https://doi.org/10.1242/jcs.180026

Brinster, R. L. (1967). PROTEIN CONTENT OF THE MOUSE EMBRYO DURING THE FIRST FIVE DAYS OF DEVELOPMENT. *Reproduction*, *13*(3), 413-420. https://doi.org/10.1530/jrf.0.0130413

Burkart, A. D., Xiong, B., Baibakov, B., Jiménez-Movilla, M., & Dean, J. (2012). Ovastacin, a cortical granule protease, cleaves ZP2 in the zona pellucida to prevent polyspermy. *J Cell Biol*, *197*(1), 37-44. https://doi.org/10.1083/jcb.201112094

Cai, N., Bai, Z., Nanda, V., & Runnels, L. W. (2017). Mass Spectrometric Analysis of TRPM6 and TRPM7 Phosphorylation Reveals Regulatory Mechanisms of the Channel-Kinases. *Sci Rep*, *7*, 42739. https://doi.org/10.1038/srep42739

Carvacho, I., Ardestani, G., Lee, H. C., McGarvey, K., Fissore, R. A., & Lykke-Hartmann, K. (2016). TRPM7-like channels are functionally expressed in oocytes and modulate post-fertilization embryo development in mouse. *Sci Rep*, *6*, 34236. https://doi.org/10.1038/srep34236

Carvacho, I., Lee, H. C., Fissore, R. A., & Clapham, D. E. (2013). TRPV3 channels mediate strontium-induced mouse-egg activation. *Cell Rep*, *5*(5), 1375-1386. https://doi.org/10.1016/j.celrep.2013.11.007

Cheng, F. P., Fazeli, A., Voorhout, W. F., Marks, A., Bevers, M. M., & Colenbrander, B. (1996). Use of peanut agglutinin to assess the acrosomal status and the zona pellucida-induced acrosome reaction in stallion spermatozoa. *J Androl*, *17*(6), 674-682.

Chubanov, V., Ferioli, S., Wisnowsky, A., Simmons, D. G., Leitzinger, C., Einer, C., Jonas, W., Shymkiv, Y., Bartsch, H., Braun, A., Akdogan, B., Mittermeier, L., Sytik, L., Torben, F., Jurinovic, V., van der Vorst, E. P., Weber, C., Yildirim Ö, A., Sotlar, K., . . . Gudermann, T.

(2016). Epithelial magnesium transport by TRPM6 is essential for prenatal development and adult survival. *Elife*, *5*. https://doi.org/10.7554/eLife.20914

Chubanov, V., Schlingmann, K. P., Wäring, J., Heinzinger, J., Kaske, S., Waldegger, S., Mederos y Schnitzler, M., & Gudermann, T. (2007). Hypomagnesemia with secondary hypocalcemia due to a missense mutation in the putative pore-forming region of TRPM6. *J Biol Chem*, *282*(10), 7656-7667. https://doi.org/10.1074/jbc.M611117200

Clark, K., Middelbeek, J., Dorovkov, M. V., Figdor, C. G., Ryazanov, A. G., Lasonder, E., & van Leeuwen, F. N. (2008). The alpha-kinases TRPM6 and TRPM7, but not eEF-2 kinase, phosphorylate the assembly domain of myosin IIA, IIB and IIC. *FEBS Lett*, *582*(20), 2993-2997. https://doi.org/10.1016/j.febslet.2008.07.043

Dai, J., Zhang, T., Guo, J., Zhou, Q., Gu, Y., Zhang, J., Hu, L., Zong, Y., Song, J., Zhang, S., Dai, C., Gong, F., Lu, G., Zheng, W., & Lin, G. (2021). Homozygous pathogenic variants in ACTL9 cause fertilization failure and male infertility in humans and mice. *Am J Hum Genet*, *108*(3), 469-481. https://doi.org/10.1016/j.ajhg.2021.02.004

Dale, B. (1988). Primary and secondary messengers in the activation of ascidian eggs. *Exp Cell Res*, *177*(1), 205-211. https://doi.org/10.1016/0014-4827(88)90038-9

Dale, B., DeFelice, L. J., & Ehrenstein, G. (1985). Injection of a soluble sperm fraction into sea-urchin eggs triggers the cortical reaction. *Experientia*, *41*(8), 1068-1070. https://doi.org/10.1007/BF01952148

de Baaij, J. H. (2015). The art of magnesium transport. *Magnes Res*, *28*(3), 85-91. https://doi.org/10.1684/mrh.2015.0388

Desai, B. N., Krapivinsky, G., Navarro, B., Krapivinsky, L., Carter, B. C., Febvay, S., Delling, M., Penumaka, A., Ramsey, I. S., Manasian, Y., & Clapham, D. E. (2012). Cleavage of TRPM7 releases the kinase domain from the ion channel and regulates its participation in Fas-induced apoptosis. *Dev Cell*, *22*(6), 1149-1162. https://doi.org/10.1016/j.devcel.2012.04.006

Dobin, A., Davis, C. A., Schlesinger, F., Drenkow, J., Zaleski, C., Jha, S., Batut, P., Chaisson, M., & Gingeras, T. R. (2013). STAR: ultrafast universal RNA-seq aligner. *Bioinformatics*, *29*(1), 15-21. https://doi.org/10.1093/bioinformatics/bts635

Ducibella, T., & Matson, S. (2007). Secretory mechanisms and Ca2+ signaling in gametes: similarities to regulated neuroendocrine secretion in somatic cells and involvement in emerging pathologies. *Endocr Pathol*, *18*(4), 191-203. https://doi.org/10.1007/s12022-007-0015-7

Dufner-Beattie, J., Weaver, B. P., Geiser, J., Bilgen, M., Larson, M., Xu, W., & Andrews, G. K. (2007). The mouse acrodermatitis enteropathica gene Slc39a4 (Zip4) is essential for early development and heterozygosity causes hypersensitivity to zinc deficiency. *Hum Mol Genet*, *16*(12), 1391-1399. https://doi.org/10.1093/hmg/ddm088

Elizondo, M. R., Arduini, B. L., Paulsen, J., MacDonald, E. L., Sabel, J. L., Henion, P. D., Cornell, R. A., & Parichy, D. M. (2005). Defective skeletogenesis with kidney stone formation in dwarf zebrafish mutant for trpm7. *Curr Biol*, *15*(7), 667-671. https://doi.org/10.1016/j.cub.2005.02.050

Escoffier, J., Lee, H. C., Yassine, S., Zouari, R., Martinez, G., Karaouzène, T., Coutton, C., Kherraf, Z. E., Halouani, L., Triki, C., Nef, S., Thierry-Mieg, N., Savinov, S. N., Fissore, R., Ray, P. F., & Arnoult, C. (2016). Homozygous mutation of PLCZ1 leads to defective human oocyte activation and infertility that is not rescued by the WW-binding protein PAWP. *Hum Mol Genet*, *25*(5), 878-891. https://doi.org/10.1093/hmg/ddv617

Franken, G. A. C., Huynen, M. A., Martínez-Cruz, L. A., Bindels, R. J. M., & de Baaij, J. H. F. (2022). Structural and functional comparison of magnesium transporters throughout evolution. *Cell Mol Life Sci*, *79*(8), 418. https://doi.org/10.1007/s00018-022-04442-8

Fukami, K., Nakao, K., Inoue, T., Kataoka, Y., Kurokawa, M., Fissore, R. A., Nakamura, K., Katsuki, M., Mikoshiba, K., Yoshida, N., & Takenawa, T. (2001). Requirement of phospholipase Cdelta4 for the zona pellucida-induced acrosome reaction. *Science*, *292*(5518), 920-923. https://doi.org/10.1126/science.1059042

Fukami, K., Yoshida, M., Inoue, T., Kurokawa, M., Fissore, R. A., Yoshida, N., Mikoshiba, K., & Takenawa, T. (2003). Phospholipase Cdelta4 is required for Ca2+ mobilization essential for acrosome reaction in sperm. *J Cell Biol*, *161*(1), 79-88. https://doi.org/10.1083/jcb.200210057

Galione, A., Jones, K. T., Lai, F. A., & Swann, K. (1997). A cytosolic sperm protein factor mobilizes Ca2+ from intracellular stores by activating multiple Ca2+ release mechanisms independently of low molecular weight messengers. *J Biol Chem*, *272*(46), 28901-28905. https://doi.org/10.1074/jbc.272.46.28901

Govin, J., Caron, C., Escoffier, E., Ferro, M., Kuhn, L., Rousseaux, S., Eddy, E. M., Garin, J., & Khochbin, S. (2006). Post-meiotic shifts in HSPA2/HSP70.2 chaperone activity during mouse spermatogenesis. *J Biol Chem*, *281*(49), 37888-37892. https://doi.org/10.1074/jbc.M608147200

Grasa, P., Coward, K., Young, C., & Parrington, J. (2008). The pattern of localization of the putative oocyte activation factor, phospholipase Czeta, in uncapacitated, capacitated, and ionophore-treated human spermatozoa. *Hum Reprod*, *23*(11), 2513-2522. https://doi.org/10.1093/humrep/den280

Hachem, A., Godwin, J., Ruas, M., Lee, H. C., Ferrer Buitrago, M., Ardestani, G., Bassett, A., Fox, S., Navarrete, F., de Sutter, P., Heindryckx, B., Fissore, R., & Parrington, J. (2017a). PLCzeta is the physiological trigger of the Ca(2+) oscillations that induce embryogenesis in mammals but conception can occur in its absence. *Development*, *144*(16), 2914-2924. https://doi.org/10.1242/dev.150227

Hachem, A., Godwin, J., Ruas, M., Lee, H. C., Ferrer Buitrago, M., Ardestani, G., Bassett, A., Fox, S., Navarrete, F., de Sutter, P., Heindryckx, B., Fissore, R., & Parrington, J. (2017b). PLCζ is the physiological trigger of the Ca(2+) oscillations that induce embryogenesis in mammals but conception can occur in its absence. *Development*, *144*(16), 2914-2924. https://doi.org/10.1242/dev.150227

Hanano, T., Hara, Y., Shi, J., Morita, H., Umebayashi, C., Mori, E., Sumimoto, H., Ito, Y., Mori, Y., & Inoue, R. (2004). Involvement of TRPM7 in cell growth as a spontaneously activated Ca2+ entry pathway in human retinoblastoma cells. *J Pharmacol Sci*, *95*(4), 403-419. https://doi.org/10.1254/jphs.fp0040273

Hara, T., Yoshigai, E., Ohashi, T., & Fukada, T. (2022). Zinc transporters as potential therapeutic targets: An updated review. *J Pharmacol Sci*, *148*(2), 221-228. https://doi.org/10.1016/j.jphs.2021.11.007

Harbuz, R., Zouari, R., Pierre, V., Ben Khelifa, M., Kharouf, M., Coutton, C., Merdassi, G., Abada, F., Escoffier, J., Nikas, Y., & al., e. (2011). A recurrent deletion of DPY19L2 causes infertility in man by blocking sperm head elongation and acrosome formation. *Am J Hum Genet*, *88*(3), 351-361. https://doi.org/10.1016/j.ajhg.2011.02.007

Horr, B., Kurtz, R., Pandey, A., Hoffstrom, B. G., Schock, E., LaBonne, C., & Alfandari, D. (2023). Production and characterization of monoclonal antibodies to Xenopus proteins. *Development*, *150*(4). https://doi.org/10.1242/dev.201309

Inselman, A. L., Nakamura, N., Brown, P. R., Willis, W. D., Goulding, E. H., & Eddy, E. M. (2010). Heat shock protein 2 promoter drives Cre expression in spermatocytes of transgenic mice. *Genesis*, *48*(2), 114-120. https://doi.org/10.1002/dvg.20588

Iritani, A., Utsumi, K., Miyake, M., Hosoi, Y., & K., S. (1988). In vitro fertilization by a routine method and by micromanipulation. *Ann N Y Acad Sci.*, *541*, 583-590.

Ito, M., Shikano, T., Kuroda, K., & Miyazaki, S. (2008). Relationship between nuclear sequestration of PLCzeta and termination of PLCzeta-induced Ca2+ oscillations in mouse eggs. *Cell Calcium*, *44*(4), 400-410. https://doi.org/10.1016/j.ceca.2008.02.003

Jaffe, L. A., & Egbert, J. R. (2017). Regulation of Mammalian Oocyte Meiosis by Intercellular Communication Within the Ovarian Follicle. *Annu Rev Physiol*, *79*, 237-260. https://doi.org/10.1146/annurev-physiol-022516-034102

Ji, Q. S., Winnier, G. E., Niswender, K. D., Horstman, D., Wisdom, R., Magnuson, M. A., & Carpenter, G. (1997). Essential role of the tyrosine kinase substrate phospholipase C-gamma1 in mammalian growth and development. *Proc Natl Acad Sci U S A*, *94*(7), 2999-3003. https://doi.org/10.1073/pnas.94.7.2999

Jin, J., Desai, B. N., Navarro, B., Donovan, A., Andrews, N. C., & Clapham, D. E. (2008). Deletion of Trpm7 disrupts embryonic development and thymopoiesis without altering Mg2+ homeostasis. *Science*, *322*(5902), 756-760. https://doi.org/10.1126/science.1163493

Jin, J., Wu, L. J., Jun, J., Cheng, X., Xu, H., Andrews, N. C., & Clapham, D. E. (2012). The channel kinase, TRPM7, is required for early embryonic development. *Proc Natl Acad Sci U S A*, *109*(5), E225-233. https://doi.org/10.1073/pnas.1120033109

Johnson, M. H., & Ziomek, C. A. (1983). Cell interactions influence the fate of mouse blastomeres undergoing the transition from the 16- to the 32-cell stage. *Dev Biol*, *95*(1), 211-218. https://doi.org/10.1016/0012-1606(83)90019-2

Jones, K. T. (2007). Intracellular calcium in the fertilization and development of mammalian eggs. *Clin Exp Pharmacol Physiol*, *34*(10), 1084-1089. https://doi.org/10.1111/j.1440-1681.2007.04726.x

Jones, K. T. (2018). Mammalian sperm contain two factors for calcium release and egg activation: Phospholipase C zeta and a cryptic activating factor. *Mol Hum Reprod*, *24*(10), 465-468. https://doi.org/10.1093/molehr/gay038

Jones, K. T., Matsuda, M., Parrington, J., Katan, M., & Swann, K. (2000). Different Ca2+-releasing abilities of sperm extracts compared with tissue extracts and phospholipase C isoforms in sea urchin egg homogenate and mouse eggs. *Biochem J*, *346 Pt 3*, 743-749. https://www.ncbi.nlm.nih.gov/pubmed/10698702

Kambe, T., Tsuji, T., Hashimoto, A., & Itsumura, N. (2015). The Physiological, Biochemical, and Molecular Roles of Zinc Transporters in Zinc Homeostasis and Metabolism. *Physiol Rev*, *95*(3), 749-784. https://doi.org/10.1152/physrev.00035.2014

Kang, W., Harada, Y., Yamatoya, K., Kawano, N., Kanai, S., Miyamoto, Y., Nakamura, A., Miyado, M., Hayashi, Y., Kuroki, Y., Saito, H., Iwao, Y., Umezawa, A., & Miyado, K. (2020). Extra-mitochondrial citrate synthase initiates calcium oscillation and suppresses age-dependent sperm dysfunction. *Lab Invest*, *100*(4), 583-595. https://doi.org/10.1038/s41374-019-0353-3

Kashir, J., Nomikos, M., Lai, F. A., & Swann, K. (2014). Sperm-induced Ca2+ release during egg activation in mammals. *Biochem Biophys Res Commun*, *450*(3), 1204-1211. https://doi.org/10.1016/j.bbrc.2014.04.078

Kashir, J., Nomikos, M., Swann, K., & Lai, F. A. (2015). PLCζ or PAWP: revisiting the putative mammalian sperm factor that triggers egg activation and embryogenesis. *Mol Hum Reprod*, *21*(5), 383-388. https://doi.org/10.1093/molehr/gav009

Kim, A. M., Bernhardt, M. L., Kong, B. Y., Ahn, R. W., Vogt, S., Woodruff, T. K., & O'Halloran, T. V. (2011). Zinc sparks are triggered by fertilization and facilitate cell cycle resumption in mammalian eggs. *ACS Chem Biol*, *6*(7), 716-723. https://doi.org/10.1021/cb200084y

Kim, A. M., Vogt, S., O'Halloran, T. V., & Woodruff, T. K. (2010). Zinc availability regulates exit from meiosis in maturing mammalian oocytes. *Nat Chem Biol*, *6*(9), 674-681. https://doi.org/10.1038/nchembio.419

Knott, J. G., Kurokawa, M., & Fissore, R. A. (2003). Release of the Ca(2+) oscillation-inducing sperm factor during mouse fertilization. *Dev Biol*, *260*(2), 536-547. https://doi.org/10.1016/s0012-1606(03)00251-3

Komiya, Y., Mandrekar, N., Sato, A., Dawid, I. B., & Habas, R. (2014). Custos controls β-catenin to regulate head development during vertebrate embryogenesis. *Proc Natl Acad Sci U S A*, *111*(36), 13099-13104. https://doi.org/10.1073/pnas.1414437111

Kong, B. Y., Duncan, F. E., Que, E. L., Kim, A. M., O'Halloran, T. V., & Woodruff, T. K. (2014). Maternally-derived zinc transporters ZIP6 and ZIP10 drive the mammalian oocyte-to-egg transition. *Mol Hum Reprod*, *20*(11), 1077-1089. https://doi.org/10.1093/molehr/gau066

Kono, T., Carroll, J., Swann, K., & Whittingham, D. G. (1995). Nuclei from fertilized mouse embryos have calcium-releasing activity. *Development*, *121*(4), 1123-1128. https://www.ncbi.nlm.nih.gov/pubmed/7743925

Krapivinsky, G., Krapivinsky, L., Manasian, Y., & Clapham, D. E. (2014). The TRPM7 chanzyme is cleaved to release a chromatin-modifying kinase. *Cell*, *157*(5), 1061-1072. https://doi.org/10.1016/j.cell.2014.03.046

Krauchunas, A. R., & Wolfner, M. F. (2013). Molecular changes during egg activation. *Curr Top Dev Biol*, *102*, 267-292. https://doi.org/10.1016/b978-0-12-416024-8.00010-6

Kunert-Keil, C., Bisping, F., Krüger, J., & Brinkmeier, H. (2006). Tissue-specific expression of TRP channel genes in the mouse and its variation in three different mouse strains. *BMC Genomics*, *7*, 159. https://doi.org/10.1186/1471-2164-7-159

Kurokawa, M., & Fissore, R. A. (2003). ICSI-generated mouse zygotes exhibit altered calcium oscillations, inositol 1,4,5-trisphosphate receptor-1 down-regulation, and embryo development. *Mol Hum Reprod*, *9*(9), 523-533. https://doi.org/10.1093/molehr/gag072

Kurokawa, M., Sato, K., Wu, H., He, C., Malcuit, C., Black, S. J., Fukami, K., & Fissore, R. A. (2005). Functional, biochemical, and chromatographic characterization of the complete [Ca2+]i oscillation-inducing activity of porcine sperm. *Dev Biol*, *285*(2), 376-392. https://doi.org/10.1016/j.ydbio.2005.06.029

Larman, M. G., Saunders, C. M., Carroll, J., Lai, F. A., & Swann, K. (2004). Cell cycle-dependent Ca2+ oscillations in mouse embryos are regulated by nuclear targeting of PLCzeta. *J Cell Sci*, *117*(Pt 12), 2513-2521. https://doi.org/10.1242/jcs.01109

Li, M., Jiang, J., & Yue, L. (2006). Functional characterization of homo- and heteromeric channel kinases TRPM6 and TRPM7. *J Gen Physiol*, *127*(5), 525-537. https://doi.org/10.1085/jgp.200609502

Liao, Y., Smyth, G. K., & Shi, W. (2014). featureCounts: an efficient general purpose program for assigning sequence reads to genomic features. *Bioinformatics*, *30*(7), 923-930. https://doi.org/10.1093/bioinformatics/btt656

Lichten, L. A., & Cousins, R. J. (2009). Mammalian zinc transporters: nutritional and physiologic regulation. *Annu Rev Nutr*, *29*, 153-176. https://doi.org/10.1146/annurev-nutr-033009-083312

Liu, W., Su, L. T., Khadka, D. K., Mezzacappa, C., Komiya, Y., Sato, A., Habas, R., & Runnels, L. W. (2011). TRPM7 regulates gastrulation during vertebrate embryogenesis. *Dev Biol*, *350*(2), 348-357. https://doi.org/10.1016/j.ydbio.2010.11.034

Love, M. I., Huber, W., & Anders, S. (2014). Moderated estimation of fold change and dispersion for RNA-seq data with DESeq2. *Genome Biol*, *15*(12), 550. https://doi.org/10.1186/s13059-014-0550-8

M, M. (2011). Cutadapt removes adapter sequences from high-throughput sequencing reads.

Mazur, A., Maier, J. A., Rock, E., Gueux, E., Nowacki, W., & Rayssiguier, Y. (2007). Magnesium and the inflammatory response: potential physiopathological implications. *Arch Biochem Biophys*, *458*(1), 48-56. https://doi.org/10.1016/j.abb.2006.03.031

Mehregan, A., Ardestani, G., Akizawa, H., Carvacho, I., & Fissore, R. (2021). Deletion of TRPV3 and CaV3.2 T-type channels in mice undermines fertility and Ca2+ homeostasis in oocytes and eggs. *J Cell Sci*, *134*(13). https://doi.org/10.1242/jcs.257956

Messerschmidt, D. M., Knowles, B. B., & Solter, D. (2014). DNA methylation dynamics during epigenetic reprogramming in the germline and preimplantation embryos. *Genes Dev*, *28*(8), 812-828. https://doi.org/10.1101/gad.234294.113

Miao, X., Sun, T., Golan, M., Mager, J., & Cui, W. (2020). Loss of POLR1D results in embryonic lethality prior to blastocyst formation in mice. *Mol Reprod Dev*, *87*(11), 1152-1158. https://doi.org/10.1002/mrd.23427

Middelbeek, J., Kuipers, A. J., Henneman, L., Visser, D., Eidhof, I., van Horssen, R., Wieringa, B., Canisius, S. V., Zwart, W., Wessels, L. F., Sweep, F. C., Bult, P., Span, P. N., van Leeuwen, F. N., & Jalink, K. (2012). TRPM7 is required for breast tumor cell metastasis. *Cancer Res*, *72*(16), 4250-4261. https://doi.org/10.1158/0008-5472.Can-11-3863

Mishieva, N., Martazanova, B., Bogatyreva, K., Korolkova, A., Kirillova, A., Veyukova, M., Burmenskaya, O., Abubakirov, A., & Sukhikh, G. T. (2020). Cumulus cell gene expression in luteal-phase-derived oocytes after double stimulation in one menstrual cycle. *Reprod Biomed Online*, *41*(3), 518-526. https://doi.org/10.1016/j.rbmo.2020.05.002

Mittermeier, L., Demirkhanyan, L., Stadlbauer, B., Breit, A., Recordati, C., Hilgendorff, A., Matsushita, M., Braun, A., Simmons, D. G., Zakharian, E., Gudermann, T., & Chubanov, V. (2019). TRPM7 is the central gatekeeper of intestinal mineral absorption essential for postnatal survival. *Proc Natl Acad Sci U S A*, *116*(10), 4706-4715. https://doi.org/10.1073/pnas.1810633116

Miyazaki, S. (1993). IP3 receptor-mediated spatial and temporal Ca2+ signaling of the cell. *Jpn J Physiol*, *43*(4), 409-434. https://doi.org/10.2170/jjphysiol.43.409

Miyazaki, S., & Ito, M. (2006). Calcium signals for egg activation in mammals. *J Pharmacol Sci*, *100*(5), 545-552. https://doi.org/10.1254/jphs.cpj06003x

Monteilh-Zoller, M. K., Hermosura, M. C., Nadler, M. J., Scharenberg, A. M., Penner, R., & Fleig, A. (2003). TRPM7 provides an ion channel mechanism for cellular entry of trace metal ions. *J Gen Physiol*, *121*(1), 49-60. https://doi.org/10.1085/jgp.20028740

Nadler, M. J., Hermosura, M. C., Inabe, K., Perraud, A. L., Zhu, Q., Stokes, A. J., Kurosaki, T., Kinet, J. P., Penner, R., Scharenberg, A. M., & Fleig, A. (2001). LTRPC7 is a Mg.ATP-regulated divalent cation channel required for cell viability. *Nature*, *411*(6837), 590-595. https://doi.org/10.1038/35079092

Nakamura, Y., & Fukami, K. (2017). Regulation and physiological functions of mammalian phospholipase C. *J Biochem*, *161*(4), 315-321. https://doi.org/10.1093/jb/mvw094

Navarrete, F. A., Aguila, L., Martin-Hidalgo, D., Tourzani, D. A., Luque, G. M., Ardestani, G., Garcia-Vazquez, F. A., Levin, L. R., Buck, J., Darszon, A., Buffone, M. G., Mager, J., Fissore, R. A., Salicioni, A. M., Gervasi, M. G., & Visconti, P. E. (2019). Transient Sperm Starvation Improves the Outcome of Assisted Reproductive Technologies. *Front Cell Dev Biol*, *7*, 262. https://doi.org/10.3389/fcell.2019.00262

Nozawa, K., Satouh, Y., Fujimoto, T., Oji, A., & Ikawa, M. (2018). Sperm-borne phospholipase C zeta-1 ensures monospermic fertilization in mice. *Sci Rep*, *8*(1), 1315. https://doi.org/10.1038/s41598-018-19497-6

Ozil, J. P., Sainte-Beuve, T., & Banrezes, B. (2017). [Mg(2+)](o)/[Ca(2+)](o) determines Ca(2+) response at fertilization: tuning of adult phenotype? *Reproduction*, *154*(5), 675-693. https://doi.org/10.1530/rep-16-0057

Palermo, G., Joris, H., Devroey, P., & Van Steirteghem, A. C. (1992). Pregnancies after intracytoplasmic injection of single spermatozoon into an oocyte. *Lancet*, *340*(8810), 17-18. https://doi.org/10.1016/0140-6736(92)92425-f

Palmer, A. E., Jin, C., Reed, J. C., & Tsien, R. Y. (2004). Bcl-2-mediated alterations in endoplasmic reticulum Ca2+ analyzed with an improved genetically encoded fluorescent sensor. *Proc Natl Acad Sci U S A*, *101*(50), 17404-17409. https://doi.org/10.1073/pnas.0408030101

Park, S. J., Shirahige, K., Ohsugi, M., & Nakai, K. (2015). DBTMEE: a database of transcriptome in mouse early embryos. *Nucleic Acids Res*, *43*(Database issue), D771-776. https://doi.org/10.1093/nar/gku1001

Paudel, B., Gervasi, M. G., Porambo, J., Caraballo, D. A., Tourzani, D. A., Mager, J., Platt, M. D., Salicioni, A. M., & Visconti, P. E. (2019). Sperm capacitation is associated with phosphorylation of the testis-specific radial spoke protein Rsph6a^{+}. *Biol Reprod*, *100*(2), 440-454. https://doi.org/10.1093/biolre/ioy202

Peres, A. (1987). The calcium current of mouse egg measured in physiological calcium and temperature conditions. *J Physiol*, *391*, 573-588. https://doi.org/10.1113/jphysiol.1987.sp016757

Rice, A., Parrington, J., Jones, K. T., & Swann, K. (2000). Mammalian sperm contain a Ca(2+)-sensitive phospholipase C activity that can generate InsP(3) from PIP(2) associated with intracellular organelles. *Dev Biol*, *228*(1), 125-135. https://doi.org/10.1006/dbio.2000.9929

Rivera, R. M., & Ross, J. W. (2013). Epigenetics in fertilization and preimplantation embryo development. *Prog Biophys Mol Biol*, *113*(3), 423-432. https://doi.org/10.1016/j.pbiomolbio.2013.02.001

Romani, A. M. (2011). Cellular magnesium homeostasis. *Arch Biochem Biophys*, *512*(1), 1-23. https://doi.org/10.1016/j.abb.2011.05.010

Runft, L. L., Jaffe, L. A., & Mehlmann, L. M. (2002). Egg activation at fertilization: where it all begins. *Dev Biol*, *245*(2), 237-254. https://doi.org/10.1006/dbio.2002.0600

Runnels, L. W., Yue, L., & Clapham, D. E. (2001). TRP-PLIK, a bifunctional protein with kinase and ion channel activities. *Science*, *291*(5506), 1043-1047. https://doi.org/10.1126/science.1058519

Ryazanova, L. V., Hu, Z., Suzuki, S., Chubanov, V., Fleig, A., & Ryazanov, A. G. (2014). Elucidating the role of the TRPM7 alpha-kinase: TRPM7 kinase inactivation leads to magnesium deprivation resistance phenotype in mice. *Sci Rep*, *4*, 7599. https://doi.org/10.1038/srep07599

Ryazanova, L. V., Rondon, L. J., Zierler, S., Hu, Z., Galli, J., Yamaguchi, T. P., Mazur, A., Fleig, A., & Ryazanov, A. G. (2010). TRPM7 is essential for Mg(2+) homeostasis in mammals. *Nat Commun*, *1*, 109. https://doi.org/10.1038/ncomms1108

Sahni, J., Tamura, R., Sweet, I. R., & Scharenberg, A. M. (2010). TRPM7 regulates quiescent/proliferative metabolic transitions in lymphocytes. *Cell Cycle*, *9*(17), 3565-3574. https://doi.org/10.4161/cc.9.17.12798

Saunders, C. M., Larman, M. G., Parrington, J., Cox, L. J., Royse, J., Blayney, L. M., Swann, K., & Lai, F. A. (2002). PLC zeta: a sperm-specific trigger of Ca(2+) oscillations in eggs and embryo

development. *Development*, *129*(15), 3533-3544. https://www.ncbi.nlm.nih.gov/pubmed/12117804

Schmitz, C., Perraud, A. L., Johnson, C. O., Inabe, K., Smith, M. K., Penner, R., Kurosaki, T., Fleig, A., & Scharenberg, A. M. (2003). Regulation of vertebrate cellular Mg2+ homeostasis by TRPM7. *Cell*, *114*(2), 191-200. https://doi.org/10.1016/s0092-8674(03)00556-7

Schütz, A., Richter, C., Weissgerber, P., Tsvilovskyy, V., Hesse, M., Ottenheijm, R., Zimmermann, F., Buchholz, S., Medert, R., Dlugosz, S., Kuryshev, V., Benes, V., Flockerzi, V., Fleischmann, B. K., Cavalié, A., & Freichel, M. (2021). Trophectoderm cell failure leads to peri-implantation lethality in Trpm7-deficient mouse embryos. *Cell Rep*, *37*(3), 109851. https://doi.org/10.1016/j.celrep.2021.109851

Sone, Y., Ito, M., Shirakawa, H., Shikano, T., Takeuchi, H., Kinoshita, K., & Miyazaki, S. (2005). Nuclear translocation of phospholipase C-zeta, an egg-activating factor, during early embryonic development. *Biochem Biophys Res Commun*, *330*(3), 690-694. https://doi.org/10.1016/j.bbrc.2005.03.032

Stein, P., Savy, V., Williams, A. M., & Williams, C. J. (2020). Modulators of calcium signalling at fertilization. *Open Biol*, *10*(7), 200118. https://doi.org/10.1098/rsob.200118

Stice, S. L., & Robl, J. M. (1990). Activation of mammalian oocytes by a factor obtained from rabbit sperm. *Mol Reprod Dev*, *25*(3), 272-280. https://doi.org/10.1002/mrd.1080250309

Stricker, S. A. (1999). Comparative biology of calcium signaling during fertilization and egg activation in animals. *Dev Biol*, *211*(2), 157-176. https://doi.org/10.1006/dbio.1999.9340

Sun, J., Wu, X., Xu, X., Jin, L., Han, N., & Zhou, R. (2012). A comparison of epidural magnesium and/or morphine with bupivacaine for postoperative analgesia after cesarean section. *Int J Obstet Anesth*, *21*(4), 310-316. https://doi.org/10.1016/j.ijoa.2012.05.006

Suzuki, T., Yoshida, N., Suzuki, E., Okuda, E., & Perry, A. C. (2010). Full-term mouse development by abolishing Zn2+-dependent metaphase II arrest without Ca2+ release. *Development*, *137*(16), 2659-2669. https://doi.org/10.1242/dev.049791

Swann, K. (1990). A cytosolic sperm factor stimulates repetitive calcium increases and mimics fertilization in hamster eggs. *Development*, *110*(4), 1295-1302. https://www.ncbi.nlm.nih.gov/pubmed/2100264

Swann, K., & Lai, F. A. (2016). Egg Activation at Fertilization by a Soluble Sperm Protein. *Physiol Rev*, *96*(1), 127-149. https://doi.org/10.1152/physrev.00012.2015

Tashiro, M., Inoue, H., & Konishi, M. (2014). Physiological pathway of magnesium influx in rat ventricular myocytes. *Biophys J*, *107*(9), 2049-2058. https://doi.org/10.1016/j.bpj.2014.09.015

Thanassoulas, A., Swann, K., Lai, F. A., & Nomikos, M. (2022). SPERM FACTORS AND EGG ACTIVATION: The structure and function relationship of sperm PLCZ1. *Reproduction*, *164*(1), F1-f8. https://doi.org/10.1530/rep-21-0477

Tokuhiro, K., & Dean, J. (2018). Glycan-Independent Gamete Recognition Triggers Egg Zinc Sparks and ZP2 Cleavage to Prevent Polyspermy. *Dev Cell*, *46*(5), 627-640.e625. https://doi.org/10.1016/j.devcel.2018.07.020

Tourzani, D. A., Paudel, B., Miranda, P. V., Visconti, P. E., & Gervasi, M. G. (2018). Changes in Protein O-GlcNAcylation During Mouse Epididymal Sperm Maturation. *Front Cell Dev Biol*, *6*, 60. https://doi.org/10.3389/fcell.2018.00060

Trapani, V., & Wolf, F. I. (2019). Dysregulation of Mg(2+) homeostasis contributes to acquisition of cancer hallmarks. *Cell Calcium*, *83*, 102078. https://doi.org/10.1016/j.ceca.2019.102078

Uehara, T., & Yanagimachi, R. (1976). Microsurgical injection of spermatozoa into hamster eggs with subsequent transformation of sperm nuclei into male pronuclei. *Biol Reprod*, *15*(4), 467-470. https://doi.org/10.1095/biolreprod15.4.467

Uehara, T., & Yanagimachi, R. (1977). Activation of hamster eggs by pricking. *J Exp Zool*, *199*(2), 269-274. https://doi.org/10.1002/jez.1401990211

Wakai, T., & Fissore, R. A. (2019). Constitutive IP(3)R1-mediated Ca(2+) release reduces Ca(2+) store content and stimulates mitochondrial metabolism in mouse GV oocytes. *J Cell Sci*, *132*(3). https://doi.org/10.1242/jcs.225441

Wakai, T., Vanderheyden, V., & Fissore, R. A. (2011). Ca2+ signaling during mammalian fertilization: requirements, players, and adaptations. *Cold Spring Harb Perspect Biol*, *3*(4). https://doi.org/10.1101/cshperspect.a006767

Wathlet, S., Adriaenssens, T., Segers, I., Verheyen, G., Janssens, R., Coucke, W., Devroey, P., & Smitz, J. (2012). New candidate genes to predict pregnancy outcome in single embryo transfer cycles when using cumulus cell gene expression. *Fertil Steril*, *98*(2), 432-439.e431-434. https://doi.org/10.1016/j.fertnstert.2012.05.007

Wathlet, S., Adriaenssens, T., Segers, I., Verheyen, G., Van de Velde, H., Coucke, W., Ron El, R., Devroey, P., & Smitz, J. (2011). Cumulus cell gene expression predicts better cleavage-stage embryo or blastocyst development and pregnancy for ICSI patients. *Hum Reprod*, *26*(5), 1035-1051. https://doi.org/10.1093/humrep/der036

Wolf, F. I., Maier, J. A., Nasulewicz, A., Feillet-Coudray, C., Simonacci, M., Mazur, A., & Cittadini, A. (2007). Magnesium and neoplasia: from carcinogenesis to tumor growth and progression or treatment. *Arch Biochem Biophys*, *458*(1), 24-32. https://doi.org/10.1016/j.abb.2006.02.016

Wozniak, K. L., & Carlson, A. E. (2020). Ion channels and signaling pathways used in the fast polyspermy block. *Mol Reprod Dev*, *87*(3), 350-357. https://doi.org/10.1002/mrd.23168

Wu, D., & Dean, J. (2020). Maternal factors regulating preimplantation development in mice. *Curr Top Dev Biol*, *140*, 317-340. https://doi.org/10.1016/bs.ctdb.2019.10.006

Wu, H., He, C. L., Jehn, B., Black, S. J., & Fissore, R. A. (1998). Partial characterization of the calcium-releasing activity of porcine sperm cytosolic extracts. *Dev Biol*, *203*(2), 369-381. https://doi.org/10.1006/dbio.1998.9070

Xu, J., Shu, Y., Yao, G., Zhang, Y., Niu, W., Zhang, Y., Ma, X., Jin, H., Zhang, F., Shi, S., Wang, Y., Song, W., Dai, S., Cheng, L., Zhang, X., Xie, W., Hsueh, A. J., & Sun, Y. (2021). Parental methylome reprogramming in human uniparental blastocysts reveals germline memory transition. *Genome Res*, *31*(9), 1519-1530. https://doi.org/10.1101/gr.273318.120

Y, T. (1971). Studies on the fertilization of mouse eggs in vitro.

Yassine, S., Escoffier, J., Martinez, G., Coutton, C., Karaouzene, T., Zouari, R., Ravanat, J. L., Metzler-Guillemain, C., Lee, H. C., Fissore, R., Hennebicq, S., Ray, P. F., & Arnoult, C. (2015). Dpy19l2-deficient globozoospermic sperm display altered genome packaging and DNA damage that compromises the initiation of embryo development. *Mol Hum Reprod*, *21*(2), 169-185. https://doi.org/10.1093/molehr/gau099

Yoon, S. Y., & Fissore, R. A. (2007). Release of phospholipase C zetaand [Ca2+]i oscillation-inducing activity during mammalian fertilization. *Reproduction*, *134*(5), 695-704. https://doi.org/10.1530/REP-07-0259

Yoon, S. Y., Jellerette, T., Salicioni, A. M., Lee, H. C., Yoo, M. S., Coward, K., Parrington, J., Grow, D., Cibelli, J. B., Visconti, P. E., Mager, J., & Fissore, R. A. (2008). Human sperm devoid of PLC, zeta 1 fail to induce Ca(2+) release and are unable to initiate the first step of embryo development. *J Clin Invest*, *118*(11), 3671-3681. https://doi.org/10.1172/JCI36942

Young, C., Grasa, P., Coward, K., Davis, L. C., & Parrington, J. (2009). Phospholipase C zeta undergoes dynamic changes in its pattern of localization in sperm during capacitation and the acrosome reaction. *Fertil Steril*, *91*(5 Suppl), 2230-2242. https://doi.org/10.1016/j.fertnstert.2008.05.021

Zeng, F., Baldwin, D. A., & Schultz, R. M. (2004). Transcript profiling during preimplantation mouse development. *Dev Biol*, *272*(2), 483-496. https://doi.org/10.1016/j.ydbio.2004.05.018

Zhu, D., Su, Y., Young, M. L., Ma, J., Zheng, Y., & Tang, L. (2017). Biological Responses and Mechanisms of Human Bone Marrow Mesenchymal Stem Cells to Zn and Mg Biomaterials. *ACS Appl Mater Interfaces*, *9*(33), 27453-27461. https://doi.org/10.1021/acsami.7b06654

Zou, Z. G., Rios, F. J., Montezano, A. C., & Touyz, R. M. (2019). TRPM7, Magnesium, and Signaling. *Int J Mol Sci*, *20*(8). https://doi.org/10.3390/ijms20081877